**POLITECNICO DI MILANO**

Facoltà di Ingegneria dei Processi Industriali

Corso di Laurea Specialistica in Ingegneria Elettrica


# EXPERIMENTAL CHARACTERIZATION OF MAGNETIC SENSORS FOR CURRENT MEASUREMENT APPLICATIONS

Relatore: Prof. Roberto OTTOBONI

Tesi di Laurea Specilistica di:

Erlind DHAMI

Matr. n. 755998

Anno Accademico 2011 – 2012

# EXPERIMENTAL CHARACTERIZATION OF MAGNETIC SENSORS FOR CURRENT MEASUREMENT APPLICATIONS

## MASTER THESIS


**ERLIND DHAMI**


July 2012

**Thesis Supervisor:**

Prof. Roberto OTTOBONI



**POLITECNICO DI MILANO**

Facoltà di Ingegneria dei Processi Industriali

Corso di Laurea Specialistica in Ingegneria Elettrica

# Abstract

CURRENT MEASUREMENT is a fundamental practice in the electricity sector. Today it is common practice to measure large currents in many applications (power measurements, protection, etc.): therefore, the current transducer must operate with current values that reach several thousand hundreds of amperes, exhibit good linearity in a wide range temperature (typically -25 $^{0}$ C to +100 $^{0}$ C) and currents, ensure adequate accuracy, and, last but not least, a good noise rejection. According to the principle of operation, can be substantially identified four techniques of measurement of an electric current, which can be classified as follows: Ohm's Law, the law of Faraday, the Faraday's effect and the detection of the magnetic field. It is natural that there are limitations and disadvantages to each of these principles; both from a technical and an economical point of view and thus each solution is a compromise between different requirements.

In this view, an attractive approach to current measurement is represented by the array of magnetic sensors, in which the measure of the current is reduced to the measurement of a magnetic field produced by it. Due to the linearity between the magnetic field and current that produces it, the latter can be reconstructed, by means of specific algorithms, starting from the values collected by a suitable array of magnetic sensors placed in proximity of the conductor in which circulates the current to be measured.

A magnetic field sensor which is very popular and widely used in these arrays is the Hall effect sensor. This sensor is relatively inexpensive, which allows the use of arrays even with a high number of sensors, very sensitive and characterized by good linearity. Currently there are several companies that produce the Hall effect sensors, which, as officially declared, exhibit excellent linearity in a wide range of temperatures and currents. The objective of this thesis is to verify experimentally the real characteristics of products from different manufacturers, in order to get a complete and comparative view of the performance of these sensors, specifically evaluated under the conditions provided for use in arrays for current measurement. The following chapters provide a report of all the tests that were performed to study

the performance of these sensors on a temperature range between -20 $^0$ C and +100 $^0$ C, and with variations in current from 50A up to 2500A.

Finally we have also carried out tests on a different transducer, but certainly of great and renewed interest: a Rogowski coil with a non-circular geometry. This type of current transducer has a very good performance in terms of linearity, crosstalk rejection, bandwidth, and is not subject to saturation phenomena. This last feature makes the Rogowski coil the ideal transducer even for measuring short-circuit currents. Several comparative tests between the two new types of Rogowski coils are reported in this thesis.

***Keywords:*** Current measurement; Hall-effect sensors; magnetic sensor array; Rogowski coil; crosstalk rejection

*"To all those people that made this work possible"*

Erlind Dhami

# Acknowledgements

GRADUATING FROM POLITECNICO DI MILANO is a big step for me, and I like to thank all the people that supported me during this beautiful journey.

First and foremost, I would like to thank my supervisor, Prof. Roberto Ottoboni, for his support, continuous help, understanding and willingness throughout the period that led to the realization of this thesis. Moreover, spending his precious time with me is appreciated far more than I have words to express. I am very grateful to work with such a knowledgeable and insightful professor.

I would like also to express my appreciation to all my professors who, with their way of teaching, have increased my passion for engineering.

A special thanks goes to my family, for giving me the opportunity of earning a better education at Politecnico di Milano, which is a dream come true. I am very grateful to them for their moral support and financial sacrifices, so that I may have a brighter future.

Next I want to thank my girlfriend Alma, who has always been present and shared with me every second of this beautiful and important part of my life. She has proven to me that, relying on each other, every difficulty is nothing else that a station by which you have to pass-by, in order to arrive on the destination. She made this journey easier.

Lastly I want to thank all the friends that I made while studying at Politecnico di Milano, especially Federico, Fabio, and Rabah, who have helped me in several occasions.

# Table of Contents

# 1

# Preface

## 1.1. Introduction of Current Measurement in Electrical Devices

NOWADAYS ELECTRICAL DEVICES are spread throughout the entire landscape of human existence. We find them in almost every application that aids the human existence around the globe; they are in different shapes and sizes, and different purposes. These devices are used for measurement, automation control, monitoring, switching operation, etc..

In the electrical engineering landscape electrical devices are used for protection purposes. They protect the electrical equipment from damages caused by various faults, like short circuits, over-loads, etc., and common examples are: current transformers, voltage transformers, circuit breakers, etc..

A lot of intelligence is being introduced in electrical devices, such as micro-electronics, computer science, power electronics, and cutting-edge sensing techniques. A crucial point in proper operation of electrical devices is current measurement, and many different approaches are available in today's market. They are differentiated from one another based on specifications required by different applications, such as the measurement of peak to peak value, RMS value, accuracy, bandwidth, robustness, cost, etc..

Different technologies include: The old school shunt resistor based on the Ohm's Law which is the simplest way to measure a current; AC current

measurements carried out by traditional current transformers, and Rogowski coils; Magnetic-field based transducers such as Hall-Effect transducers in three different configurations, – open-loop, closed-loop, and ETA –; Fluxgate based transducers which are very sensitive magnetic-field based transducers; fiber-optic current sensors based on the Faraday's Effect; and other technologies such the magneto-resistance effect (MR).

Current sensing technologies must fulfill various requirements, for various applications. Generally, the common requirements are:

- High accuracy and linearity
- Wide bandwidth
- DC and AC measurement
- Low temperature drift
- Interference rejection
- IC packaging
- Low power consumption
- Low price

## 1.2. Current Sensing Techniques: The State of the Art

INFORMATION regarding current flow is required in a wide range of applications. High performance electrical/electronic devices require high performance sensing techniques to meet the demands in terms of cost, isolation, precision, bandwidth, measurement range, or size. To satisfy these demands, different current measurement methods have been developed.

The following paragraphs are a thorough review of current sensing techniques. We can classify these techniques based upon the underlying physical principle in order to have some understanding of the performance and the limitations of each one [1].

These principles are as follows:

i. Ohm's law of resistance
ii. Faraday's law of induction
iii. Faraday effect
iv. Magnetic field sensors

We'll also discuss known sensing techniques, such as open – loop, closed – loop, particularly magnetic field – based sensors and the use of these sensors in combination to meet performance requirements.

### 1.2.1. Current Sensors Based on Ohm's Law

OHM'S LAW is a simplification of the Lorentz law that states

$$\mathbf{J} = \sigma (\mathbf{E} + v \times \mathbf{B}) \tag{1-1}$$

where:

**J** is the current density
**E** the electric field
v the charge velocity
**B** the magnetic flux density acting on the charge
σ the material conductivity

Generally, the moving charge has a velocity that is sufficiently small so that the second term can be neglected. Therefore we can write

$$\mathbf{J} = \sigma \mathbf{E}, \tag{1-2}$$

This equation is the Ohm's law and states that the voltage drop across a resistor is proportional to the current going through it. This relationship can be used to sense currents. Sensors based on this simple relationship are well known for their lower costs, and reliability due to this simple principle.

## SHUNT RESISTOR

A COMMON AND SIMPLE approach to current sensing is the use of a shunt resistor. The voltage drop across the shunt is proportional to its current flow. Both alternating currents (AC) and direct currents (DC) can be measured with the shunt resistor. Due to its introduction into the current's path, the shunt resistor generates a power loss that can be calculated via the Ohm's law ($i^2R$). From this relationship, is quite clear that the loss increases with the square of the current, thus restricting the usage of the shunt resistor in high current applications.

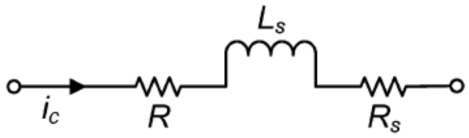


**Figure 1-1** Equivalent circuit diagram for a shunt resistor

Fig. 1-1 depicts the equivalent circuit of a shunt resistor with nominal resistance $R$ alongside a parasitic inductance $L_S$ and a series resistance $R_S$, due to the skin effect [2]. The parasitic inductance $L_S$ is often a source of confusion since it is frequently assumed to be related to the self-inductance of the shunt resistor. Hence, the connection of the sense wires is crucial to achieve good performance. Significant research has been conducted to reduce $L_S$ and the skin effect in order to increase the measurement bandwidth [3 – 5].

The high – performance coaxial shunt have been widely used for many applications – fast-rise time transient currents and high amplitudes – but, for highly integrated electronic devices are preferred low-cost surface-mounted-devices (SMDs)[6], because of their small sizes and relatively low prices.

Fast-response for measuring high-impulse or heavy-surge currents is the common requirement for shunt resistors. In 1981 Malewski[7], designed a circuit to eliminate the skin effect and later in 1999 the flap-strap sandwich shunt (FSSS)[8] was introduced from a flat-strap sandwich resistor. The

properties of the FSSS in terms of response time, power loss and frequency characteristics, are the same as the shunt resistor but the cost is lower and the construction technique is less sophisticated, compared to Malewski and the coaxial shunt.

### TRACE RESISTANCE SENSING

IT IS POSSIBLE to exploit the intrinsic resistance of a conducting element, (usually a copper trace) instead of a shunt resistor. Since no additional resistor is required this approach promises a low-cost and space saving configuration with no additional power losses either. Naturally, the voltage drop of a copper trace is very low due to its very low resistance, making the presence of a high gain amplifier mandatory in order to get a useful signal.

There are several physical effects which may alter the current measurement process: thermal drift of the copper trace, initial conditions of the trace resistance etc. Therefore, this approach is not suitable for applications that require a reasonable accuracy due to the large thermal drift. In order to overcome the problems associated with the temperature drift, a digital controller can be used for thermal drift compensation and calibration of the copper trace [9].

Ohm's law provides the simplest way to measure currents. A significant drawback of this kind of current sensor is the unavoidable electrical connection between the current to be measured and the sense circuit. By employing a so-called isolation amplifier, electrical isolation can be added. However, these amplifiers are expensive and can also deteriorate the bandwidth, accuracy and thermal drift of the original current sensing technique. For these reasons, current sensing techniques based on physical principles that provide intrinsic electrical isolation deliver a better performance at lower costs in applications where isolation is required.

## 1.2.2. Current Sensors Technology that Uses Faraday's Law

FARADAY'S LAW of induction – that states: the total electromotive force induced in a closed circuit is proportional to the time rate of change of the total magnetic flux linking the circuit – has been largely employed in current sensing techniques. Two major sensing devices based on Faraday's law are Current transformers (CTs) and Rogowski coils. These sensors provide an intrinsic electrical isolation between the current we want to measure and the output signal, thus making these current sensing devices mandatory, where safety standards demand electrical isolation.

ROGOWSKI COIL

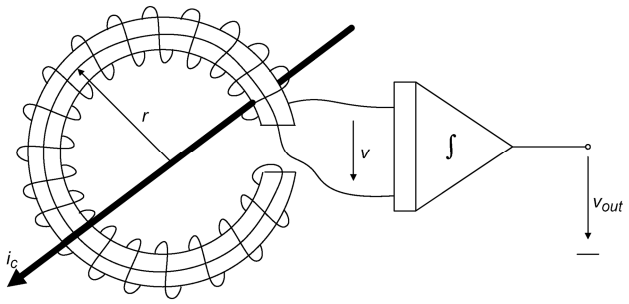


**Figure 1-2** Rogowski coil as a transducer. An integrator is required to get an output voltage $v_{out}$ proportional to the primary current $i_c$

In figure 1-2 is depicted a basic configuration of a Rogowski coil – also called air-cored coils – which is a classic example of a sensing technique based on the Faraday's law of induction. The coil's working principle can be explained starting from Ampere's law that defines the path integral of the magnetic flux density $\boldsymbol{B}$ inside the coil

$$\oint_C \vec{B} \cdot \overrightarrow{dl} = \mu_0 i_C \tag{1-3}$$

The current $i_C$ passes through an enclosed curve $\boldsymbol{C}$. For a simple analysis, let's suppose that the cross section diameter of the coil is much smaller than the radius $\boldsymbol{r}$. This is valid for most coil designs. If the current $i_C$ passes through the center of the coil, the magnetic flux density $\boldsymbol{B}$ can written as:

$$B = \frac{\mu_0 i_C}{2\pi r} \tag{1-4}$$

Applying the Faraday's law of induction, we can determine the induced voltage into the Rogowski coil due to the current $\boldsymbol{i_C}$

$$v = -N\frac{d\phi}{dt} = -NA\frac{dB}{dt} = -\frac{NA\mu_0}{2\pi r}\frac{di_C}{dt} \tag{1-5}$$

where:

**A** is the cross sectional area of the coil

**N** is the number of turns

Voltage $\boldsymbol{v}$ is proportional to the derivative of the current $\boldsymbol{i_C}$ that we want to measure. Using an integrator with an integrating constant $\boldsymbol{k}$, and infinitely high input impedance the exact expression of $\boldsymbol{v_{out}}$ can be found.

$$v_{out} = -\frac{NA\mu_0}{2\pi r}k\int_t \frac{di_C}{dt}dt + v_{out}(0) = -k\frac{NA\mu_0}{2\pi r}i_C + v_{out}(0) \tag{1-6}$$

Expression (1-6) is theoretically valid even if the conductor isn't in the center of the Rogowski coil, but a quick look at the characteristics of commercial Rogowski coils, shows that the typical measurement error is increased if the coil is not centered on the conductor, as shown in figure 1-3.

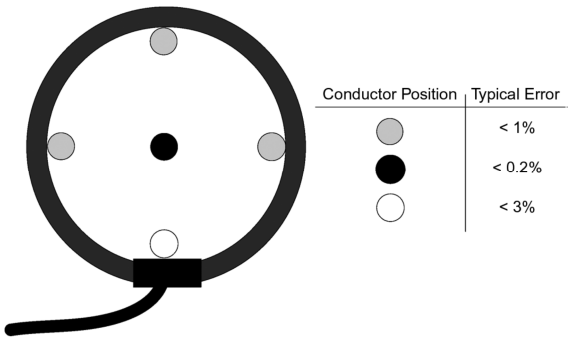


**Figure 1-3** Accuracy of the Rogoski coil based on the position of the conductor.

This error derives from the fact that in reality the winding density is not perfectly constant along the entire coil, and is even worse in the proximity of the mechanical clip, where the density cannot be even. Also from expression (1-6) can be noticed that the coil can be used to measure

DC currents. But, we have to remember that the working principle is based on the detection of the flux change, which is proportional to the current change. From (1-6) we have to know the initial condition at $t = 0$, which is $v_{out}(0)$ in order to reconstruct a DC current. Since practical integrators are not perfect and may exhibit a small offset voltage, the frequency response of the Rogowski coil must be modified, in order to reduce the gain at low frequency. Therefore, practical Rogowski coils are not suitable for low-frequency currents measurement [10], [11], [12]. To extend the use to these currents, it has been proposed to combine the Rogowski coil with an open-loop magnetic field sensor in order to measure DC currents [13].

Many different designs of Rogowski coils have been proposed. For higher performance, a coil with a current output has been proposed, which uses its self-inductance for passive integration. Reducing the bulk of the coil, by introducing a PCB Rogowski coil, is another example of different Rogowski coil design.

Compared to the current transformer, the Rogowski coil has a low sensitivity. This is because of the absence of a high permeability magnetic core, that the current transformer can take advantage of. However, this can be compensated by adding more windings on the Rogowski coil or using an integrator with a higher gain $k$. More windings increase the self-capacitance and self-inductance, and higher integrator gain means an amplifier with a large gain-bandwidth product. As always in engineering, trade-offs must be made depending on specific applications.

Fig. 1-4 displays the operating limits of Rogowski coils [14]

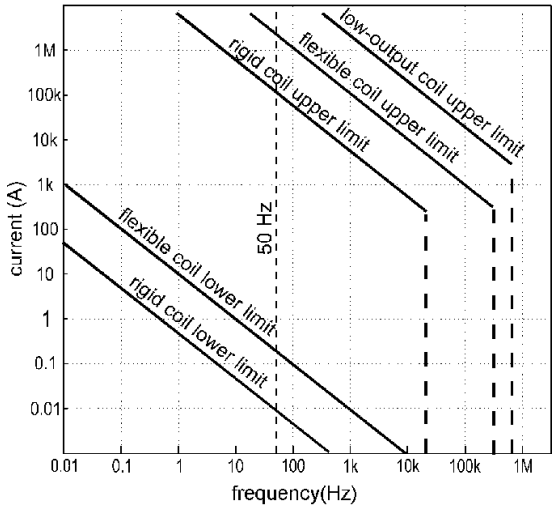


**Figure 1-4** Operating limits of Rogowski coils. Rigid coils have the advantage of being able to measure at smaller frequencies, whereas flexible coils have improved handling capability, and usually can measure at higher frequencies.

Upper limits:

The direct output from the coil depends on the rate of change of current. For sufficiently high currents and frequencies the output can be large enough to cause a voltage breakdown. Coils with a low mutual inductance are best for high currents and frequencies.

Resonance Limits:

Every coil has a self-resonant frequency caused by its self-inductance and inter-turn capacitance. The resonance also depends on other factors such as cable capacitance. The resonance can be controlled by suitable damping circuitry, but generally it is not feasible to use a coil above its resonant frequency. The vertical broken lines show these limits.

Lower Limits:

At low currents and low frequencies the direct output from the coil is very low and the usefulness of the current transducer is limited by noise effects. Rigid coils which have a large mutual inductance are best for very low current measurements. The low current limit can be extended by using multiple primary turns round the coil or in the case of a flexible coil by

wrapping the coil several times round the conductor. Electronic methods of signal recovery such as filters or phase-sensitive detectors are also useful.

One of the key features of Rogowski transducers is the fact that they don't exhibit saturation and are intrinsically linear due to the absence of magnetic material. Being able to measure high currents makes the Rogoskwi transducer an exceptional tool to measure the amplitude of the current pulse, even when it is unknown. The cost is comparable with that of current transformers but with the advantage of less insertion impedance and, in the case of flexible coils, higher user-friendliness. The coil can be used in a wide range of applications, such as: short-circuit testing systems, current measurements in power-distribution systems, slip-ring induction motors, etc..

## CURRENT TRANSFORMER (CT)

THE CURRENT TRANSFORMER (CT) is similar to the Rogowski coil, with one primary turn and several secondary turns but it uses a core material with high relative permeability. The secondary winding of a CT is loaded with a sense resistor. The secondary current that passes through the sense resistor generates a magnetic flux that opposes the flux generated by the primary current.

A basic model of the current transformer is shown in fig. 1-5(a). This equivalent circuit neglects stray inductances, core losses, and winding resistance. However, it gives sufficient insights to understand the working principle of the transformer. The secondary current is generally standardized at 1A, 2A, 5A (the third value is the most common).

There are two errors that must be kept in mind when using this approach in current measurement:

- **Ratio error:** is described as the deviation from the nominal ratio $K_n$, thus preventing a correct identification of the primary current.

– **Phase shift error:** is the deviation in the phase displacement of primary and secondary current.

The quality of the measurement is certified by the accuracy class of the CT which ranges from 0.1 to 3; these values represent the maximum allowed error in percentage, at the rated current.

An advantage of a CT over the Rogowski coil is that integration of the output is not required since the output voltage is directly proportional to the primary current, thus preventing the deterioration of the accuracy by the offset or saturation of the integration circuit. Furthermore, the position of the current carrying conductor influences less on the accuracy of the CT compared with Rogowski coil. However, must be kept in mind that the magnetizing inductance $L_m$ [fig. 1-5(a)] is not ideal, and exhibits hysteresis and saturation. For this reason, the peak magnetizing current must not saturate the core, and the core losses must not cause overheating of the transformer. Saturation problems are critical especially for CTs used in protection relays.

Current transformers are very popular in power conversion applications because of their low cost, and the ability to provide an output signal that is directly compatible with an analog-to-digital converter. They are also intensively employed in power distribution networks at 50/60 Hz line frequency.

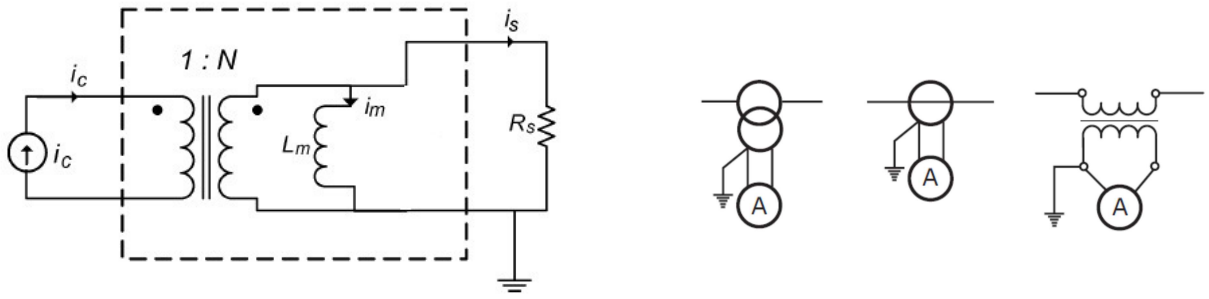


(a) (b)

**Figure 1-5** (a) current transformer model, (b) insertion scheme.

## 1.2.3. Current Sensors that Employ Faraday's Effect

THE FARADAY'S EFFECT is used in optical fiber current sensing. It is a magnetically induced circular birefringence. If the intrinsic circular birefringence of a medium is negligible small, a beam of light traveling through the medium will have its linear polarization rotated by an angle $\boldsymbol{\theta}$ equal to the integral of applied magnetic field $\boldsymbol{H}$ along the path $\boldsymbol{s}$

$$\theta = V \int \vec{H} \cdot d\vec{s} \tag{1-6}$$

where:

**V** – is the Verdet constant

Extensive research has been done in optical current transformers. They provide an attractive alternative in applications such as: power distribution systems measurements, where electrical isolation is a key requirement. In such applications the cost of traditional current transformers increases, since the construction process has to take into account the challenges that arise, in terms of isolation material design, with increased levels of voltage. To this is added the need to avoid saturation of the core. Optical current sensors can measure DC currents beyond 100kA.

A direct way to use the Faraday's effect for current measurement is shown in figure 1-6.

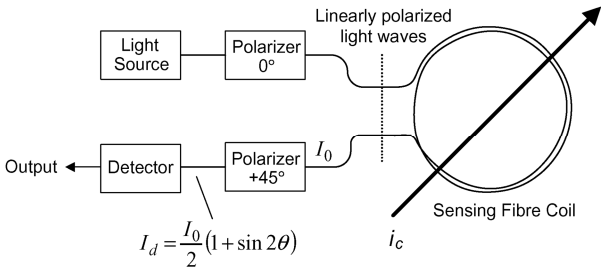


**Figure 1-6** Schematic of a fiber polarimeter – the simplest way to measure the current $\boldsymbol{i_c}$, using Faraday's effect.

Linear polarized light is feed into a fiber-optic coil that revolves $\boldsymbol{N}$ times around the current $\boldsymbol{i_C}$ to be measured. The rotation $\boldsymbol{\theta}$ of the linear polarized light can be calculated using Ampere's law

$$\theta = VNi_C \tag{1-7}$$

An advantage of using fiber-optic coils is that only the magnetic fields internal to the coil – resulting from the flow of current $\boldsymbol{i_C}$ – are detected since external dispersion magnetic fields will commonly cancel out. Moreover, the position of the current conductor inside the sensor has no significant influence on the measurement accuracy [1].

Another advanced technique based on the Faraday's effect is by means of two counter propagating light beams using a Sagnac interferometer [1]. This technique delivers a better scale factor stability, excellent zero point stability, and provides significantly increased measurement range over the previous method.

A commercially available fiber-optic sensor can measure up to 500kA [1]. In order to avoid stress on the fiber-optic cable, the cable is packaged so as to protect the cable from any stress due to mounting and transportation of the current sensor. This current sensor introduces a significant reduction in power loss and is less bulky compared to alternative technologies used in power distribution systems. However, for smaller currents other technologies are more feasible mainly due to their lower costs, and because the fiber-optic principle will require many turns in order to provide the desired sensitivity. Special and expensive materials are required in order to avoid bend stress, which otherwise will deteriorate performance of these sensors. As mentioned above, fiber-optic sensors do not have the need for magnetic centering of the conductor carrying the current to measure, and are especially useful in HV systems due to their intrinsic electrical isolation, and in environments with high electromagnetic – interference. They are usually employed in power metering, fault detection and electro winning applications.

### 1.2.4. Magnetic Field – Based Current Sensors

MAGNETIC FIELD SENSORS are solid state devices that are becoming more and more popular because they can be used in many different types of application such as sensing position, velocity or directional movement [15]. They are widely used due to their non-contact wear free operation, low maintenance, robust design and as sealed Hall Effect devices are immune to vibration, dust and water. The wide ranges of applications – from automobiles to aircrafts – make the magnetic field sensors very popular devices.

#### HALL– EFFECT SENSORS

HALL-EFFECT SENSORS are devices based on the Hall-effect, which was discovered by Edwin Hall in 1879 based on the physical principle of the Lorentz force. They are activated by an external magnetic field. Figure 1-7(a) shows a block diagram of a sensing device based on the Hall Effect sensor. In this generalized device, the Hall sensor senses the magnetic field produced by the magnetic system. This system responds to the quantity to be sensed (current, temperature, position, velocity, etc.) through the input interface. The output interface then converts the electrical signal from the Hall sensor – the Hall voltage – to a signal that is significant to the application context.

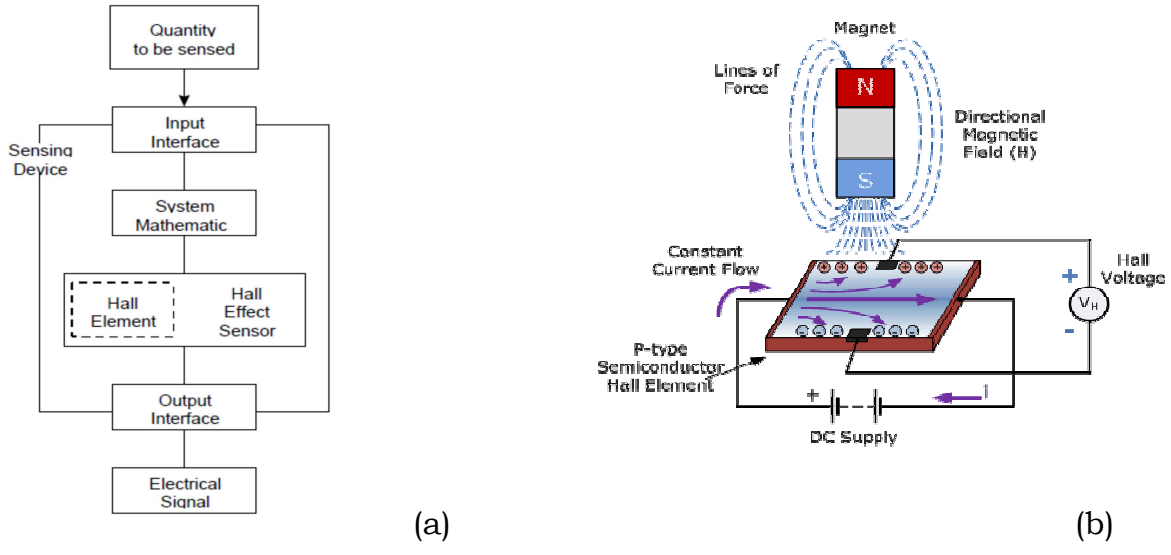


**Figure 1-7** (a) General sensor based on Hall Effect [16] , (b) Basic principle of the Hall Effect

The basic principle of the Hall Effect it is shown in figure 1-7(b). The magnetic field has two important characteristics; flux density ***B*** and ***polarity***. The output signal from a Hall Effect sensor is the function of magnetic field density around the device. When the magnetic flux density around the sensor exceeds a certain preset threshold, the sensor detects it and generates an output voltage called the **Hall Voltage, *V***.

Hall Effect Sensors consist basically of a thin piece of rectangular p-type semiconductor material such as gallium arsenide (GaAs), indium antimonide (InSb) or indium arsenide (InAs) passing a continuous current through itself. When the device is placed within a magnetic field, the magnetic flux lines exert a force on the semiconductor material which deflects the charge carriers, electrons and holes, to either side of the semiconductor slab. This movement of charge carriers is a result of the magnetic force they experience passing through the semiconductor material. As these electrons and holes move side wards a potential difference (**the Hall Voltage, *V***) is produced between the two sides of the semiconductor material by the build-up of these charge carriers. Then the movement of electrons through the semiconductor material is affected by the presence of an external magnetic field which is at right angles to it and this effect is greater in a flat rectangular shaped material.

Generally, Hall Effect sensors and switches are designed to be in the ***"OFF"***, (open circuit condition) when there is no magnetic field present. They only turn ***"ON"***, (closed circuit condition) when subjected to a magnetic field of sufficient strength and polarity. At zero magnetic field, an offset voltage is present, also known as misalignment voltage. Therefore, to use the Hall-effect device as a current transducer, additional circuitry is required in order to compensate this offset voltage.

## SENSING CONFIGURATIONS

THERE ARE THREE DIFFERENT sensing configurations; open – loop, closed – loop, and a third one that combines magnetic field sensors with a current transformer or a Rogowski coil [1]. The followings will provide a quick review of each one these sensing configurations.

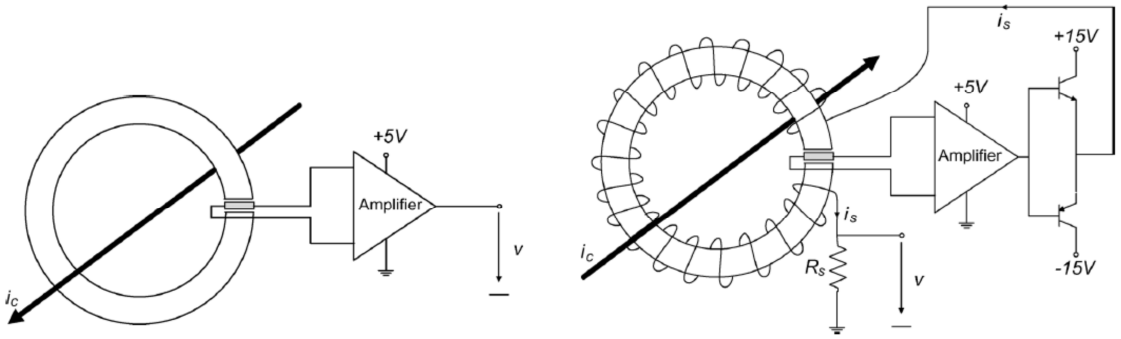


(a) (b)

**Figure 1-8** (a) Open – loop current sensor, (b) Closed – loop current sensor

Figure 1-8(a) is a schematic of an open – loop configuration that uses a magnetic core to concentrate the field from the primary current $\boldsymbol{i_C}$ onto the sensing device. This configuration reduces the influence of external magnetic fields. It is possible to measure DC, AC, and impulse currents with galvanic insulation between the primary and the secondary circuit. When the primary current $\boldsymbol{i_C}$, flows through the sensor, it creates a primary magnetic flux. The Hall sensor placed in the air gap of the magnetic circuit, will provide a voltage $\boldsymbol{V}$ (Hall voltage), that is proportional to this flux, which itself is proportional to the primary current $\boldsymbol{i_C}$ to be measured. The amplifier then amplifies the Hall voltage $\boldsymbol{V}$ to be further processed.

The closed – loop configuration, just like the open – loop configuration; provides galvanic insulation between the primary and the secondary circuit. Same considerations can be made regarding the waveforms that can be measured. Figure 1-8(b) shows a schematic of this configuration. The primary current $\boldsymbol{i_C}$ flowing through the sensing device creates a primary

magnetic flux. The Hall sensor placed in the air gap of this circuit provides a voltage that is proportional to this flux. This voltage is then processed by the electronic circuit and is converted to a secondary current $i_S$, which is then fed to the secondary winding. Current $i_S$ multiplied by the number of turns of the secondary winding cancels out the primary magnetic flux. The formula $N_P \cdot I_P = N_S \cdot I_S$ is true at any given time. Therefore, the secondary current $i_S$ is proportional to the primary current at any moment. This secondary current can be passed through a measuring resistance $R_S$. The voltage drop $V$ on this resistance is proportional to the primary current $i_C$.

Some key features of these configurations can be summed up as follows; the open – loop have a good accuracy that ranges from direct to several tens of kHz. It provides high reliability, low power consumption, reduced weight and volume and cost effectiveness. The closed – loop on the other hand, features a high accuracy under frequencies that span from direct to more than 100 kHz, while delivering high dynamic performance, high overload capabilities and high reliability. Both these configurations measure instantaneous values.

The third configuration, as mention above, is a combination of a magnetic sensor and a current transformer or a Rogowski coil. This combination is very interesting, since it takes advantage of DC measurements offered by the magnetic sensor, and the accuracy and bandwidth offered by the CT/Rogowski coil. An example of this configuration is the Eta current sensing principle developed by LEM.

This transducer is the combination of an open – loop Hall-effect sensor with a magnetic core that uses the CT principle, as shown in figure 1-9. Since no compensation current is required, the power consumption has been greatly reduced, and the sensor can work with a unipolar supply [17]. Eta technology is almost the same as the closed – loop technology in terms of both performance and cost. The current transformer covers the high – frequency range, while the open – loop Hall-effect works on the low – frequency range.

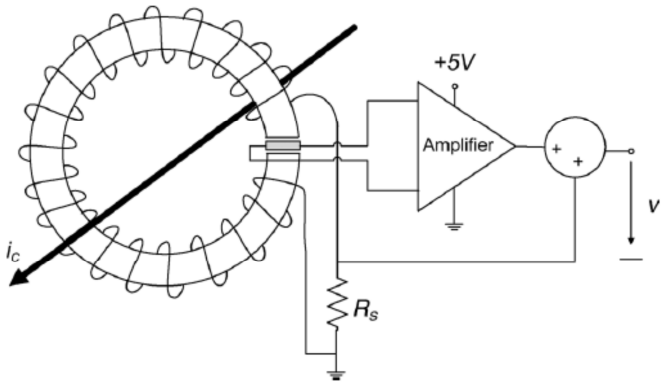


**Figure 1-9** A schematic of the Eta technology

The combination of magnetic field sensor and CT has been pushed further to build the so-called current probes, which are sensors that achieve a measurement bandwidth up to 100 MHz and accuracy around 2%. Other designs use a Rogowski coil to measure the high – frequency part of the current. Despite of all these advantages, active current probes are used mainly in measurement equipment, and are not mass-produced due to their complex design, large volume, and expensiveness.

### THE FLUXGATE PRINCIPLE

THE FLUXGATE TECHNOLOGY is known for decades, and is one of the most accurate field sensors available today. The basic fluxgate principle exploits the nonlinear relation that exists between the magnetic field, ***H***, and the magnetic flux density, ***B***, within a magnetic material. These sensors are able to measure DC or low-frequency AC magnetic fields. Fluxgate sensors can sense the direction of magnetic fields in the range of up to 1mT that can go even down to 10 pT [18].

Fig. 1-10 shows the mechanics of the fluxgate principle. The core is magnetically saturated (in both directions) by means of an excitation coil that is driven by an excitation current $\boldsymbol{I_{exc}}$ that can be a sine or a square waveform. In saturation the core permeability drops down and the DC flux associated with the measured DC magnetic field $\boldsymbol{B_0}$ decreases (flux collapse). During the next half cycle of the excitation waveform the core recovers from

saturation, and the DC flux associated with magnetic field $\boldsymbol{B_0}$ increases (flux recovery); the cycle than repeats. This process of "gating" flux in and out the sense coil gives the name to the device. Due to this flux change, a voltage $\boldsymbol{V_{ind}}$ is induced into the sensing (pick-up) coil placed around the core.

From fig. 1-10(b) can be seen that the sense voltage has a frequency that is twice compared to the excitation current $\boldsymbol{I_{exc}}$. For this reason, often the voltage $\boldsymbol{V_{ind}}$ is extracted using a 2nd harmonic demodulation scheme. There are some fluxgates the work in short – circuited mode, providing a current – output.

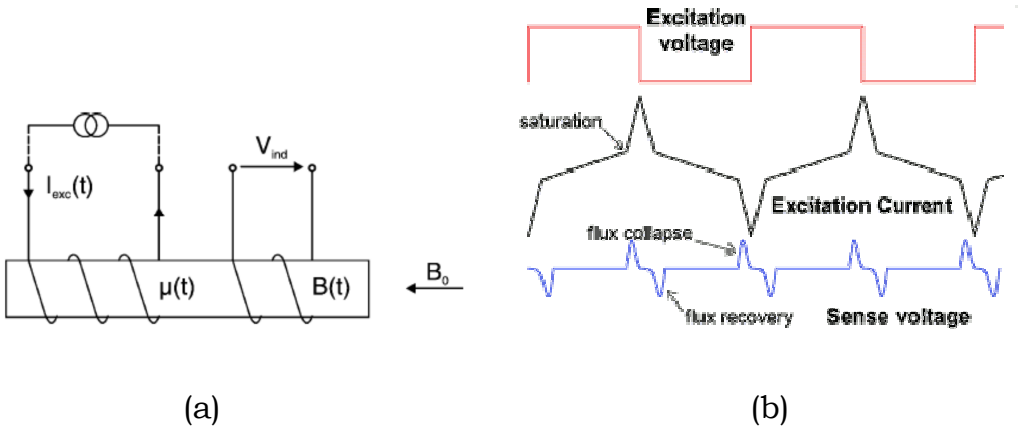


**Figure 1-10** (a) the fluxgate principle, (b) ideal flux waveforms [19]

The main problem of using this basic single-core design is that the sense coil will pick up the excitation current $\boldsymbol{I_{exc}}$ as well as the induced voltage $\boldsymbol{V_{ind}}$, because the sensor acts as a transformer. Thus, the single-core design is used mainly for simple devices and special applications. In order to overcome this flaw, double cores (either double-rod or ring-core) are normally used. Some popular configurations of fluxgate-based magnetic sensors are shown in fig. 1-11.

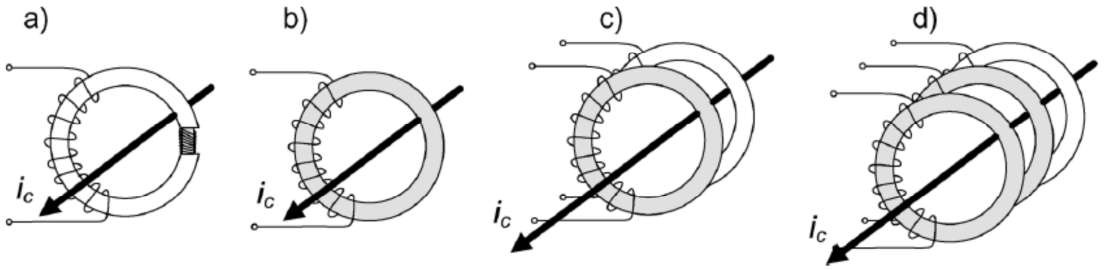


**Figure 1-11**[1] Different types of fluxgate configurations. (a) Closed – loop configuration, (b) low – frequency version, (c) Additional CT to extend the bandwidth, (d) three core configuration for enhanced performance.

In the closed – loop configuration or "The standard fluxgate configuration" [fig. 1-11(a)], the magnetic field is concentrated by the magnetic core. The secondary winding is used to compensate this concentrated magnetic field. High accuracy is achieved, due to high sensitivity and temperature stability offered by the fluxgate. A low – frequency version consisting of a single closed annular magnetic core, with no pick-up coil is depicted in [fig. 1-11(b)]. Because of the absence of the pick-up coil, the current on the excitation coil is processed in order to determine the primary current $\boldsymbol{i_C}$. This is a low-cost configuration, with a very low thermal drift, but with a limited bandwidth. This configuration can be extended using a current transformer in order to increase the bandwidth [fig. 1-11(c)]. The current transformer provides the measurements of high-frequency signals, while the fluxgate measures low-frequency signals. Finally, the most advanced and most costly configuration is depicted in figure [fig. 1-11(d)], where a third core is used for enhanced performance and bandwidth.

Many different fluxgate-based sensors have been proposed, and there are efforts in integrating open-loop fluxgate sensors with PCB technology which is certainly a promising development towards low-cost applications. Standalone fluxgate sensors are commercially successful but so far only in high precision applications because of the high cost and size requirements. Due to the very high accuracy, fluxgates are often employed in calibration systems, diagnosis systems, laboratory equipment, and medical systems.

## MAGNETO RESISTANCE EFFECT (MR)

IT IS POSSIBLE TO BUILD structures in which the electrical resistance varies as a function of applied magnetic field. These structures can be used as magnetic sensors. Normally these resistors are assembled in a bridge configuration to compensate for thermal drift [1]. Popular magneto resistance-based sensors are: Anisotropic Magneto Resistance (AMR), Giant Magneto Resistance (GMR), Giant Magneto Impendence (GMI) and Tunnel Magneto Resistance (TMR).

All these MR-based sensors have higher sensitivity compared to Hall-effect sensors. Despite of this, these sensors (GMR, CMR, and TMR) are still more expensive than Hall-effect devices, have serious drawbacks related with nonlinear behavior, distinct thermal drift, and a very strong external field can permanently alter the sensor behavior (GMR). GMI and TMR sensors are even more sensitive than GMR based sensors, but still in the test phase and no commercial version are available today [1].

## 1.3. Arrays of Magnetic Sensors for Current Measurements

CURRENT TRANSDUCERS based on sensor array are widely known for their low cost, small size, and interface with a PC. They are primarily Hall-effect sensors arranged in different configurations based on specific requirements of the application.

The simplest way to measure the current is to place a single magnetic sensor near the current that we want to measure, but crosstalk fields may limit the accuracy of the sensor. A single sensor cannot distinguish the field generated by the current under measurement from external magnetic fields. Ampere's Law states that the current flowing in a conductor is proportional to the sum of the sensors' outputs located around the conductor, so fitting as many sensors as possible in the area around the conductor is the next step. The third way to sense a current is to use a sensor array. Once the array has been located, the next step is to process the data from such array. Finally specific algorithms are employed to reconstruct the original current, based on the linear relationship between the current and magnetic field.

A circular array of magnetic sensors is an example of a modern current transducer. This approach has been employed for current sensing in a three-phase bus-bar system, with four sensors per phase, $\theta_0 = \pi$. The transducer was tested in a 50-500 Hz frequency range and the effects of a bar placed in the proximity of the array have been experimentally investigated. A high current testing showed that the transducer belongs to the 1% accuracy class.

When dealing with DC currents, two algorithms have been proposed to improve the accuracy and to reduce the crosstalk effect of external magnetic fields. Paper [20] presents and algorithm based on spatial harmonic analysis of the magnetic field. The DFT and the numerical solution of the proposed systems can be performed by a DSP. The new method can thus be applied in the realization of an intelligent current sensor made of low-cost magnetic sensors. The current under measurement $I_1$ and the crosstalk current $I_2$ are both considered filamentary. Because of the linearity of the field equations,

taking into account only one crosstalk current is sufficient to generalize the problem. An environmental homogenous magnetic field $H_0$, e.g. the earth magnetic field, may also be present.

Let us now consider a circular array of radius $d < D$ centered on current $I_1$ and made of $N$ magnetic sensors, that are of the same type and have the same sensitivity $S$. The sensors are tangentially directed and distributed equally on the circumference, in positions $\theta_n=2\pi n/N$ , where $n=1,\ldots,N-1$ as shown in [Fig.1-12].

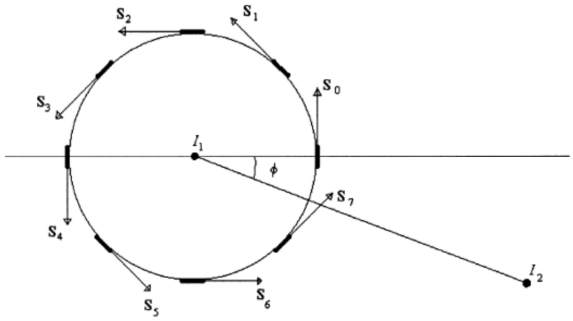


**Figure 1-12** Circular array made of sensors and their sensitivity vectors

The sensor output can be expressed as a complex Fourier series

$$V(\theta) = \sum_{m=-\infty}^{+\infty} c_m e^{im\theta} \tag{1-8}$$

where:

$\boldsymbol{c_m}$ is the Fourier coefficient

Taking into account the aliasing phenomenon, the relation between the DFT transformation of $V(\theta)$ and the Fourier coefficients is as follows

$$\tilde{v}_m = DFT\{v_n\} = e^{-jm\phi}\left(c_m + c_{N+m}e^{-jm\phi} + c_{-N+m}e^{-jm\phi}\right), \qquad m = 0, \ldots., N-1 \tag{1-9}$$

The quantities $\tilde{v}_m$, $c_m$, $c_{N+m}$ and $c_{-N+m}$ are all known, so $I_1$, $I_2$ and their distance can be calculated by solving a nonlinear formulation.

The algorithm described above can be used only in the case of a circular bus-bar. In [21] is presented a generalized version of this algorithm that can be applied both in circular and rectangular bus-bars.

Due to the symmetrical magnetic field generated by the conductor $H^{bar}$ and $v^{bar}$ can be expanded in a spatial Fourier series of only cosinusoidal terms

$$v^{bar} = S \sum_{\substack{m\geq 0 \\ m=even}} I^{bar}\, b_m(r) cosm\theta \tag{1-10}$$

where:

coefficients $\boldsymbol{b_m}$ depend on $\boldsymbol{r}$ and on the dimensions of the bus-bar

$\boldsymbol{I^{bar}}$ is the current under measurement flowing in the bar

Let us now consider again a circular array centered on the bar and made of $N$ magnetic sensors, that are tangentially directed and distributed equally on the circumference, in positions $\theta_n=2\pi n/N$, where $n=1,\ldots,N-1$. The sensor output is given by

$$V_n = V(r=d, \theta=\theta_n) = V^{bar}(d,\theta_n) + V^{crosstalk}(d,\theta_n) = V_n^{bar} + V_n^{crosstalk} \tag{1-11}$$

The DFT transform $\tilde{V}_m^{bar}$ of $V_n^{bar}$ taking into account aliasing is given by

$$\tilde{V}_m^{bar} = S(b_m + b_{N+m} + b_{N-m} + b_{2N+m} + b_{2N-m}) \cdot I^{bar} \tag{1-12}$$

The DFT of the magnetic sensor signals due to crosstalk current is the same as (1-9). For the linearity of the DFT operator, the DFT $\tilde{V}_m$ of the sensor outputs $V_n = V_n^{bar} + V_n^{crosstalk}$ is given by the sum of $\tilde{V}_m^{bar}$ and $\tilde{V}_m^{crosstalk}$. Thus, in order to calculate $I^{bar}$ the nonlinear system of the two complex equations (12a) and (12b) in [20] must be inverted.

For the AC current measurement, let us consider a circular array of magnetic sensors and a current to be measured flowing in bus-bar placed at the center of the array [Fig.1-13].

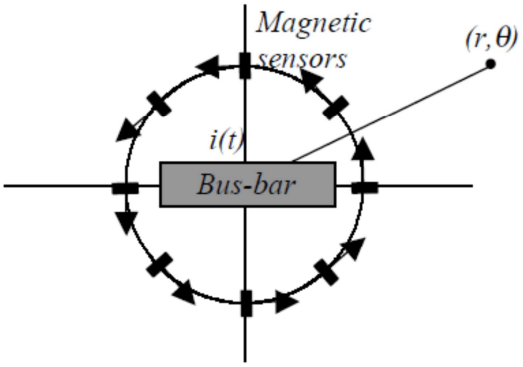


**Figure 1-13** A circular array of *N*=8 magnetic sensors and a bus-bar current under measurement. Arrows indicate the sensitivity direction of the sensors

The sum of magnetic sensors signals is proportional to a discretization of the Ampère's circulation and so realizes the measurement of the encircled current *i(t)*, being:

$$i(t) = \oint \vec{H} \cdot dl \tag{1-13}$$

$$\oint \vec{H} \cdot dl \cong d\frac{2\pi}{N}\sum_{n=1}^{N}\frac{v_n(t)}{S} \tag{1-14}$$

where:

- ***N*** is the number of sensors
- ***S*** is the sensitivity of the sensors (equal for all)
- ***d*** is the radius of the array
- ***$v_n(t)$*** is the output voltage of the $n^{th}$ sensor

In the case of an AC current, in many applications the crosstalk field is generated by a density current distribution that is symmetric with respect to the axis *θ=0*; the corresponding magnetic scalar potential of the crosstalk field can be expressed in M cylindrical harmonics [22]. Then the sum of the output signals of the crosstalk field can be defined as [23]

$$\frac{1}{N}\sum_{n=1}^{N} v_n^{crosstalk} \begin{cases} \cong -SNd^N b_n cosN\theta_0 & if\ N \le M \\ = 0 & otherwise \end{cases} \tag{1-15}$$

where:

$\boldsymbol{v_n}$ is the output voltage of the $n^{th}$ sensor of the crosstalk field

$\boldsymbol{b_n}$ is the coefficient of cylindrical harmonics

Eq. (1-15) says that rotating the array at values of $\boldsymbol{\theta_0}$ that are multiple of $\boldsymbol{\pi/2N}$ the contribution of the external field to measurement error becomes zero. This property can be usefully applied in many poly-phase systems. An example is shown in [Fig.1-14]. It is an application on a typical low-voltage protection circuit-breakers designed for rated current $I_n$=*3200 A*. Thanks to property (1-15) four sensors per-phase are enough for cross-talk error rejection rotating the arrays at $\boldsymbol{\theta_0=\pi/8}$.

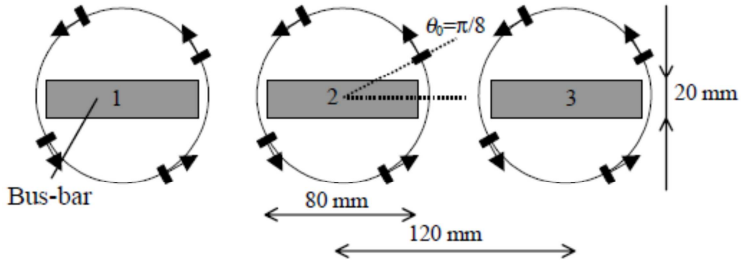


**Figure 1-14** Properly rotated four sensor arrays in a three-phase bus-bar system.

At last we review an AC current transducer for protective applications that consists of a magnetic sensor array. This new transducer proposed in [24-26] is designed for low-voltage power circuit breakers. The principle of measuring *P* periodic currents flowing in parallel conductors by processing *N* magnetic field data can be applied to a generic multi-conductor system. Once the $p^{th}$ current and the $n^{th}$ sensor voltage signal have been expanded in Fourier series, we can indicate with $\tilde{V}_{k,n}$ the phasor of the $k^{th}$ harmonic of the $n^{th}$ sensor voltage and similarly with $\tilde{I}_{k,p}$ the phasor $k^{th}$ harmonic of the $p^{th}$ current. Thanks to the linearity of the electromagnetic problem, it is possible to write the linear system

$$\begin{bmatrix} \tilde{V}_{k,1} \\ \vdots \\ \tilde{V}_{k,N} \end{bmatrix} = \begin{bmatrix} \tilde{c}_{k,11} & \cdots & \tilde{c}_{k,1P} \\ \vdots & \ddots & \vdots \\ \tilde{c}_{k,N1} & \cdots & \tilde{c}_{k,NP} \end{bmatrix} \cdot \begin{bmatrix} \tilde{I}_{k,1} \\ \vdots \\ \tilde{I}_{k,P} \end{bmatrix} \qquad (1\text{-}16)$$

$\tilde{V}_{k,n} = V_{k,n}e^{j\phi_{k,n}}$ , $\tilde{I}_{k,p=}I_{k,p}e^{j\phi_{k,p}}$ , $\tilde{V}_{k,n}$ , $\tilde{I}_{k,p}$ are all phasors. The trans-impedances $\tilde{c}_{k,np}$ are given by

$$\tilde{c}_{k,np} = \frac{\tilde{V}_{k,n}}{\tilde{I}_{k,p}}\Big|\tilde{I}_{k,q\neq p} = 0 \tag{1-17}$$

The trans-impedances can be estimated through numerical simulations on the FEM or the direct calibration. A Monte Carlo simulation shows that the procedure based on direct calibration guarantees a lower uncertainty than the one based on numerical analysis.

Accuracy specifications for protection current transformers are fulfilled not only at the nominal frequency, but also in the whole bandwidth. Preliminary experimental results are promising. The measurement model has been verified, and the experimental results are in accordance with numerical simulations.

## 1.4. Thesis Objective

IN THE PREVIOUS part, we briefly introduce the existing current sensing techniques and the recent development in the field of magnetic sensor arrays. But, let's go back to magnetic sensors. It is very clear that prior to any signal processing done by the algorithms aforementioned is sensing the magnetic field generated by the current under measurement. Therefore, it is of paramount importance an investigation of their performance. The most popular magnetic field sensors used in sensor arrays, are the Hall sensors, primarily due to their cost-effectiveness, and wide operating temperature range.

# 2

# Characterization of Hall sensors

## 2.1. Overview of the Tests

THIS CHAPTER discloses the experimental tests performed on Hall-effect sensors that were done entirely at Dipartimento di Elettrotecnica of Politecnico di Milano. The main purpose of this investigation was to verify the performance of each design both for linearity and temperature drift. The tests were designed to give a complete and very clear view of the real behavior of these magnetic sensors that can be used later in magnetic sensor arrays.

## 2.2. Metrological Characterization of Type 1 Sensors

THE MEASURING SYSTEM was made up of a DC current generator, magnetic sensors, a voltage generator, five digital multimeters, and a climatic chamber that was able to simulate a temperature from – 40 $^{o}$C up to 180 $^{o}$C. We dedicated a great deal of attention to ChenYang CYSJ362A [27] sensors, because of their low cost. They have a nominal hall voltage of 156~204 mV on B=100mT, an offset voltage of ±8 mV and a thermal drift of –0.06 %/$^{o}$C. CYSJ362A series Hall-effect element is a ion-implanted magnetic field sensor made of monocrystal gallium arsenide (GaAs) semiconductor material group III-V using ion-implanted technology.

A simple board was designed to drive the sensors with 1 mA, 1.5 mA, 2 mA, and 3 mA. The sensors were placed on the board with their magnetic sensitivity vectors alternated. The system was then placed in the temperature chamber alongside a copper bar connected to a current generator able to generate up to 500A DC. The sensors were touching the bar perpendicularly in order to have a signal high enough to be measured

with good accuracy, when the current was passing through the bar [Fig.2-1]. The first batch made up of four sensors was tested from ambient temperature (23 – 27 $^{o}$C) up to 100 $^{o}$C. This was done for 1 mA, 1.5 mA, 2 mA, and 3 mA. We took two measures for each temperature step:

a) The offset voltage (no current flowing on the bar)
b) The gain voltage (200A flowing on the bar)

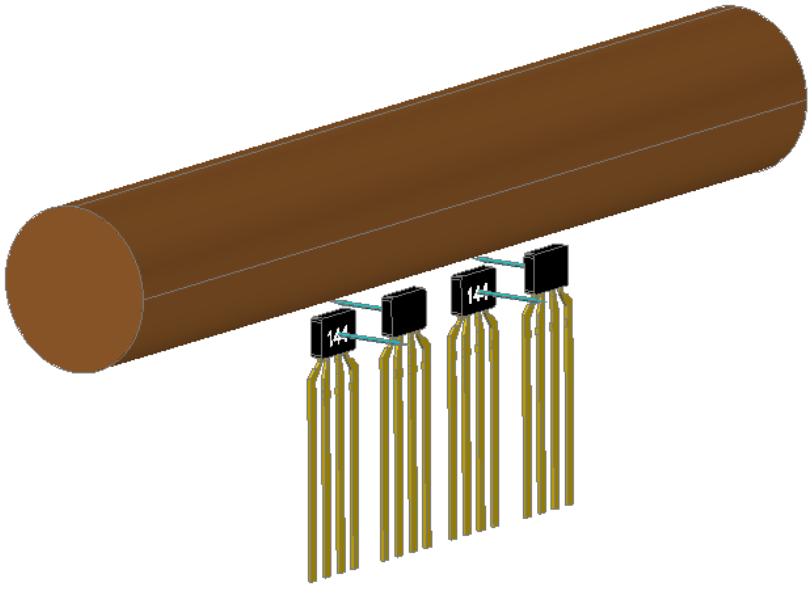

**Figure 2-1** Sensors' position for the case of CYSJ362A

We used different currents in order to determine which one led to the lowest relative error referred to the hall voltage measured at room temperature.

Then, we repeated exactly the same procedure with another batch of four sensors to verify the repeatability of the measurements. A side by side analyzes of the two batches is carried out at the end.

***Note1.*** *We couldn't simulate the –20 $^{o}$C point because the temperature chamber was unable to go under 20 $^{o}$C when we did the tests.*

***Note2.*** *200A was the max current supported by the conductors connecting the generator to the bar, because at 100 °C was impossible to go up to 500A due to insulation issues.*

***Note3.*** *We were unable to start from a fixed temperature every time due to stabilization problems of the temperature chamber around room temperature (23 – 27 °C), that as a matter of fact when these tests were done was always relatively high.*

***Note4.*** *We are going to refer to a group of sensors as the* ***first batch****, and the other group as the* ***second batch****.*

Below we report the measurements for 1 mA, 1.5 mA, and 2 mA for both batches.

i. *First batch + second batch 1mA*

**Tab. 2-1 (first batch 1mA)**

| Tsens [°C] | Isbarra [A] | Vs1 [mV] | Vs2 [mV] | Vs3 [mV] | Vs4 [mV] | Err_rel_ % Vs1-Vs2 | Err_rel_ %Vs3-Vs4 | Err_rel_ % Vs1 | Err_rel_ %Vs2 | Err_rel_ % Vs3 | Err_rel_ %Vs4 |
|---|---|---|---|---|---|---|---|---|---|---|---|
| 27,5 | 0 | -0,452 | -0,356 | -0,419 | -0,165 | | | | | | |
| 27,5 | 200 | 2,358 | -3,173 | 2,342 | -2,986 | | | | | | |
| 40 | 0 | -0,492 | -0,369 | -0,429 | -0,169 | | | | | | |
| 40 | 200 | 2,312 | -3,172 | 2,322 | -2,986 | -0,8497559 | -0,3753754 | -1,9508058 | -0,0315159 | -0,853971 | 0 |
| 60 | 0 | -0,516 | -0,373 | -0,457 | -0,175 | | | | | | |
| 60 | 200 | 2,269 | -3,161 | 2,279 | -2,961 | -1,8260712 | -1,6516517 | -3,7743851 | -0,378191 | -2,6900085 | -0,8372405 |
| 80 | 0 | -0,536 | -0,376 | -0,485 | -0,171 | | | | | | |
| 80 | 200 | 2,228 | -3,143 | 2,218 | -2,927 | -2,8927861 | -3,4346847 | -5,5131467 | -0,9454775 | -5,29462 | -1,9758875 |
| 100 | 0 | -0,559 | -0,357 | -0,514 | -0,155 | | | | | | |
| 100 | 200 | 2,188 | -3,099 | 2,156 | -2,855 | -4,4114988 | -5,9496997 | -7,2094996 | -2,3321777 | -7,94193 | -4,38714 |

Table 2-1 shows the offset voltage (***in black***), and the gain voltage (***in red***). Also the relative error in percentage referred to the hall voltage measured at room temperature is shown. It is interesting to see the relative error in percentage of the difference $V_{s1}$-$V_{s2}$ and $V_{s3}$-$V_{s4}$ referred to the same differences taken at room temperature**.** We recall that sensors 1-2 and 3-4 have been installed on the board with their sensitivity vectors alternated.

The same information is reported on [Table 2-2] for the second batch.

| Tab. 2-2 (second batch 1mA) | | | | | | | | | | | |
|---|---|---|---|---|---|---|---|---|---|---|---|
| Tsens [ºC] | Isbarra [A] | Vs1 [mV] | Vs2 [mV] | Vs3 [mV] | Vs4 [mV] | Err_rel_ % Vs1-Vs2 | Err_rel_ %Vs3-Vs4 | Err_rel_ % Vs1 | Err_rel_ %Vs2 | Err_rel_ % Vs3 | Err_rel_ %Vs4 |
| 26.5 | 0 | -0.296 | -0.545 | 0.087 | 0.106 | | | | | | |
| 26.5 | 200 | 2.479 | -3.295 | 2.794 | -2.695 | | | | | | |
| 40 | 0 | -0.303 | -0.573 | 0.069 | 0.098 | | | | | | |
| 40 | 200 | 2.454 | -3.307 | 2.762 | -2.693 | -0.2251472 | -0.6194207 | -1.0084712 | 0.3641882 | -1.1453114 | -0.0742115 |
| 60 | 0 | -0.317 | -0.622 | 0.038 | 0.073 | | | | | | |
| 60 | 200 | 2.409 | -3.334 | 2.694 | -2.694 | -0.5368895 | -1.8400437 | -2.8237192 | 1.1836115 | -3.5790981 | -0.0371058 |
| 80 | 0 | -0.335 | -0.675 | 0.003 | 0.059 | | | | | | |
| 80 | 200 | 2.369 | -3.373 | 2.635 | -2.691 | -0.5542085 | -2.9695755 | -4.4372731 | 2.3672231 | -5.6907659 | -0.148423 |
| 100 | 0 | -0.355 | -0.706 | -0.016 | 0.053 | | | | | | |
| 100 | 200 | 2.323 | -3.378 | 2.593 | -2.676 | -1.2642882 | -4.008016 | -6.29286 | 2.5189681 | -7.1939871 | -0.7050093 |

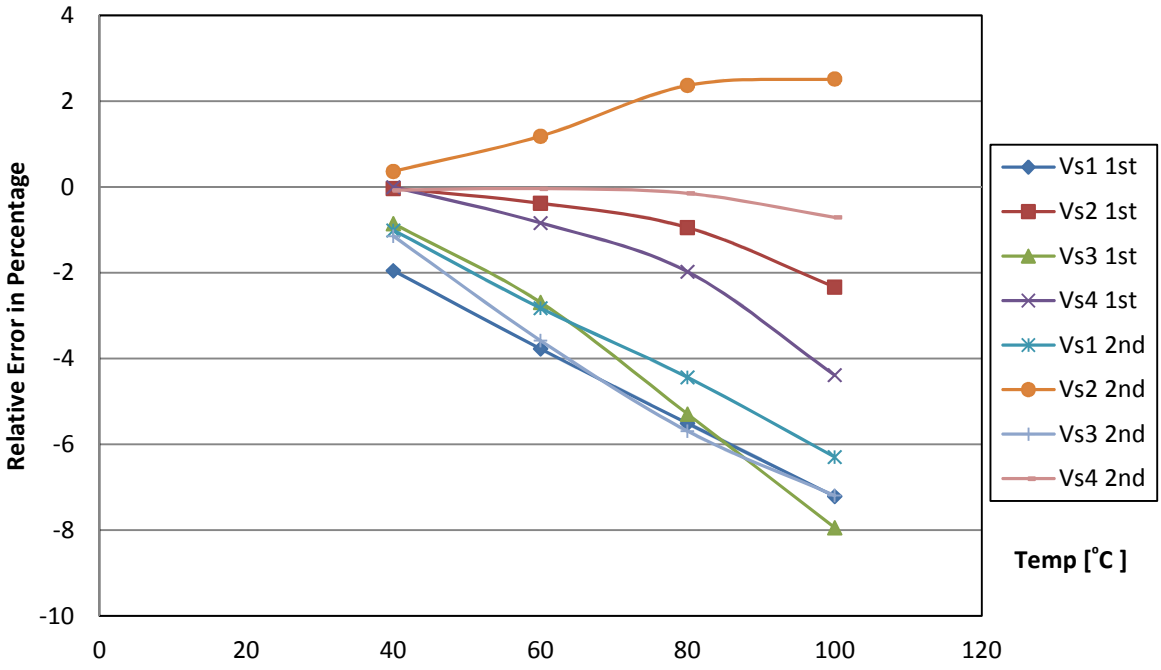


**Figure 2-2** Relative error in % of the gain voltage referred to room temperature

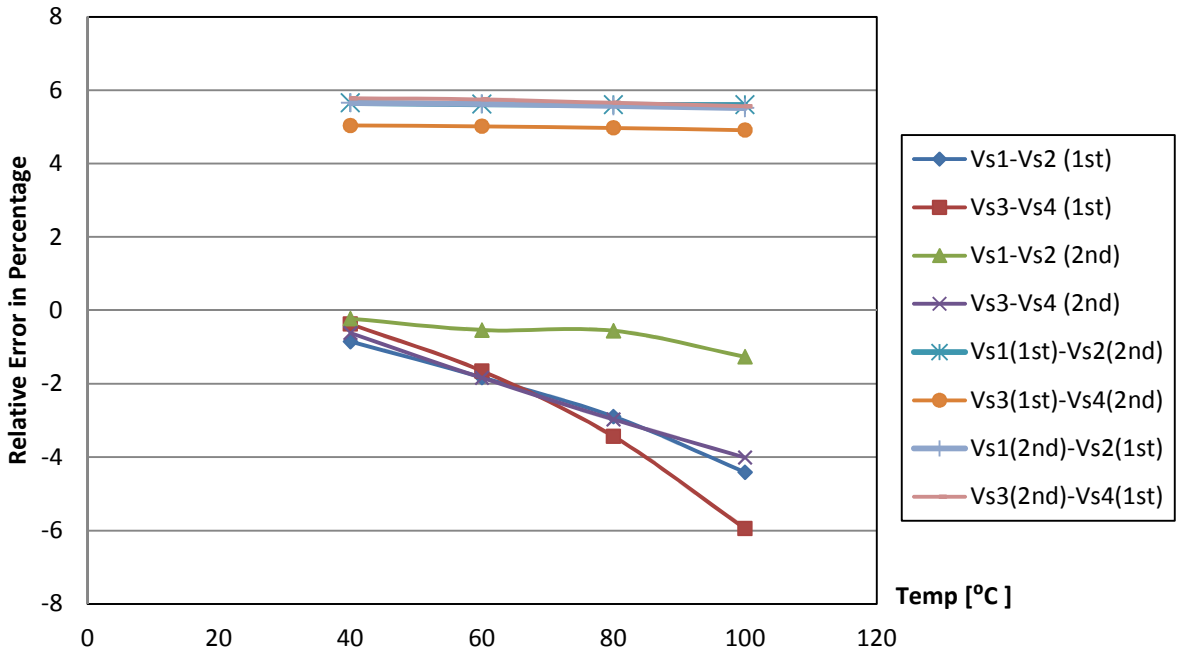


**Figure 2-3** Relative error in % of the voltage differences and the combined voltage differences

On [Fig. 2-2] is plotted the relative error in percentage for the eight sensors tested on 1mA. It shows only the case of the gain voltage. It can be easily noted that in both batches, sensors #1 and #3 have the maximum error of up to 5.3% and 7.1% respectively.

From [Fig. 2-3] can be noted that the second batch has a lower relative error with respect to the first batch, particularly $V_{s1}$-$V_{s2}(2^{nd})$. On the other hand all the combined differences have a relative error that is below 0.5% in all cases. This is very interesting because the tests for the two batches were done in different days.

### *ii. First batch + second batch 1.5mA*

We repeated the same tests for both batches, but now the sensors are fed 1.5mA. Again we report the results on the tables below.

**Tab. 2-3 (first batch 1.5 mA)**

| Tsens [ºC] | Isbarra [A] | Vs1 [mV] | Vs2 [mV] | Vs3 [mV] | Vs4 [mV] | Err_rel_ % Vs1-Vs2 | Err_rel_ %Vs3-Vs4 | Err_rel_ % Vs1 | Err_rel_ %Vs2 | Err_rel_ % Vs3 | Err_rel_ %Vs4 |
|---|---|---|---|---|---|---|---|---|---|---|---|
| 27.1 | 0 | -0.701 | -0.453 | -0.649 | -0.129 | | | | | | |
| 27.1 | 200 | 3.337 | -4.687 | 3.389 | -4.386 | | | | | | |
| 40 | 0 | -0.735 | -0.463 | -0.678 | -0.157 | | | | | | |
| 40 | 200 | 3.272 | -4.677 | 3.325 | -4.375 | -0.8497559 | -0.3753754 | -1.9478574 | -0.2133561 | -1.8884627 | -0.250798 |
| 60 | 0 | -0.781 | -0.489 | -0.709 | -0.179 | | | | | | |
| 60 | 200 | 3.188 | -4.671 | 3.254 | -4.363 | -1.8260712 | -1.6516517 | -4.4650884 | -0.3413697 | -3.983476 | -0.5243958 |
| 80 | 0 | -0.824 | -0.508 | -0.754 | -0.188 | | | | | | |
| 80 | 200 | 3.105 | -4.662 | 3.198 | -4.346 | -2.8927861 | -3.4346847 | -6.9523524 | -0.5333902 | -5.6358808 | -0.9119927 |
| 100 | 0 | -0.866 | -0.527 | -0.791 | -0.199 | | | | | | |
| 100 | 200 | 3.092 | -4.645 | 3.156 | -4.325 | -4.4114988 | -5.9496997 | -7.3419239 | -0.8960956 | -6.8751844 | -1.3907889 |

**Tab. 2-4 (second batch 1.5 mA)**

| Tsens [ºC] | Isbarra [A] | Vs1 [mV] | Vs2 [mV] | Vs3 [mV] | Vs4 [mV] | Err_rel_ % Vs1-Vs2 | Err_rel_ %Vs3-Vs4 | Err_rel_ % Vs1 | Err_rel_ %Vs2 | Err_rel_ % Vs3 | Err_rel_ %Vs4 |
|---|---|---|---|---|---|---|---|---|---|---|---|
| 24 | 0 | -0.456 | -0.814 | 0.128 | 0.066 | | | | | | |
| 24 | 200 | 3.695 | -5.002 | 4.284 | -4.082 | | | | | | |
| 40 | 0 | -0.477 | -0.878 | 0.082 | 0.035 | | | | | | |
| 40 | 200 | 3.645 | -5.035 | 4.209 | -4.081 | -0.1954697 | -0.9084389 | -1.35318 | 0.6597361 | -1.7507003 | -0.0244978 |
| 60 | 0 | -0.505 | -0.894 | -0.032 | -0.006 | | | | | | |
| 60 | 200 | 3.591 | -5.069 | 4.112 | -4.078 | -0.4254341 | -2.1037533 | -2.8146143 | 1.3394642 | -4.0149393 | -0.0979912 |
| 80 | 0 | -0.537 | -1.011 | -0.025 | -0.012 | | | | | | |
| 80 | 200 | 3.546 | -5.106 | 3.995 | -4.027 | -0.5174198 | -4.1118814 | -4.0324763 | 2.0791683 | -6.7460317 | -1.3473787 |
| 100 | 0 | -0.581 | -1.068 | -0.036 | -0.01 | | | | | | |
| 100 | 200 | 3.454 | -5.122 | 3.953 | -3.983 | -1.3912844 | -5.1398518 | -6.5223275 | 2.3990404 | -7.7264239 | -2.4252817 |

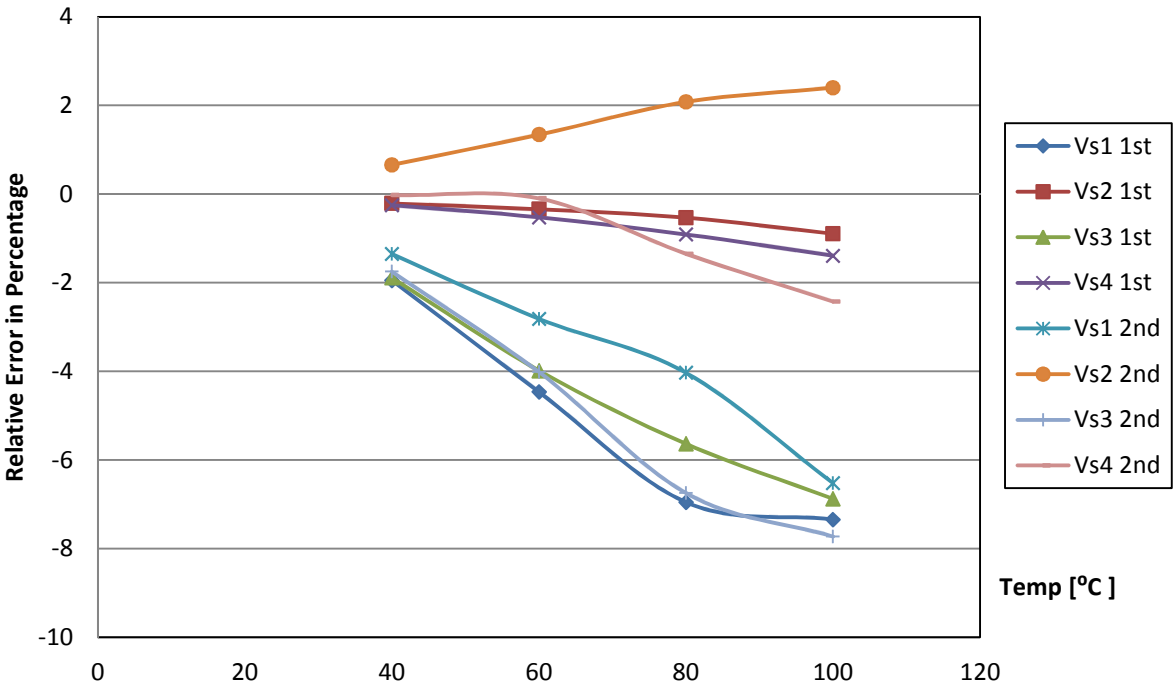


**Figure 2-4** Relative error in % of the gain voltage referred to room temperature

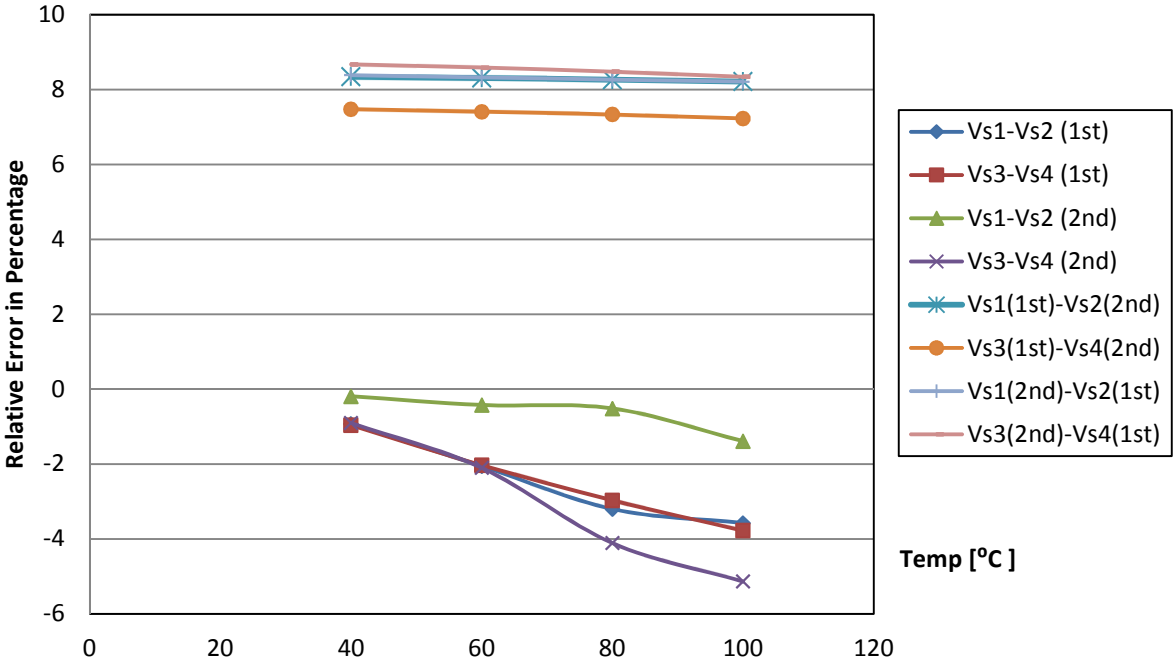


**Figure 2-5** Relative error in % of the voltage differences and the combined voltage differences

Same as before, on [Fig. 2-4] we see the relative error in percentage for the eight sensors tested on 1.5 mA, and only the case of the gain voltage is

shown again. It can be noted that, sensor #1 and #3 of both batches have the maximum error of up to 5.4% and 5.9% respectively.

From [Fig. 2-5] we see the same trend as the first case of 1 mA, with $V_{s1}$-$V_{s2}$(2nd) being the lowest error. Again the combined differences have a relative error that is below 0.5% in all case.

*iii.* *First batch + second batch 2mA*

At last we repeated the tests for the case of 2mA while using again the same sensors.

**Tab. 2-5 (first batch 2 mA)**

| Tsens [ºC] | Isbarra [A] | Vs1 [mV] | Vs2 [mV] | Vs3 [mV] | Vs4 [mV] | Err_rel_% Vs1-Vs2 | Err_rel_%Vs3-Vs4 | Err_rel_% Vs1 | Err_rel_%Vs2 | Err_rel_% Vs3 | Err_rel_%Vs4 |
|---|---|---|---|---|---|---|---|---|---|---|---|
| 24.5 | 0 | -0.916 | -0.625 | -0.782 | -0.252 | | | | | | |
| 24.5 | 200 | 4.674 | -6.112 | 4.735 | -5.898 | | | | | | |
| 40 | 0 | -0.967 | -0.648 | -0.836 | -0.256 | | | | | | |
| 40 | 200 | 4.421 | -6.221 | 4.558 | -5.885 | -1.335064 | -1.7868899 | -5.4129226 | 1.783377 | -3.7381204 | -0.2204137 |
| 60 | 0 | -1.033 | -0.678 | -0.901 | -0.271 | | | | | | |
| 60 | 200 | 4.322 | -6.211 | 4.461 | -5.861 | -2.3456332 | -2.9248566 | -7.5310227 | 1.6197644 | -5.7866948 | -0.6273313 |
| 80 | 0 | -1.085 | -0.706 | -0.973 | -0.291 | | | | | | |
| 80 | 200 | 4.241 | -6.204 | 4.366 | -5.837 | -3.1615057 | -4.0440139 | -9.2640137 | 1.5052356 | -7.7930306 | -1.0342489 |
| 100 | 0 | -1.135 | -0.732 | -1.033 | -0.295 | | | | | | |
| 100 | 200 | 4.131 | -6.194 | 4.289 | -5.802 | -4.274059 | -5.0973385 | -11.617458 | 1.341623 | -9.4192186 | -1.6276704 |

**Tab. 2-6 (second batch 2 mA)**

| Tsens [ºC] | Isbarra [A] | Vs1 [mV] | Vs2 [mV] | Vs3 [mV] | Vs4 [mV] | Err_rel_% Vs1-Vs2 | Err_rel_%Vs3-Vs4 | Err_rel_% Vs1 | Err_rel_%Vs2 | Err_rel_% Vs3 | Err_rel_%Vs4 |
|---|---|---|---|---|---|---|---|---|---|---|---|
| 24.5 | 0 | -0.642 | -1.078 | 0.165 | 0.238 | | | | | | |
| 24.5 | 200 | 4.843 | -6.545 | 5.769 | -5.387 | | | | | | |
| 40 | 0 | -0.667 | -1.145 | 0.106 | 0.218 | | | | | | |
| 40 | 200 | 4.774 | -6.587 | 5.677 | -5.388 | -0.2370917 | -0.8157046 | -1.4247367 | 0.6417112 | -1.5947305 | 0.0185632 |
| 60 | 0 | -0.696 | -1.223 | 0.062 | 0.163 | | | | | | |
| 60 | 200 | 4.721 | -6.621 | 5.607 | -5.394 | -0.403934 | -1.3893869 | -2.5190997 | 1.1611917 | -2.8081123 | 0.1299425 |
| 80 | 0 | -0.734 | -1.331 | 0.013 | 0.132 | | | | | | |
| 80 | 200 | 4.637 | -6.685 | 5.505 | -5.382 | -0.5795574 | -2.4112585 | -4.2535618 | 2.1390374 | -4.576183 | -0.092816 |
| 100 | 0 | -0.786 | -1.392 | -0.016 | 0.109 | | | | | | |
| 100 | 200 | 4.582 | -6.683 | 5.409 | -5.364 | -1.0800843 | -3.4331302 | -5.3892216 | 2.1084798 | -6.2402496 | -0.4269538 |

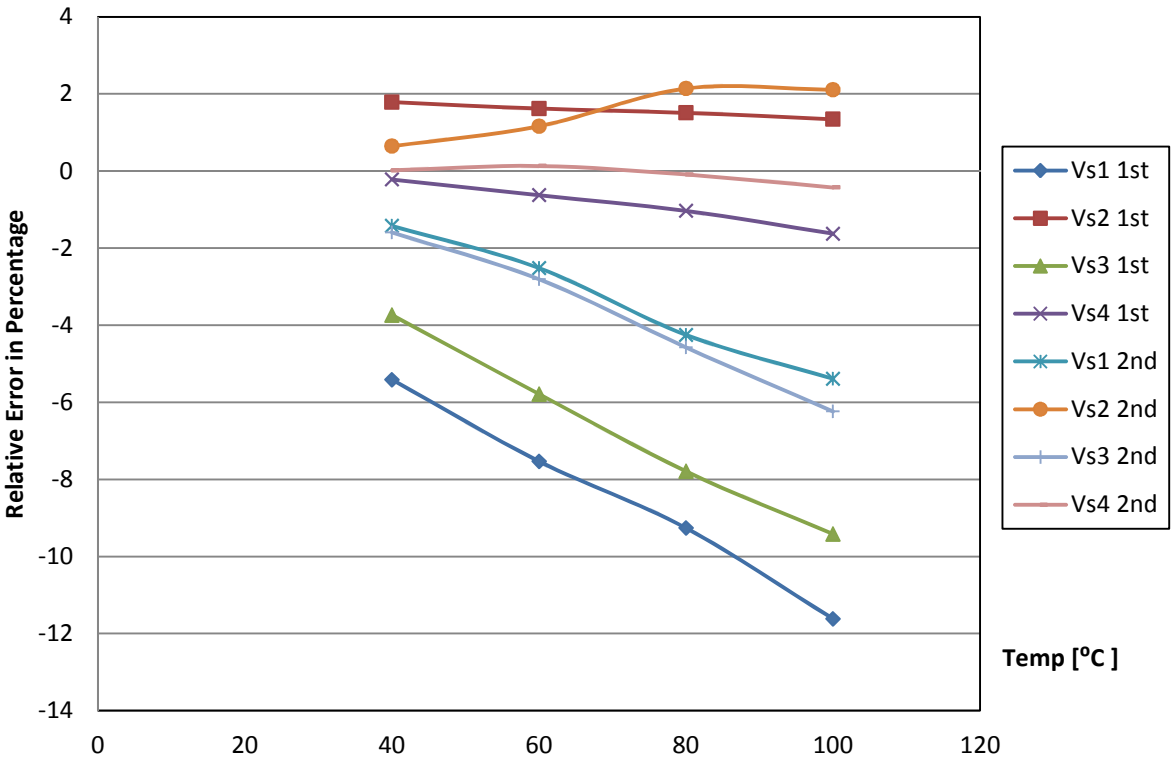


**Figure 2-6** Relative error in % of the gain voltage referred to room temperature

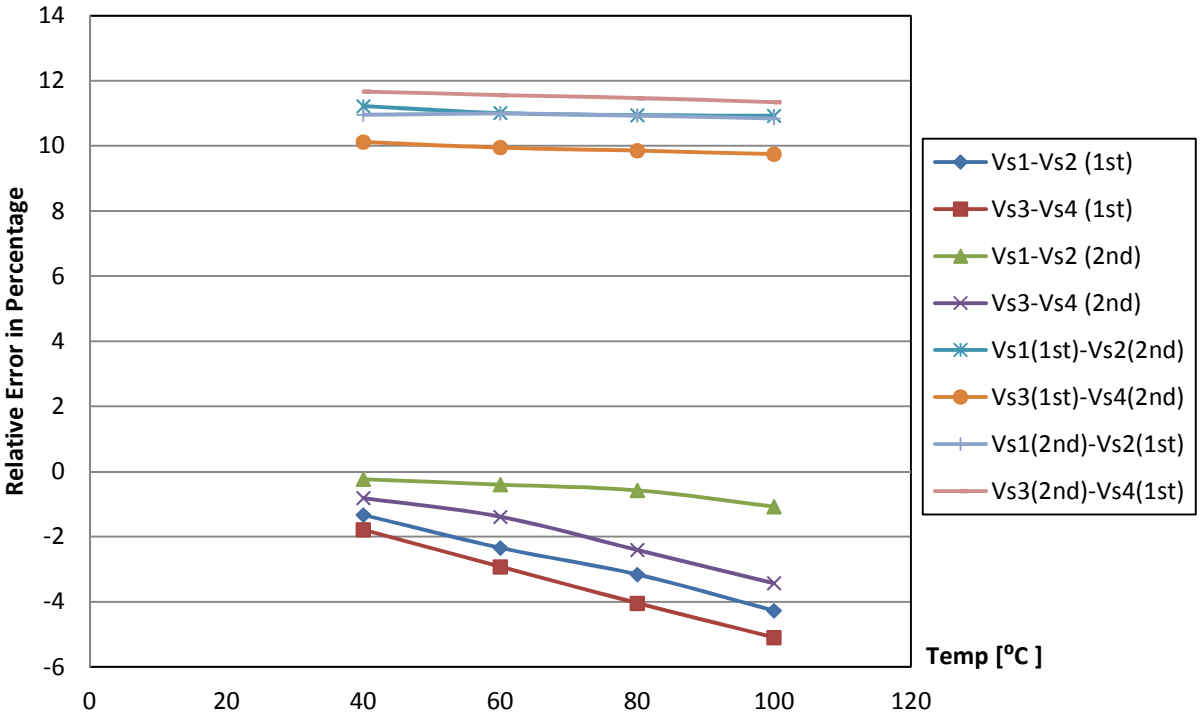


**Figure 2-7** Relative error in % of the voltage differences and the combined voltage differences

Just like the other two cases, on [Fig. 2-6] is plotted the relative error in percentage for the eight sensors tested on 2 mA, and only the case of the gain voltage is shown again. The trend is quite obvious; sensors #1 and #3 of both batches have again the maximum error that respectively goes up to 6.2% and 5.7%.

Again [Fig. 2-7] shows that $V_{s1}$-$V_{s2}$(2nd) has the lowest error, and it is the lowest among the three cases analyzed in this section. At 2 mA the combined differences remained under 0.5%.

### 2.2.1. Summary and Conclusions

THE SENSORS analyzed in this section were the most economical ones and claimed good performance in a wide range of operating temperature. While half the sensors had a somewhat acceptable performance, the other half had an error that went up to 7%. We also did test these sensors with 3 mA and 5mA. Moreover, even though the latter corresponds to the one on the datasheet, the error went far beyond 10%, making this recommended driving current totally useless for good performance of the sensors. We also drove the sensors with 6 VDC (again the set point used by the manufacturer) and the error went up to 9%.

We can conclude that sensor #2 and sensor #4 from both batches performed the better, while sensor #1 and #3 had a greater relative error referred to the voltage taken at room temperature. In all the cases, the difference $V_{s1}$-$V_{s2}$ (2nd) produced the smaller error with respect to the other differences. Another observation is that the combined differences had an error that was under 0.5% in all the cases analyzed.

From this section we can conclude that 2 mA is the upper limit driving current, in order to have the best performance of these sensors, but looking at the overall experimental results it is safe to say that they don't meet the specifications required for applications such as magnetic sensor arrays working as current transducers.

## 2.3. Changes in the Experimental Setup

WE CONTINUED the experimental activity with a different experimental setup [Fig.2-8], and four other types of sensors from three different manufacturers. All these tests were done at room temperature and the current flowing through the bar varied from 50 A up to 2500 A. So in this case we were not testing their thermal drift. The arrangement of the sensors changed too. Now they were on a circumference around the copper bar that was now fixed at much better support because we were out of the climatic chamber, and more room was available to mount the bar. Of course another PCB was designed to mount the sensors in such configuration. Two types of sensors have been fed with a constant 5 VDC, and the other two types with a 1mA current according to their datasheets.

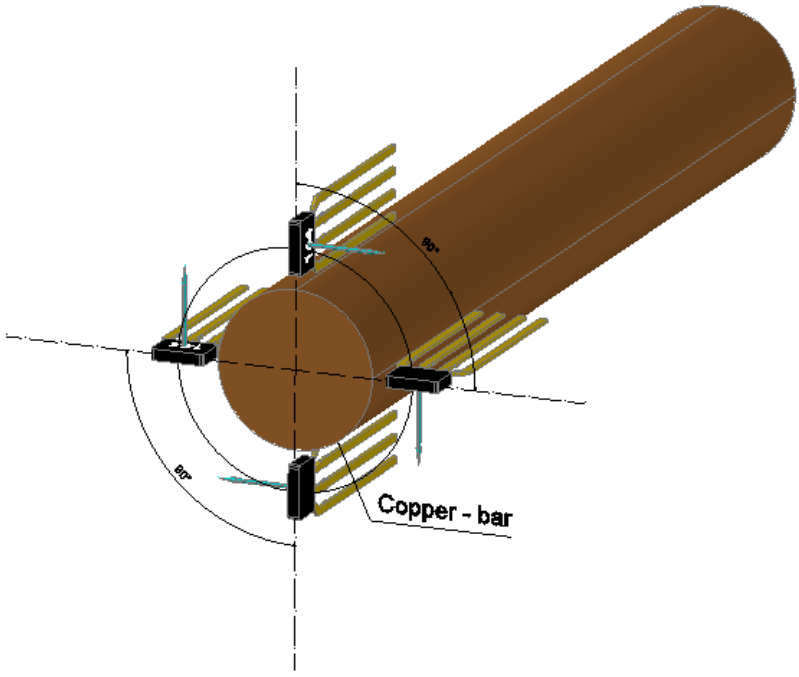


**Figure 2-8** Four Hall sensors forming a circular array

The followings explain in more detail the experimental activity along with the results that we obtained from it. The order in which we lay out the results does not correspond to the order in which we tested the sensors. All the measurements were done using a bar with a diameter of 9 mm, sensor distance 8.89 mm.

## 2.4. Metrological Characterization of Type 2 Sensors

THIS SECTION shows the measurement results for the Asahi-Kasei's HG-362A GaAs Hall elements [28]. They have a nominal hall voltage of 78~102 mV on B=50mT, an offset voltage of ±8 mV when driven with 6 VDC and a maximum thermal drift of –0.06 %/°C when driven with 1mA under a temperature range 25~125°C. The packaging of these sensors is identical to the CYSJ362A sensors that we tested earlier. The measurement setup, as we anticipated above, was changed with respect to the case of the CYSJ362A sensors. The copper bar was fed using a DC generator that was able to go up to 2500A in the first test, and then with a more precise DC current generator able to go up to 500A. We switched the DC current generator to the more precise one; because we noticed that the first generator was not very stable.

Below we show the results first for the case when the less precise DC current generator is used, and then the case when the more precise DC current generator is used, with their respective graphs. In these tests we used the same sensors for both cases. The sensors are driven with a current equal to 1mA and the max allowed induction is 300mT per sensor.

*i. Case #1 – current from 100A to 2500A*

Below we show the measurement results for one sensor at a time along with the linearity and error calculations.

**Tab. 2-9**

| Linearity and errors for sensor #1 | | | | | |
|---|---|---|---|---|---|
| I [A] | $Vs_1$ [mV] | Ieq. Regr. [A] | E%punt. Regr. | Ieq. EndP [A] | E%punt. EndP. |
| 100 | 0.7993 | 96.5983373 | -3.401662699 | 100 | 0 |
| 200 | 1.5062 | 186.1234317 | -6.938284173 | 189.2348637 | -5.382568127 |
| 300 | 2.4354 | 303.801629 | 1.267209652 | 306.5315611 | 2.177187049 |
| 400 | 3.2233 | 403.584939 | 0.89623474 | 405.9913845 | 1.497846131 |
| 500 | 4.0091 | 503.1022952 | 0.620459044 | 505.1861164 | 1.037223271 |
| 600 | 4.7987 | 603.1009011 | 0.516816852 | 604.8605377 | 0.810089609 |
| 700 | 5.5867 | 702.8968756 | 0.413839368 | 704.3329844 | 0.618997777 |
| 800 | 6.3833 | 803.7819939 | 0.472749241 | 804.8910442 | 0.611380527 |
| 900 | 7.1633 | 902.5648113 | 0.284979032 | 903.3536184 | 0.372624272 |

| Linearity and errors for sensor #1 | | | | | |
|---|---|---|---|---|---|
| I [A] | $Vs_1$ [mV] | Ieq. Regr. [A] | E%punt. Regr. | Ieq. EndP [A] | E%punt. EndP. |
| 1000 | 7.9457 | 1001.651576 | 0.165157579 | 1002.119154 | 0.211915444 |
| 1100 | 8.7318 | 1101.206925 | 0.109720495 | 1101.351756 | 0.122886954 |
| 1200 | 9.5183 | 1200.812933 | 0.067744413 | 1200.634852 | 0.052904348 |
| 1300 | 10.3024 | 1300.114993 | 0.008845641 | 1299.614986 | -0.029616455 |
| 1400 | 11.0844 | 1399.1511 | -0.060635716 | 1398.330028 | -0.119283682 |
| 1500 | 11.8746 | 1499.225693 | -0.051620491 | 1498.08019 | -0.12798732 |
| 1600 | 12.664 | 1599.19897 | -0.0500644 | 1597.729365 | -0.141914708 |
| 1700 | 13.4475 | 1698.425043 | -0.092644518 | 1696.633758 | -0.198014227 |
| 1800 | 14.2359 | 1798.271676 | -0.096018027 | 1796.156699 | -0.213516747 |
| 1900 | 15.0188 | 1897.421762 | -0.135696719 | 1894.985352 | -0.263928864 |
| 2000 | 15.8092 | 1997.521684 | -0.123915804 | 1994.76076 | -0.261961993 |
| 2100 | 16.6065 | 2098.495454 | -0.07164507 | 2095.407184 | -0.218705535 |
| 2200 | 17.3986 | 2198.810671 | -0.054060409 | 2195.39719 | -0.209218625 |
| 2300 | 18.1961 | 2299.80977 | -0.00827089 | 2296.068861 | -0.170919101 |
| 2400 | 18.9866 | 2399.922356 | -0.003235184 | 2395.856893 | -0.172629473 |
| 2500 | 19.8116 | 2504.404182 | 0.176167266 | 2500 | 0 |

**Tab. 2-10**

| Linearity and errors for sensor #2 | | | | | |
|---|---|---|---|---|---|
| I [A] | $Vs_2$ [mV] | Ieq. Regr. [A] | E%punt. Regr. | Ieq. EndP [A] | E%punt. EndP. |
| 100 | 0.9504 | 97.18245419 | -2.817545814 | 100 | 0 |
| 200 | 1.7782 | 185.7322054 | -7.133897305 | 188.3398919 | -5.830054025 |
| 300 | 2.8796 | 303.5489437 | 1.182981234 | 305.8774095 | 1.959136486 |
| 400 | 3.8105 | 403.1273001 | 0.781825016 | 405.2197692 | 1.304942306 |
| 500 | 4.7434 | 502.9195964 | 0.583919278 | 504.7755619 | 0.955112386 |
| 600 | 5.6799 | 603.0969846 | 0.516164108 | 604.7155339 | 0.785922319 |
| 700 | 6.6144 | 703.0604329 | 0.437204707 | 704.442073 | 0.634581852 |
| 800 | 7.5468 | 802.7992443 | 0.349905535 | 803.9445074 | 0.49306343 |
| 900 | 8.4775 | 902.3562066 | 0.261800738 | 903.2655239 | 0.36283599 |
| 1000 | 9.4048 | 1001.549471 | 0.154947107 | 1002.223704 | 0.22237044 |
| 1100 | 10.3416 | 1101.75895 | 0.159904575 | 1102.195691 | 0.199608302 |
| 1200 | 11.2696 | 1201.027094 | 0.085591145 | 1201.228573 | 0.102381111 |
| 1300 | 12.1926 | 1299.760387 | -0.018431751 | 1299.727873 | -0.020932846 |
| 1400 | 13.1273 | 1399.74523 | -0.018197891 | 1399.475755 | -0.037446046 |
| 1500 | 14.0637 | 1499.911921 | -0.005871947 | 1499.405056 | -0.039662954 |
| 1600 | 14.9943 | 1599.458186 | -0.033863365 | 1598.715401 | -0.080287467 |
| 1700 | 15.9234 | 1698.843997 | -0.068000203 | 1697.865671 | -0.125548786 |
| 1800 | 16.8574 | 1798.75396 | -0.069224452 | 1797.538851 | -0.136730474 |
| 1900 | 17.782 | 1897.658405 | -0.123241825 | 1896.208897 | -0.199531711 |
| 2000 | 18.7217 | 1998.178098 | -0.091095123 | 1996.490362 | -0.175481892 |
| 2100 | 19.663 | 2098.868942 | -0.053859918 | 2096.942573 | -0.145591752 |

| Linearity and errors for sensor #2 | | | | | |
|---|---|---|---|---|---|
| I [A] | $Vs_2$ [mV] | Ieq. Regr. [A] | E%punt. Regr. | Ieq. EndP [A] | E%punt. EndP. |
| 2200 | 20.5921 | 2198.254752 | -0.07932945 | 2196.092843 | -0.177598031 |
| 2300 | 21.5346 | 2299.07396 | -0.040262597 | 2296.673114 | -0.144647212 |
| 2400 | 22.4823 | 2400.449412 | 0.018725513 | 2397.808311 | -0.091320394 |
| 2500 | 23.4399 | 2502.883867 | 0.115354688 | 2500 | 0 |

**Tab. 2-11**

| Linearity and errors for sensor #3 | | | | | |
|---|---|---|---|---|---|
| I [A] | $Vs_3$ [mV] | Ieq. Regr. [A] | E%punt. Regr. | Ieq. EndP [A] | E%punt. EndP. |
| 100 | 0.9913 | 96.56076353 | -3.439236472 | 100 | -1.42109E-14 |
| 200 | 1.8563 | 184.8119757 | -7.594012139 | 188.0425794 | -5.97871032 |
| 300 | 3.0123 | 302.752324 | 0.917441348 | 305.7041074 | 1.901369127 |
| 400 | 3.9911 | 402.6139269 | 0.653481732 | 405.3296296 | 1.332407388 |
| 500 | 4.979 | 503.403953 | 0.680790594 | 505.88138 | 1.176276002 |
| 600 | 5.961 | 603.5920343 | 0.598672388 | 605.8326088 | 0.972101472 |
| 700 | 6.9409 | 703.5658642 | 0.50940917 | 705.5700927 | 0.795727524 |
| 800 | 7.9166 | 803.1111911 | 0.388898882 | 804.8800865 | 0.610010814 |
| 900 | 8.8934 | 902.7687449 | 0.307638322 | 904.302042 | 0.47800467 |
| 1000 | 9.8662 | 1002.018201 | 0.201820064 | 1003.316864 | 0.331686423 |
| 1100 | 10.8433 | 1101.706362 | 0.155123804 | 1102.769355 | 0.251759521 |
| 1200 | 11.8207 | 1201.42513 | 0.118760866 | 1202.25238 | 0.187698354 |
| 1300 | 12.7859 | 1299.8992 | -0.007753864 | 1300.493649 | 0.037973011 |
| 1400 | 13.7667 | 1399.964852 | -0.002510593 | 1400.322738 | 0.023052712 |
| 1500 | 14.7453 | 1499.80605 | -0.012930021 | 1499.927903 | -0.004806435 |
| 1600 | 15.7274 | 1600.004333 | 0.000270843 | 1599.889311 | -0.006918086 |
| 1700 | 16.7002 | 1699.253789 | -0.04389475 | 1698.904133 | -0.064462775 |
| 1800 | 17.6765 | 1798.860331 | -0.063314954 | 1798.275197 | -0.095822407 |
| 1900 | 18.6516 | 1898.344443 | -0.08713458 | 1897.524121 | -0.130309446 |
| 2000 | 19.6285 | 1998.012199 | -0.099390037 | 1996.956254 | -0.152187281 |
| 2100 | 20.6147 | 2098.628784 | -0.065296018 | 2097.334973 | -0.126906039 |
| 2200 | 21.593 | 2198.439374 | -0.070937534 | 2196.909604 | -0.14047256 |
| 2300 | 22.5758 | 2298.709075 | -0.056127164 | 2296.942259 | -0.132945254 |
| 2400 | 23.5637 | 2399.499101 | -0.020870781 | 2397.49401 | -0.104416266 |
| 2500 | 24.5708 | 2502.247998 | 0.089919926 | 2500 | -1.81899E-14 |

**Tab. 2-12**

| Linearity and errors for sensor #4 | | | | | |
|---|---|---|---|---|---|
| I [A] | $Vs_4$ [mV] | Ieq. Regr. [A] | E%punt. Regr. | Ieq. EndP [A] | E%punt. EndP. |
| 100 | 0.8169 | 95.27437998 | -4.725620023 | 100 | 0 |
| 200 | 1.5452 | 185.3816653 | -7.309167366 | 189.7861061 | -5.106946927 |
| 300 | 2.4943 | 302.8069357 | 0.93564524 | 306.792825 | 2.264275001 |
| 400 | 3.2976 | 402.1934279 | 0.548356981 | 405.8250632 | 1.456265795 |
| 500 | 4.1133 | 503.1140823 | 0.622816468 | 506.3859952 | 1.277199038 |
| 600 | 4.9157 | 602.3892241 | 0.398204011 | 605.3072798 | 0.884546631 |
| 700 | 5.7257 | 702.6046588 | 0.372094108 | 705.1655058 | 0.737929395 |
| 800 | 6.5512 | 804.7377962 | 0.592224526 | 806.934599 | 0.866824878 |
| 900 | 7.3604 | 904.8542527 | 0.539361411 | 906.6941996 | 0.743799955 |
| 1000 | 8.1588 | 1003.634503 | 0.363450338 | 1005.122357 | 0.512235715 |
| 1100 | 8.9505 | 1101.585812 | 0.14416469 | 1102.724527 | 0.247684264 |
| 1200 | 9.76 | 1201.739385 | 0.144948742 | 1202.521112 | 0.210092667 |
| 1300 | 10.5562 | 1300.247446 | 0.019034271 | 1300.67805 | 0.052157668 |
| 1400 | 11.3715 | 1401.118611 | 0.079900774 | 1401.189669 | 0.084976356 |
| 1500 | 12.166 | 1499.416343 | -0.038910483 | 1499.137028 | -0.057531488 |
| 1600 | 12.9789 | 1599.990573 | -0.000589159 | 1599.352771 | -0.040451828 |
| 1700 | 13.7781 | 1698.869802 | -0.066482215 | 1697.879554 | -0.124732134 |
| 1800 | 14.5771 | 1797.724287 | -0.126428517 | 1796.38168 | -0.201017759 |
| 1900 | 15.3798 | 1897.036545 | -0.155971303 | 1895.339949 | -0.245265818 |
| 2000 | 16.1836 | 1996.484899 | -0.175755059 | 1994.433829 | -0.278308574 |
| 2100 | 17.002 | 2097.739605 | -0.107637872 | 2095.327621 | -0.222494225 |
| 2200 | 17.8183 | 2198.734493 | -0.057523056 | 2195.962522 | -0.183521712 |
| 2300 | 18.6283 | 2298.949927 | -0.045655328 | 2295.820748 | -0.181706595 |
| 2400 | 19.4411 | 2399.511786 | -0.020342255 | 2396.024163 | -0.165659866 |
| 2500 | 20.2845 | 2503.859561 | 0.154382428 | 2500 | 0 |

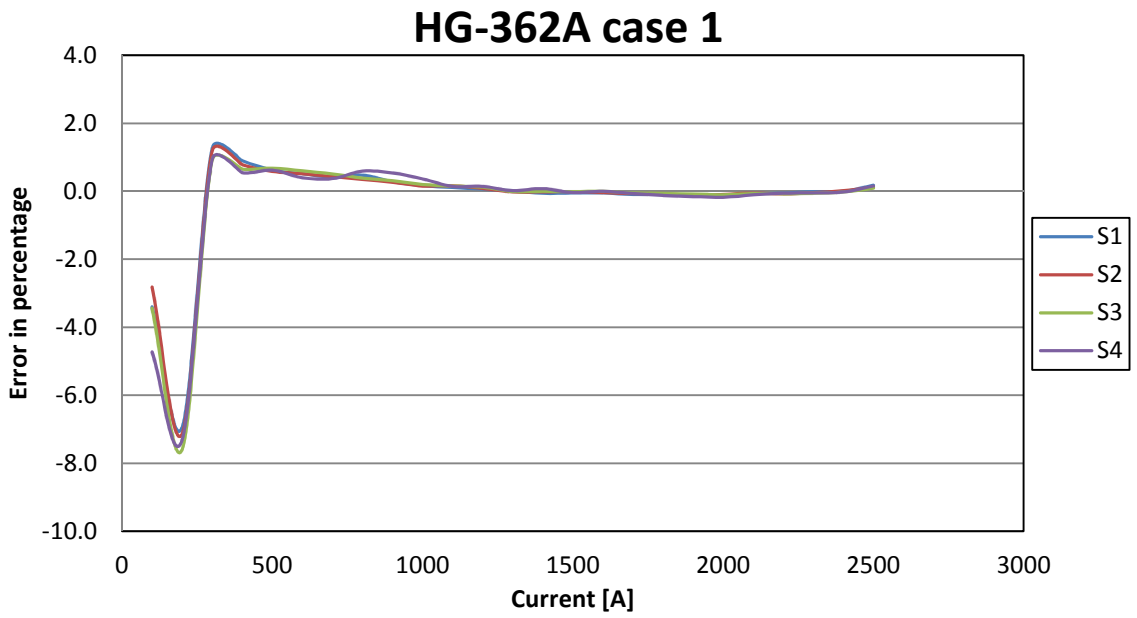


**Figure 2-9** Error in percentage referred to regression line (HG-362A sensors)

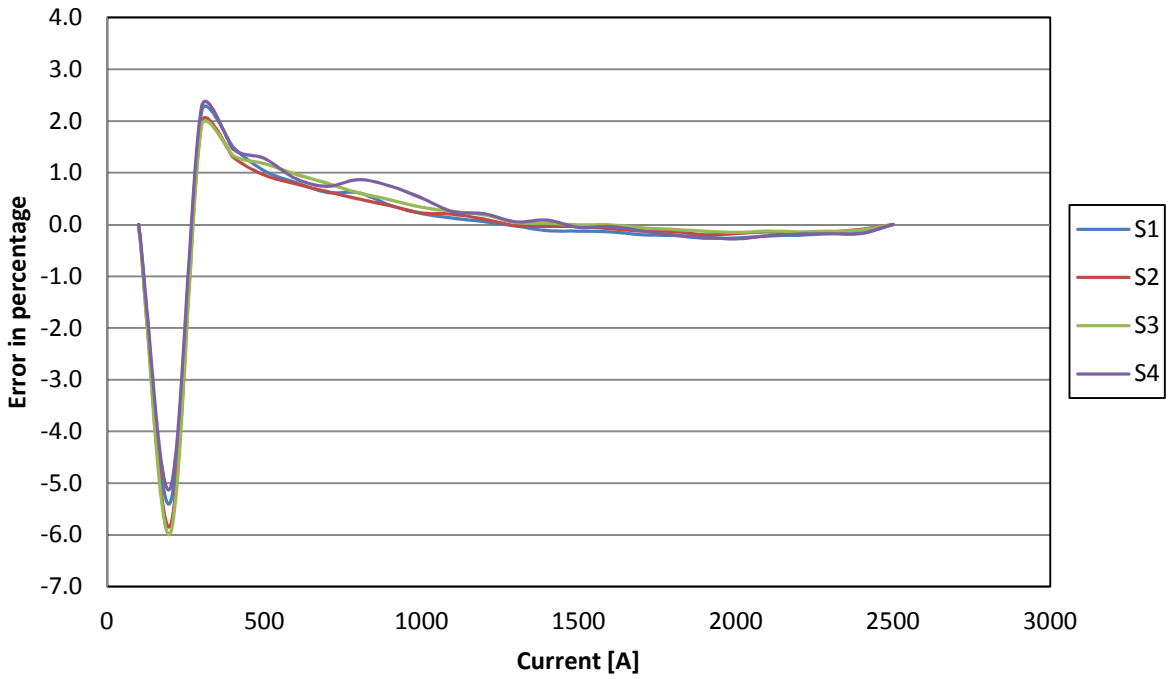


**Figure 2-10** Error in percentage referred to end points line (HG-362A sensors)

*ii. Case #2 – current from 50A to 500A*

Just like for the first case below we show the measurement results for one sensor at a time along with the linearity and error calculations.

**Tab. 2-13**

| Linearity and errors for sensor #1 | | | | | |
|---|---|---|---|---|---|
| I [A] | $Vs_1$ [mV] | Ieq. Regr. [A] | E%punt. Regr. | Ieq. EndP [A] | E%punt. EndP. |
| 50.8 | -0.4440 | 50.74472378 | -0.108811454 | 50.8 | 0 |
| 100.7 | -0.8834 | 100.4895371 | -0.208999851 | 100.5513266 | -0.147639933 |
| 150.5 | -1.3251 | 150.4947353 | -0.003498143 | 150.563072 | 0.041908335 |
| 200.4 | -1.7668 | 200.4999334 | 0.049866986 | 200.5748175 | 0.087234281 |
| 250.6 | -2.2096 | 250.6296634 | 0.011836965 | 250.7111111 | 0.044338033 |
| 300.8 | -2.6569 | 301.2688419 | 0.155864995 | 301.3569199 | 0.185146244 |
| 350.9 | -3.0951 | 350.8778023 | -0.00632592 | 350.9723758 | 0.020625755 |
| 400.9 | -3.5357 | 400.7584686 | -0.035303407 | 400.8595731 | -0.010084042 |
| 450.7 | -3.9764 | 450.650456 | -0.010992675 | 450.7580929 | 0.012889491 |
| 500.6 | -4.4166 | 500.485838 | -0.022805034 | 500.6 | 0 |

**Tab. 2-14**

| Linearity and errors for sensor #2 | | | | | |
|---|---|---|---|---|---|
| I [A] | $Vs_2$ [mV] | Ieq. Regr. [A] | E%punt. Regr. | Ieq. EndP [A] | E%punt. EndP. |
| 50.8 | -0.3934 | 50.47659628 | -0.636621504 | 50.8 | 1.39871E-14 |
| 100.7 | -0.7759 | 100.0299968 | -0.665345826 | 100.4088636 | -0.289112569 |
| 150.5 | -1.1632 | 150.2052438 | -0.195851279 | 150.6402699 | 0.093202584 |
| 200.4 | -1.5449 | 199.6550032 | -0.371754888 | 200.1453764 | -0.127057669 |
| 250.6 | -1.9356 | 250.2707249 | -0.131394674 | 250.8177504 | 0.086891601 |
| 300.8 | -2.3640 | 305.7705335 | 1.652437993 | 306.3796776 | 1.854946022 |
| 350.9 | -2.7111 | 350.7378153 | -0.046219627 | 351.3972896 | 0.141718319 |
| 400.9 | -3.0925 | 400.1487093 | -0.187401024 | 400.8634872 | -0.009107705 |
| 450.7 | -3.4760 | 449.8316611 | -0.19266449 | 450.6020472 | -0.021733474 |
| 500.6 | -3.8615 | 499.7737157 | -0.165058781 | 500.6 | 2.27101E-14 |

**Tab. 2-15**

| Linearity and errors for sensor #3 | | | | | |
|---|---|---|---|---|---|
| I [A] | $Vs_3$ [mV] | Ieq. Regr. [A] | E%punt. Regr. | Ieq. EndP [A] | E%punt. EndP. |
| 50.8 | -0.4324 | 50.52470789 | -0.541913602 | 50.8 | 1.39871E-14 |
| 100.7 | -0.8684 | 100.8373641 | 0.136409264 | 101.0763094 | 0.373693526 |
| 150.5 | -1.2959 | 150.1691544 | -0.219830988 | 150.3724614 | -0.084743287 |

| Linearity and errors for sensor #3 | | | | | |
|---|---|---|---|---|---|
| I [A] | $Vs_3$ [mV] | Ieq. Regr. [A] | E%punt. Regr. | Ieq. EndP [A] | E%punt. EndP. |
| 200.4 | -1.7331 | 200.6202858 | 0.109923056 | 200.7871459 | 0.193186575 |
| 250.6 | -2.1687 | 250.8867836 | 0.114438804 | 251.0173302 | 0.166532411 |
| 300.8 | -2.6040 | 301.1186627 | 0.105938391 | 301.2129208 | 0.137274188 |
| 350.9 | -3.0371 | 351.0966705 | 0.056047455 | 351.1548235 | 0.072619975 |
| 400.9 | -3.4660 | 400.5900152 | -0.077322237 | 400.6124132 | -0.071735306 |
| 450.7 | -3.8977 | 450.4064686 | -0.065127892 | 450.3928782 | -0.068143288 |
| 500.6 | -4.3331 | 500.6498872 | 0.009965487 | 500.6 | 0 |

**Tab. 2-16**

| Linearity and errors for sensor #4 | | | | | |
|---|---|---|---|---|---|
| I [A] | $Vs_4$ [mV] | Ieq. Regr. [A] | E%punt. Regr. | Ieq. EndP [A] | E%punt. EndP. |
| 50.8 | 0.5155 | 50.85070999 | 0.099822822 | 50.8 | -1.39871E-14 |
| 100.7 | 1.0271 | 100.6159099 | -0.083505539 | 100.5713161 | -0.127789372 |
| 150.5 | 1.5435 | 150.8480234 | 0.231244768 | 150.8096031 | 0.205716355 |
| 200.4 | 2.0501 | 200.126855 | -0.136299876 | 200.0944912 | -0.152449508 |
| 250.6 | 2.5682 | 250.5243337 | -0.03019405 | 250.4981637 | -0.04063698 |
| 300.8 | 3.0854 | 300.8342661 | 0.011391651 | 300.8142792 | 0.004747083 |
| 350.9 | 3.5982 | 350.7161944 | -0.052381192 | 350.7023381 | -0.056329993 |
| 400.9 | 4.1144 | 400.9288531 | 0.007197087 | 400.9211679 | 0.005280106 |
| 450.7 | 4.6277 | 450.8594183 | 0.035371257 | 450.8578696 | 0.035027641 |
| 500.6 | 5.1390 | 500.5954361 | -0.000911688 | 500.6 | 0 |

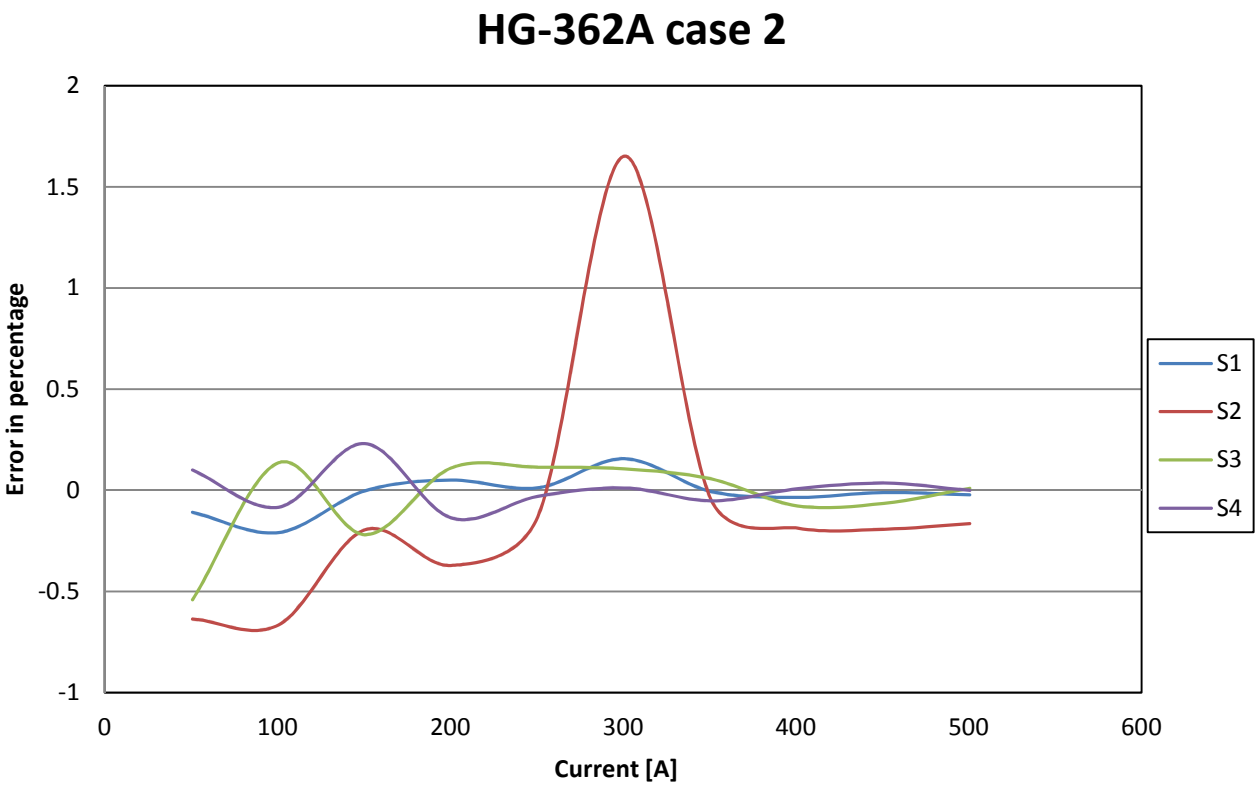


**Figure 2-11** Error in percentage referred to regression line (HG-362A sensors)

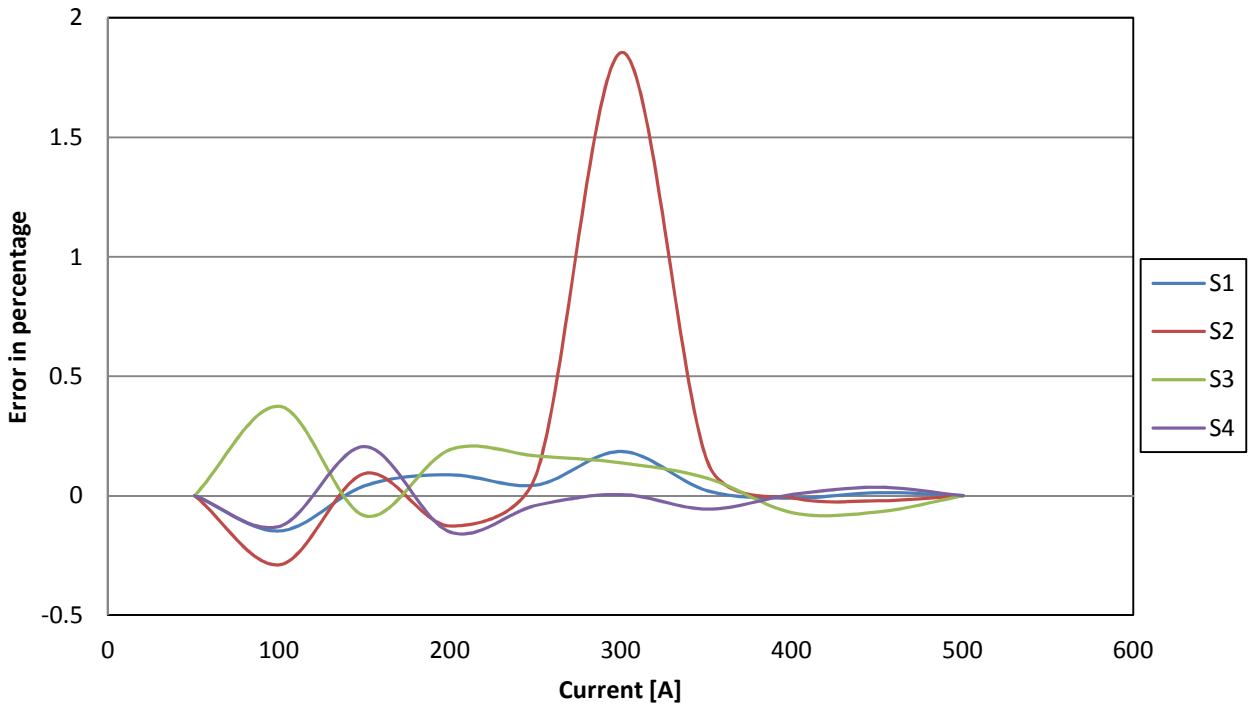


**Figure 2-12** Error in percentage referred to end points line (HG-362A sensors)

## 2.5. Metrological Characterization of Type 3 Sensors

WE CONTINUE the measurements with Hoeben's HE144 Hall elements [29]. They have a nominal hall voltage of 90~185 mV on B=0.1T when driven with the advised current of 5mA and a maximum thermal drift of –0.06 %/°C. The operating temperature is -40 to +175°C. These sensors have again the same packaging as the first two sensors that we looked before. The experimental setup is the same as the one used for the HG-362A sensors, expect that this time we used three sensors instead of four. The driving current is equal to 1mA and the maximum allowed induction is 500mT per sensor.

*iii. Case #1 – current from 100A to 2500A*

Below we report the measurement results for all three sensors together with the linearity and error calculations.

**Tab. 2-17**

| Linearity and errors for sensor #1 | | | | | |
|---|---|---|---|---|---|
| I [A] | $Vs_1$ [mV] | Ieq. Regr. [A] | E%punt. Regr. | Ieq. EndP [A] | E%punt. EndP. |
| 100 | 0.5061 | 94.47160509 | -5.528394907 | 100 | 0 |
| 200 | 1.0221 | 197.6415829 | -1.179208528 | 202.718081 | 1.359040502 |
| 300 | 1.5496 | 303.1108917 | 1.036963899 | 307.7254216 | 2.575140521 |
| 400 | 2.0464 | 402.4419866 | 0.610496662 | 406.6214344 | 1.655358609 |
| 500 | 2.5401 | 501.153262 | 0.230652394 | 504.9003426 | 0.980068512 |
| 600 | 3.0349 | 600.0844733 | 0.014078881 | 603.3982233 | 0.566370556 |
| 700 | 3.5516 | 703.3944104 | 0.484915773 | 706.2556506 | 0.893664368 |
| 800 | 4.0461 | 802.2656392 | 0.283204898 | 804.6938115 | 0.586726442 |
| 900 | 4.5449 | 901.9966178 | 0.221846419 | 903.9879565 | 0.443106278 |
| 1000 | 5.041 | 1001.187753 | 0.118775345 | 1002.744623 | 0.274462314 |
| 1100 | 5.5371 | 1100.378889 | 0.034444467 | 1101.50129 | 0.136480889 |
| 1200 | 6.0387 | 1200.669705 | 0.055808734 | 1201.35282 | 0.112734974 |
| 1300 | 6.531 | 1299.101062 | -0.069149109 | 1299.353035 | -0.049766512 |
| 1400 | 7.0276 | 1398.392168 | -0.11484513 | 1398.209235 | -0.127911785 |
| 1500 | 7.526 | 1498.04317 | -0.130455331 | 1497.423754 | -0.171749763 |
| 1600 | 8.0261 | 1598.034073 | -0.122870438 | 1596.976684 | -0.188957226 |
| 1700 | 8.5301 | 1698.804749 | -0.07030888 | 1697.305973 | -0.158472188 |
| 1800 | 9.023 | 1797.356071 | -0.14688495 | 1795.425628 | -0.254131773 |
| 1900 | 9.5239 | 1897.506927 | -0.131214352 | 1895.137812 | -0.255904644 |
| 2000 | 10.0263 | 1997.957696 | -0.102115178 | 1995.148595 | -0.242570274 |
| 2100 | 10.5318 | 2099.028285 | -0.046272133 | 2095.776482 | -0.201119905 |

| Linearity and errors for sensor #1 | | | | | |
|---|---|---|---|---|---|
| I [A] | $Vs_1$ [mV] | Ieq. Regr. [A] | E%punt. Regr. | Ieq. EndP [A] | E%punt. EndP. |
| 2200 | 11.0413 | 2200.898641 | 0.040847329 | 2197.200634 | -0.127243923 |
| 2300 | 11.535 | 2299.609917 | -0.01696015 | 2295.479542 | -0.19654166 |
| 2400 | 12.0443 | 2401.440284 | 0.060011843 | 2396.86388 | -0.130671654 |
| 2500 | 12.5624 | 2505.03014 | 0.201205596 | 2500 | 0 |

**Tab. 2-18**

| Linearity and errors for sensor #2 | | | | | |
|---|---|---|---|---|---|
| I [A] | $Vs_2$ [mV] | Ieq. Regr. [A] | E%punt. Regr. | Ieq. EndP [A] | E%punt. EndP. |
| 100 | 0.4333 | 91.9466676 | -8.053332403 | 100 | 1.42109E-14 |
| 200 | 0.8768 | 195.8197715 | -2.090114261 | 203.4975642 | 1.748782124 |
| 300 | 1.3297 | 301.8944699 | 0.631489964 | 309.1887635 | 3.062921152 |
| 400 | 1.7529 | 401.0130664 | 0.253266606 | 407.9490097 | 1.987252414 |
| 500 | 2.1776 | 500.4829812 | 0.096596247 | 507.059304 | 1.411860798 |
| 600 | 2.5998 | 599.3673656 | -0.10543907 | 605.5861848 | 0.931030795 |
| 700 | 3.0446 | 703.5449453 | 0.506420758 | 709.3871241 | 1.341017723 |
| 800 | 3.4702 | 803.2256511 | 0.403206385 | 808.7074473 | 1.088430909 |
| 900 | 3.8943 | 902.5550386 | 0.283893175 | 907.6777224 | 0.853080261 |
| 1000 | 4.3213 | 1002.563641 | 0.256364141 | 1007.324757 | 0.732475715 |
| 1100 | 4.7455 | 1101.91645 | 0.174222739 | 1106.318369 | 0.574397161 |
| 1200 | 5.1742 | 1202.323214 | 0.19360114 | 1206.362125 | 0.530177066 |
| 1300 | 5.5959 | 1301.090492 | 0.083883995 | 1304.772323 | 0.367101759 |
| 1400 | 6.0196 | 1400.326195 | 0.023299611 | 1403.649252 | 0.260660841 |
| 1500 | 6.4396 | 1498.695312 | -0.086979193 | 1501.662729 | 0.110848575 |
| 1600 | 6.8707 | 1599.664185 | -0.020988444 | 1602.266562 | 0.141660103 |
| 1700 | 7.3024 | 1700.773585 | 0.045504999 | 1703.010414 | 0.177083172 |
| 1800 | 7.7228 | 1799.236387 | -0.042422922 | 1801.117237 | 0.06206872 |
| 1900 | 8.147 | 1898.589196 | -0.074252836 | 1900.110849 | 0.005834136 |
| 2000 | 8.5726 | 1998.269902 | -0.086504905 | 1999.431172 | -0.028441411 |
| 2100 | 9.003 | 2099.074826 | -0.044055897 | 2099.871649 | -0.006111952 |
| 2200 | 9.4337 | 2199.950014 | -0.002272087 | 2200.382136 | 0.017369813 |
| 2300 | 9.8515 | 2297.803865 | -0.095484139 | 2297.882209 | -0.092077878 |
| 2400 | 10.2845 | 2399.217741 | -0.032594135 | 2398.929436 | -0.044606828 |
| 2500 | 10.7176 | 2500.655038 | 0.026201517 | 2500 | 1.81899E-14 |

**Tab. 2-19**

| Linearity and errors for sensor #3 | | | | | |
|---|---|---|---|---|---|
| I [A] | $Vs_3$ [mV] | Ieq. Regr. [A] | E%punt. Regr. | Ieq. EndP [A] | E%punt. EndP. |
| 100 | 0.4051 | 91.58298276 | -8.417017244 | 100 | 0 |
| 200 | 0.8171 | 194.8541484 | -2.572925795 | 203.1428959 | 1.571447944 |

| Linearity and errors for sensor #3 | | | | | |
|---|---|---|---|---|---|
| I [A] | $Vs_3$ [mV] | Ieq. Regr. [A] | E%punt. Regr. | Ieq. EndP [A] | E%punt. EndP. |
| 300 | 1.2399 | 300.8324223 | 0.277474096 | 308.9895376 | 2.99651253 |
| 400 | 1.6367 | 400.2935838 | 0.073395943 | 408.3271616 | 2.081790397 |
| 500 | 2.0317 | 499.3035605 | -0.13928789 | 507.2141613 | 1.442832257 |
| 600 | 2.4293 | 598.9652486 | -0.172458572 | 606.7520628 | 1.125343792 |
| 700 | 2.8452 | 703.2139811 | 0.459140154 | 710.8713113 | 1.553044471 |
| 800 | 3.2439 | 803.1513931 | 0.393924136 | 810.6845943 | 1.335574285 |
| 900 | 3.6421 | 902.963476 | 0.329275112 | 910.3727039 | 1.15252265 |
| 1000 | 4.0409 | 1002.925954 | 0.292595383 | 1010.211022 | 1.021102152 |
| 1100 | 4.4388 | 1102.662839 | 0.2420763 | 1109.824027 | 0.893093367 |
| 1200 | 4.8395 | 1203.101568 | 0.25846397 | 1210.138004 | 0.844833641 |
| 1300 | 5.2346 | 1302.13661 | 0.164354633 | 1309.050038 | 0.696156775 |
| 1400 | 5.6315 | 1401.622838 | 0.115916967 | 1408.412697 | 0.600906911 |
| 1500 | 6.0252 | 1500.306959 | 0.020463913 | 1506.974246 | 0.464949705 |
| 1600 | 6.4268 | 1600.971279 | 0.060704962 | 1607.513534 | 0.469595898 |
| 1700 | 6.8294 | 1701.886258 | 0.110956368 | 1708.30317 | 0.488421766 |
| 1800 | 7.2212 | 1800.094129 | 0.005229383 | 1806.38906 | 0.354947769 |
| 1900 | 7.6169 | 1899.279566 | -0.037917559 | 1905.451302 | 0.286910649 |
| 2000 | 8.0138 | 1998.765794 | -0.061710316 | 2004.813961 | 0.24069805 |
| 2100 | 8.4148 | 2099.279719 | -0.034299072 | 2105.203042 | 0.247763891 |
| 2200 | 8.8155 | 2199.718448 | -0.012797826 | 2205.517018 | 0.250773562 |
| 2300 | 9.2031 | 2296.873554 | -0.135932428 | 2302.551451 | 0.110932673 |
| 2400 | 9.6171 | 2400.646036 | 0.026918172 | 2406.195041 | 0.25812671 |
| 2500 | 9.9918 | 2494.567652 | -0.217293917 | 2500 | -1.81899E-14 |

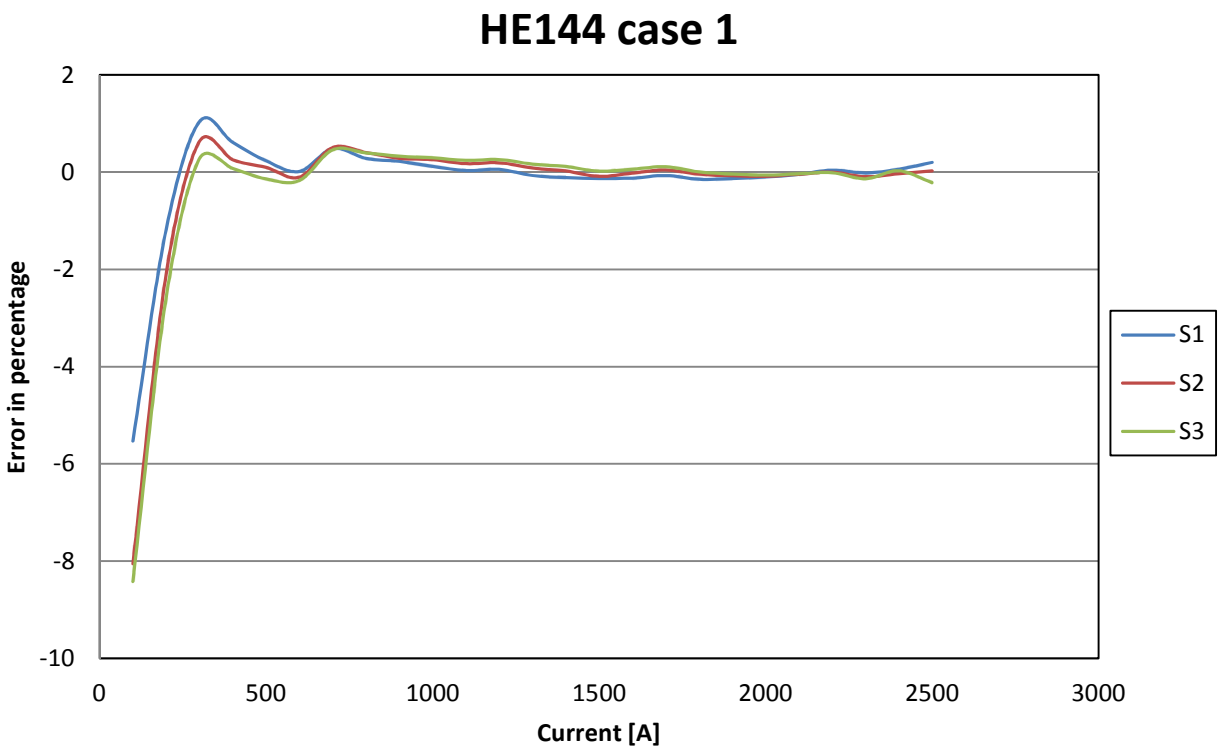


**Figure 2-13** Error in percentage referred to regression line (HE144 sensors)

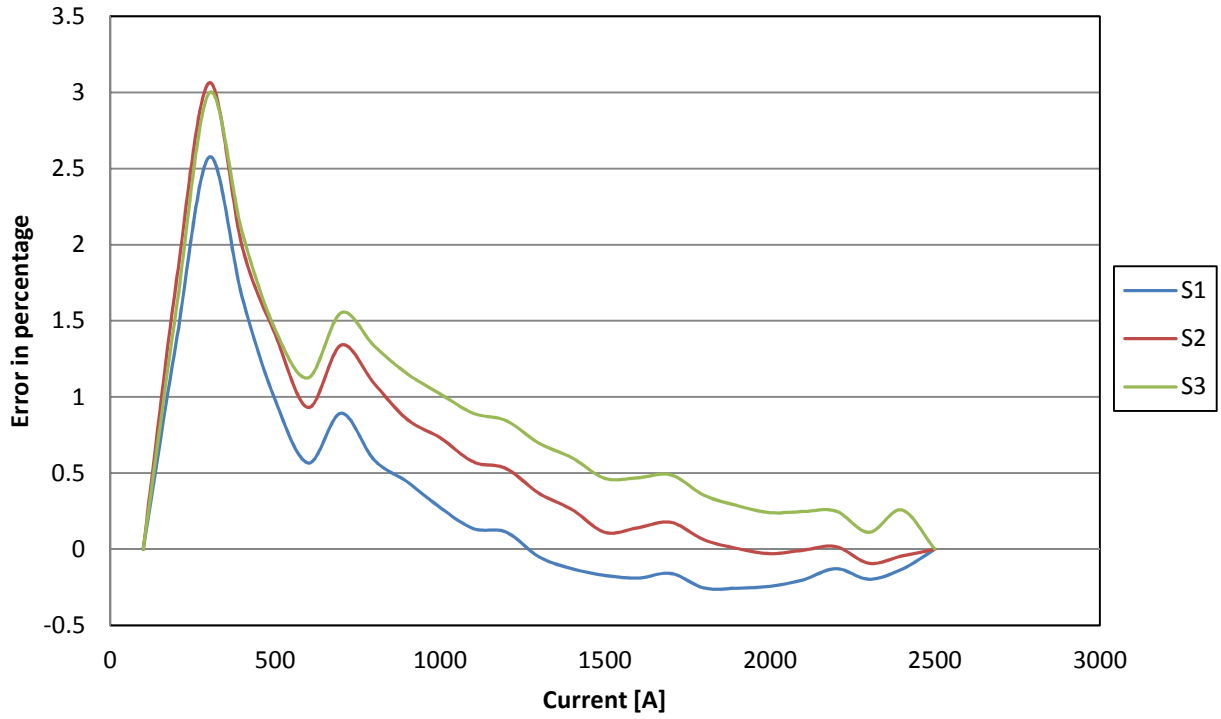


**Figure 2-14** Error in percentage referred to end points line (HE144 sensors)

*iv. Case #2 – current from 50A to 500A*

We report below the measurements done with the more precise DC current generator together with the calculations of linearity and error for each sensor.

**Tab. 2-20**

| Linearity and errors for sensor #1 | | | | | |
|---|---|---|---|---|---|
| I [A] | $Vs_1$ [mV] | Ieq. Regr. [A] | E%punt. Regr. | Ieq. EndP [A] | E%punt. EndP. |
| 50.8 | 0.2321 | 50.95968865 | 0.314347741 | 50.8 | 0 |
| 100.7 | 0.4615 | 100.5735394 | -0.125581526 | 100.4339987 | -0.264152185 |
| 150.5 | 0.6929 | 150.6199433 | 0.079696573 | 150.5007263 | 0.000482622 |
| 200.5 | 0.9234 | 200.4716983 | -0.014115538 | 200.372726 | -0.063478324 |
| 250.6 | 1.1541 | 250.3667087 | -0.093093108 | 250.2879985 | -0.124501811 |
| 300.8 | 1.3874 | 300.8240381 | 0.007991403 | 300.7658185 | -0.011363543 |
| 350.9 | 1.6186 | 350.8271868 | -0.020750425 | 350.7892732 | -0.031555095 |
| 400.9 | 1.8502 | 400.916846 | 0.00420205 | 400.8992737 | -0.000181179 |
| 450.8 | 2.0816 | 450.96325 | 0.036213389 | 450.9660013 | 0.036823702 |
| 500.6 | 2.3110 | 500.5771007 | -0.004574369 | 500.6 | -1.13551E-14 |

**Tab. 2-21**

| Linearity and errors for sensor #2 | | | | | |
|---|---|---|---|---|---|
| I [A] | $Vs_2$ [mV] | Ieq. Regr. [A] | E%punt. Regr. | Ieq. EndP [A] | E%punt. EndP. |
| 50.8 | 0.2321 | 50.65465759 | -0.286107103 | 50.8 | 1.39871E-14 |
| 100.7 | 0.4607 | 100.4452771 | -0.252952283 | 100.7462185 | 0.045897207 |
| 150.5 | 0.6902 | 150.4319226 | -0.045234172 | 150.8890756 | 0.258522013 |
| 200.5 | 0.9195 | 200.3750067 | -0.062340776 | 200.9882353 | 0.243508875 |
| 250.6 | 1.1502 | 250.6230203 | 0.009186091 | 251.3932773 | 0.316551201 |
| 300.8 | 1.3819 | 301.0888407 | 0.096024162 | 302.0168067 | 0.404523512 |
| 350.9 | 1.6128 | 351.3804156 | 0.136909555 | 352.4655462 | 0.446151672 |
| 400.9 | 1.8429 | 401.4977452 | 0.14910082 | 402.7394958 | 0.458841556 |
| 450.8 | 2.0727 | 451.5497327 | 0.166311608 | 452.9478992 | 0.476463877 |
| 500.6 | 2.2908 | 499.0533815 | -0.308952961 | 500.6 | 0 |

**Tab. 2-22**

| Linearity and errors for sensor #3 | | | | | |
|---|---|---|---|---|---|
| I [A] | $Vs_3$ [mV] | Ieq. Regr. [A] | E%punt. Regr. | Ieq. EndP [A] | E%punt. EndP. |
| 50.8 | 0.2306 | 51.33277764 | 1.048774879 | 50.8 | 1.39871E-14 |
| 100.7 | 0.4587 | 100.9608558 | 0.259042478 | 100.338593 | -0.358894719 |
| 150.5 | 0.6868 | 150.5889339 | 0.0590923 | 149.877186 | -0.413829876 |
| 200.5 | 0.9150 | 200.2387692 | -0.130289673 | 199.437497 | -0.529926692 |
| 250.6 | 1.1440 | 250.0626618 | -0.214420683 | 249.1715513 | -0.570011433 |
| 300.8 | 1.3761 | 300.5610262 | -0.079446065 | 299.5788615 | -0.405963606 |
| 350.9 | 1.6059 | 350.5589761 | -0.097185504 | 349.4866593 | -0.40277593 |
| 400.9 | 1.8356 | 400.5351687 | -0.091003059 | 399.3727391 | -0.380958063 |
| 450.8 | 2.0644 | 450.315547 | -0.107465177 | 449.0633576 | -0.385235662 |
| 500.6 | 2.3017 | 501.9452837 | 0.268734255 | 500.6 | 0 |

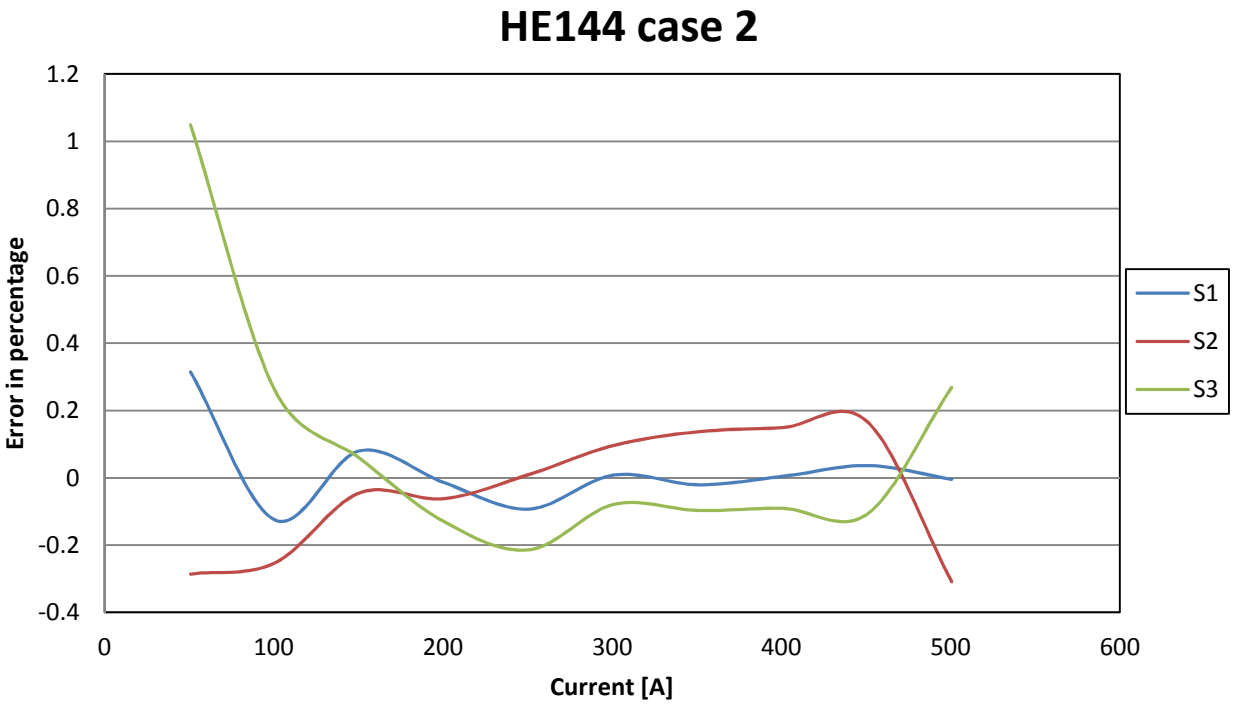


**Figure 2-15** Error in percentage referred to regression line (HE144 sensors)

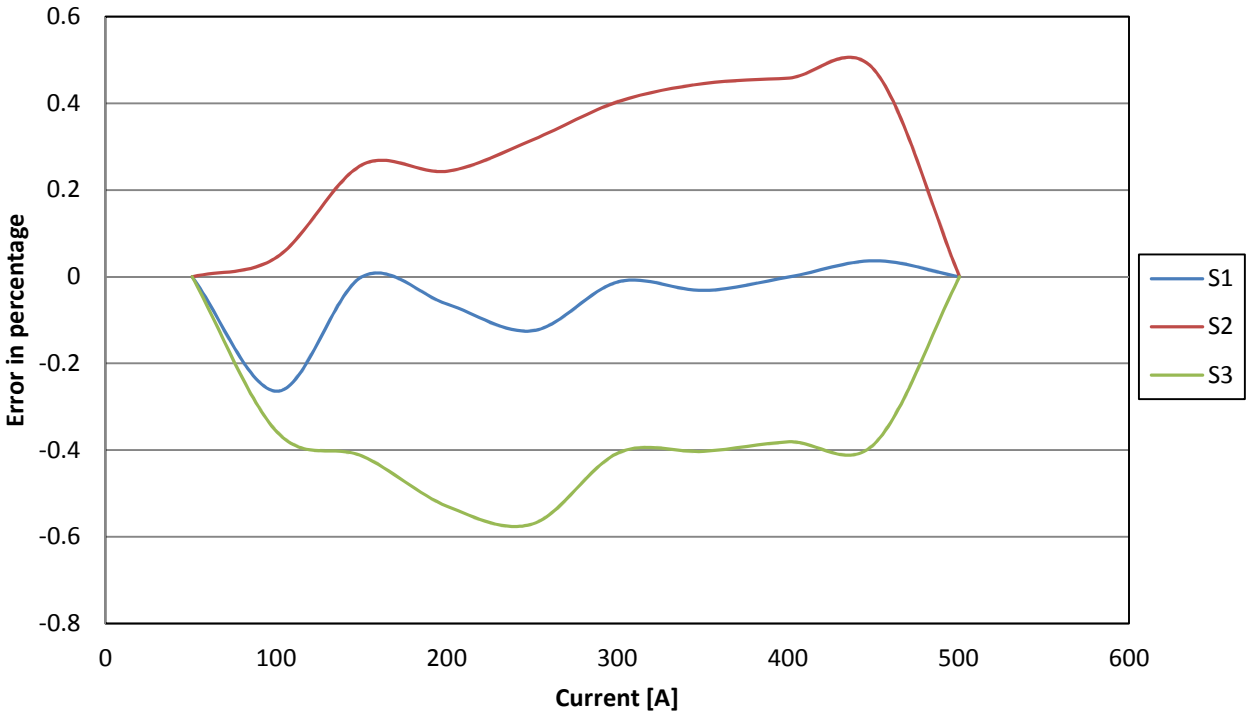


**Figure 2-16** Error in percentage referred to end points line (HE144 sensors)

## 2.6. Metrological Characterization of Type 4 Sensors

THE NEXT BATCH of sensors that we tested consisted of Honeywell SS495A1[30] sensors. They have a maximum thermal drift of ±0.04 %/°C when external magnetic field is absent, and -0.02 to +0.06%/°C in the test condition specified by the manufacturer. The chip packaging is the same again, but these sensors have only three pins, instead of four of the past ones that we tested. Again we kept the same experimental setup of the last two types. As advised by the manufacturer's datasheet we drove the sensors with a 5 VDC which adds up to a power consumption of roughly 20mA (7mA/sensor, 3 sensors on the board) with a max allowed induction of 60mT per sensor.

*v. Case #1 – current from 100A to 2500A*

Just like we did so far we report the tests results with the less stable DC generator together with linearity and error calculations.

**Tab. 2-22**

| Linearity and errors for sensor #1 | | | | | |
|---|---|---|---|---|---|
| I [A] | $Vs_1$ [V] | Ieq. Regr. [A] | E%punt. Regr. | Ieq. EndP [A] | E%punt. EndP. |
| 100 | 0.0654 | 98.3132894 | -1.686710596 | 100 | 0 |
| 200 | 0.1296 | 196.5108023 | -1.744598851 | 198.1088825 | -0.945558739 |
| 300 | 0.1993 | 303.1208747 | 1.040291569 | 304.6227316 | 1.540910538 |
| 400 | 0.2637 | 401.6242989 | 0.406074714 | 403.0372493 | 0.759312321 |
| 500 | 0.3293 | 501.9631905 | 0.392638108 | 503.2855778 | 0.657115568 |
| 600 | 0.394 | 600.9254816 | 0.154246928 | 602.1585482 | 0.359758039 |
| 700 | 0.4593 | 700.8055064 | 0.115072338 | 701.9484241 | 0.278346296 |
| 800 | 0.5246 | 800.6855312 | 0.085691396 | 801.7382999 | 0.217287488 |
| 900 | 0.5895 | 899.9537335 | -0.005140728 | 900.9169054 | 0.101878383 |
| 1000 | 0.6546 | 999.527847 | -0.047215301 | 1000.401146 | 0.040114613 |
| 1100 | 0.72 | 1099.560827 | -0.03992478 | 1100.34384 | 0.03125814 |
| 1200 | 0.7852 | 1199.287897 | -0.059341951 | 1199.980898 | -0.00159185 |
| 1300 | 0.8506 | 1299.320877 | -0.05224023 | 1299.923591 | -0.005877599 |
| 1400 | 0.9158 | 1399.047946 | -0.068003844 | 1399.560649 | -0.03138218 |
| 1500 | 0.9816 | 1499.692749 | -0.020483392 | 1500.114613 | 0.007640879 |
| 1600 | 1.0466 | 1599.113907 | -0.05538081 | 1599.446036 | -0.034622732 |
| 1700 | 1.1119 | 1698.993932 | -0.059180481 | 1699.235912 | -0.044946345 |
| 1800 | 1.1777 | 1799.638735 | -0.020070291 | 1799.789876 | -0.011673565 |
| 1900 | 1.2427 | 1899.059893 | -0.049479333 | 1899.121299 | -0.046247424 |
| 2000 | 1.309 | 2000.469474 | 0.023473688 | 2000.439351 | 0.021967526 |
| 2100 | 1.3738 | 2099.58472 | -0.019775218 | 2099.465138 | -0.025469596 |
| 2200 | 1.4397 | 2200.382479 | 0.017385408 | 2200.17192 | 0.007814535 |
| 2300 | 1.5053 | 2300.721371 | 0.031363942 | 2300.420248 | 0.018271666 |
| 2400 | 1.571 | 2401.213218 | 0.050550748 | 2400.821394 | 0.034224769 |
| 2500 | 1.6359 | 2500.48142 | 0.01925681 | 2500 | -1.81899E-14 |

**Tab. 2-23**

| Linearity and errors for sensor #2 | | | | | |
|---|---|---|---|---|---|
| I [A] | $Vs_2$ [V] | Ieq. Regr. [A] | E%punt. Regr. | Ieq. EndP [A] | E%punt. EndP. |
| 100 | 0.0695 | 99.59514156 | -0.404858442 | 100 | 0 |
| 200 | 0.138 | 198.1328331 | -0.933583471 | 198.4019 | -0.79906626 |
| 300 | 0.2116 | 304.0069074 | 1.33563581 | 304.13 | 1.376668462 |
| 400 | 0.2801 | 402.5445989 | 0.636149733 | 402.5319 | 0.632968217 |

| Linearity and errors for sensor #2 | | | | | |
|---|---|---|---|---|---|
| I [A] | $Vs_2$ [V] | Ieq. Regr. [A] | E%punt. Regr. | Ieq. EndP [A] | E%punt. EndP. |
| 500 | 0.3494 | 502.2330956 | 0.446619117 | 502.083 | 0.416591848 |
| 600 | 0.4183 | 601.3461897 | 0.224364944 | 601.0594 | 0.176572694 |
| 700 | 0.4873 | 700.6031344 | 0.086162056 | 700.1796 | 0.025652207 |
| 800 | 0.5567 | 800.4354817 | 0.054435211 | 799.8743 | -0.015711977 |
| 900 | 0.6256 | 899.5485758 | -0.050158248 | 898.8508 | -0.127690988 |
| 1000 | 0.6947 | 998.9493711 | -0.105062886 | 998.1146 | -0.188543724 |
| 1100 | 0.7641 | 1098.781718 | -0.110752869 | 1097.809 | -0.19915441 |
| 1200 | 0.8333 | 1198.326364 | -0.139469629 | 1197.217 | -0.231938708 |
| 1300 | 0.9026 | 1298.014861 | -0.152702992 | 1296.768 | -0.248629087 |
| 1400 | 0.9717 | 1397.415656 | -0.184595966 | 1396.032 | -0.283456891 |
| 1500 | 1.0416 | 1497.967257 | -0.1355162 | 1496.445 | -0.237026396 |
| 1600 | 1.1109 | 1597.655754 | -0.146515397 | 1595.996 | -0.250269348 |
| 1700 | 1.1807 | 1698.063504 | -0.113911557 | 1696.265 | -0.219703611 |
| 1800 | 1.2507 | 1798.758955 | -0.068946961 | 1796.822 | -0.176572694 |
| 1900 | 1.3201 | 1898.591302 | -0.074142 | 1896.516 | -0.183345777 |
| 2000 | 1.3908 | 2000.293708 | 0.014685384 | 1998.079 | -0.096067517 |
| 2100 | 1.4602 | 2100.126055 | 0.006002618 | 2097.773 | -0.106029124 |
| 2200 | 1.5304 | 2201.109207 | 0.05041852 | 2198.617 | -0.062847908 |
| 2300 | 1.6003 | 2301.660808 | 0.072209042 | 2299.03 | -0.042158845 |
| 2400 | 1.6707 | 2402.931662 | 0.122152571 | 2400.162 | 0.006733704 |
| 2500 | 1.7402 | 2502.90786 | 0.116314386 | 2500 | 0 |

**Tab. 2-24**

| Linearity and errors for sensor #3 | | | | | |
|---|---|---|---|---|---|
| I [A] | $Vs_3$ [V] | Ieq. Regr. [A] | E%punt. Regr. | Ieq. EndP [A] | E%punt. EndP. |
| 100 | 0.0778 | 100.4178254 | 0.417825444 | 100 | 0 |
| 200 | 0.1534 | 198.3891096 | -0.805445202 | 197.8651334 | -1.067433306 |
| 300 | 0.2354 | 304.6542591 | 1.551419691 | 304.0151458 | 1.338381931 |
| 400 | 0.3113 | 403.0143182 | 0.753579541 | 402.2686329 | 0.567158222 |
| 500 | 0.3876 | 501.8927438 | 0.378548767 | 501.0399249 | 0.207984984 |
| 600 | 0.4637 | 600.5119862 | 0.085331036 | 599.5523145 | -0.074614253 |
| 700 | 0.5406 | 700.1679618 | 0.023994537 | 699.1003139 | -0.128526583 |
| 800 | 0.6177 | 800.0831206 | 0.010390075 | 798.9072158 | -0.136598022 |
| 900 | 0.6941 | 899.0911379 | -0.100984676 | 897.8079591 | -0.243560101 |
| 1000 | 0.7709 | 998.6175218 | -0.138247818 | 997.2265073 | -0.27734927 |
| 1100 | 0.8479 | 1098.403089 | -0.145173726 | 1096.903958 | -0.281458366 |
| 1200 | 0.9248 | 1198.059065 | -0.16174462 | 1196.451957 | -0.295670216 |
| 1300 | 1.0021 | 1298.233407 | -0.135891793 | 1296.517762 | -0.267864478 |
| 1400 | 1.0788 | 1397.630199 | -0.169271504 | 1395.806859 | -0.299510089 |
| 1500 | 1.1565 | 1498.322908 | -0.111806156 | 1496.390468 | -0.240635462 |

| Linearity and errors for sensor #3 | | | | | |
|---|---|---|---|---|---|
| I [A] | $Vs_3$ [V] | Ieq. Regr. [A] | E%punt. Regr. | Ieq. EndP [A] | E%punt. EndP. |
| 1600 | 1.2333 | 1597.849292 | -0.134419278 | 1595.809016 | -0.261936483 |
| 1700 | 1.3107 | 1698.153225 | -0.108633804 | 1696.004272 | -0.23504283 |
| 1800 | 1.3883 | 1798.716342 | -0.071314311 | 1796.45843 | -0.19675389 |
| 1900 | 1.4653 | 1898.50191 | -0.078846864 | 1896.135881 | -0.203374703 |
| 2000 | 1.5434 | 1999.712985 | -0.014350756 | 1997.237295 | -0.138135255 |
| 2100 | 1.6204 | 2099.498552 | -0.023878473 | 2096.914746 | -0.146916877 |
| 2200 | 1.6993 | 2201.746361 | 0.079380024 | 2199.05177 | -0.043101377 |
| 2300 | 1.7768 | 2302.179886 | 0.09477765 | 2299.376477 | -0.027109715 |
| 2400 | 1.8547 | 2403.131778 | 0.130490748 | 2400.218988 | 0.009124514 |
| 2500 | 1.93178 | 2503.021018 | 0.120840739 | 2500 | 0 |

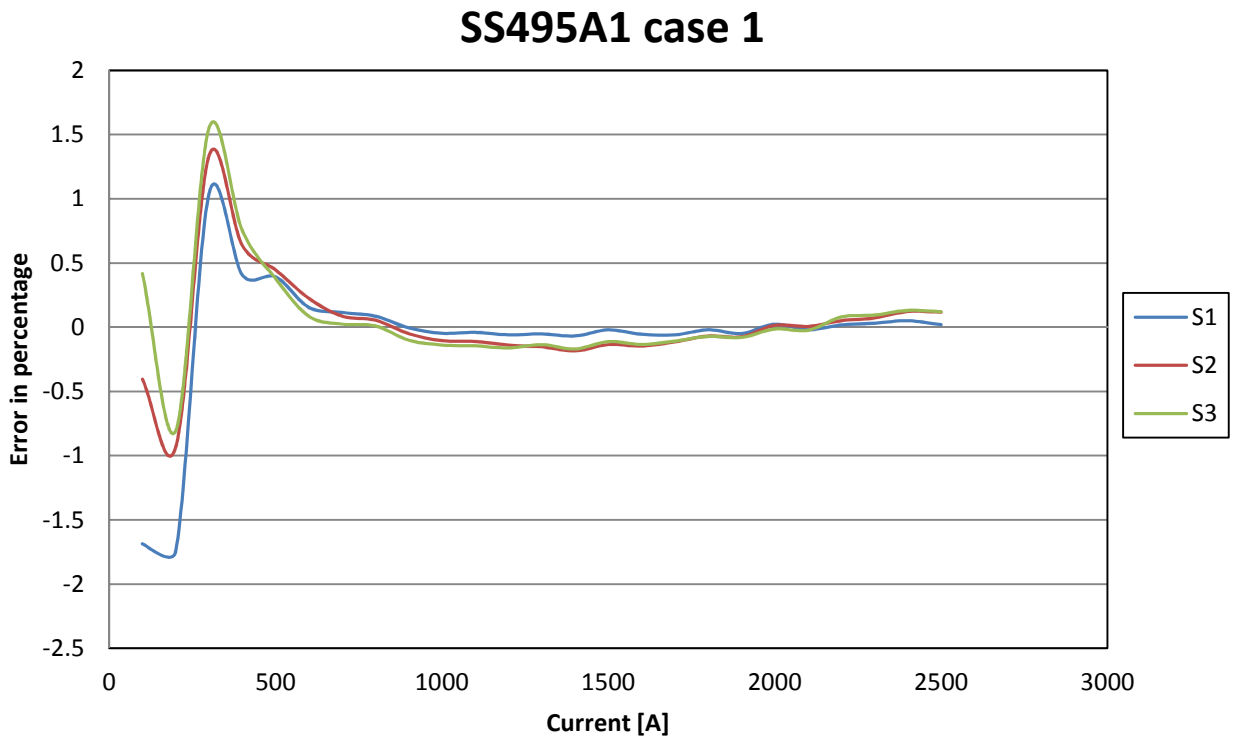


**Figure 2-17** Error in percentage referred to regression line (SS495A1 sensors)

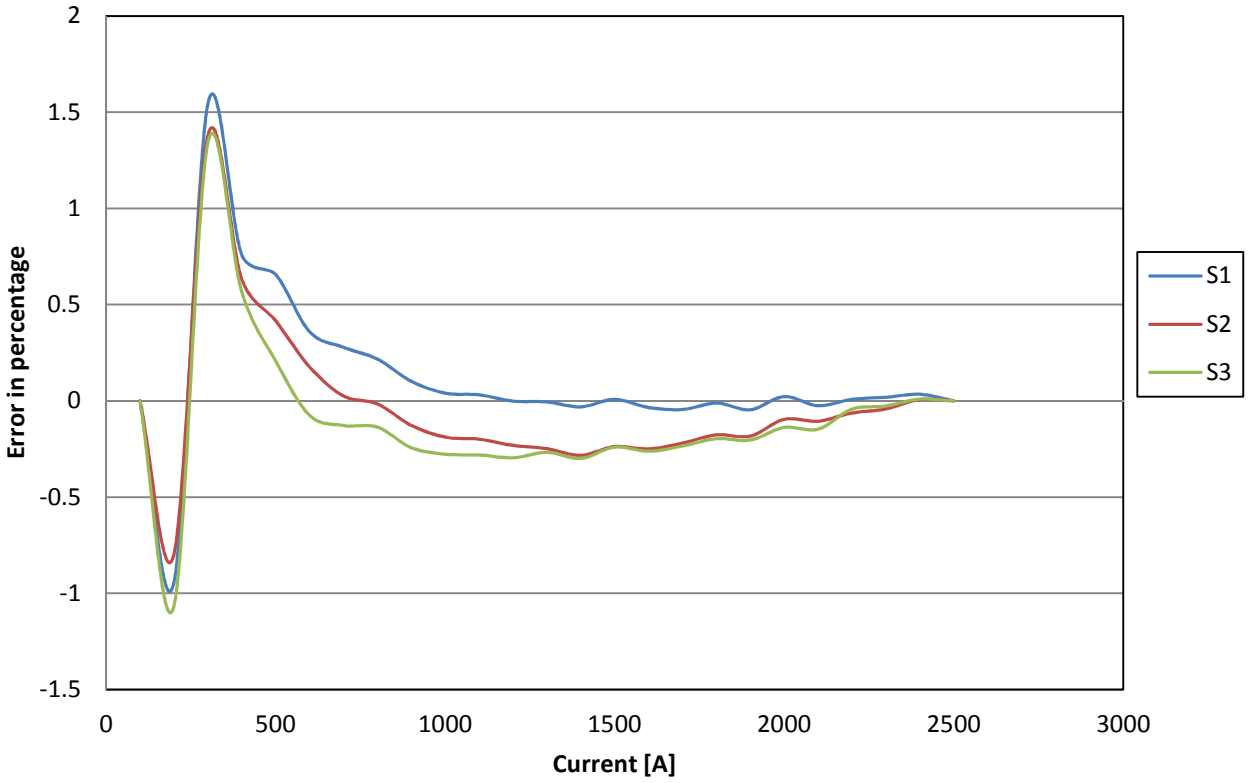


**Figure 2-18** Error in percentage referred to end points line (SS495A1 sensors)

*vi.* *Case #2 – current from 50A to 500A*

Again we report the tests results for the Honeywell sensors when the more stable DC current generator is used.

**Tab. 2-25**

| Linearity and errors for sensor #1 | | | | | |
|---|---|---|---|---|---|
| I [A] | $Vs_1$ [V] | Ieq. Regr. [A] | E%punt. Regr. | Ieq. EndP [A] | E%punt. EndP. |
| 50.8 | -0.0303 | 50.58487439 | -0.423475601 | 50.8 | 0 |
| 100.4 | -0.0608 | 100.6446971 | 0.243722256 | 100.8342643 | 0.432534119 |
| 150.6 | -0.0913 | 150.5896662 | -0.006861782 | 150.7537334 | 0.102080618 |
| 200.5 | -0.1217 | 200.4690045 | -0.015459123 | 200.6076054 | 0.053668512 |
| 250.6 | -0.1522 | 250.5780502 | -0.008758883 | 250.6910675 | 0.036339793 |
| 300.8 | -0.1829 | 300.9003958 | 0.033376271 | 300.9877206 | 0.062407107 |
| 350.9 | -0.2134 | 350.9274032 | 0.00780941 | 350.9891862 | 0.025416424 |
| 400.9 | -0.2438 | 400.8723722 | -0.006891437 | 400.9086554 | 0.002158989 |
| 450.8 | -0.2742 | 450.7188952 | -0.017991309 | 450.7297287 | -0.015588122 |
| 500.6 | -0.3046 | 500.6146412 | 0.002924722 | 500.6 | 0 |

**Tab. 2-26**

| Linearity and errors for sensor #2 | | | | | |
|---|---|---|---|---|---|
| I [A] | $Vs_2$ [V] | Ieq. Regr. [A] | E%punt. Regr. | Ieq. EndP [A] | E%punt. EndP. |
| 50.8 | -0.0337 | 50.61911913 | -0.356064712 | 50.8 | 0 |
| 100.4 | -0.0675 | 100.5432665 | 0.142695709 | 100.7121 | 0.310884144 |
| 150.6 | -0.1014 | 150.5560628 | -0.029174747 | 150.7129 | 0.074955506 |
| 200.5 | -0.1352 | 200.5393095 | 0.019605742 | 200.6841 | 0.091818334 |
| 250.6 | -0.1691 | 250.6555297 | 0.022158681 | 250.7882 | 0.075119703 |
| 300.8 | -0.2031 | 300.8456239 | 0.015167534 | 300.9663 | 0.055272789 |
| 350.9 | -0.2370 | 350.9175196 | 0.004992761 | 351.0261 | 0.035936435 |
| 400.9 | -0.2709 | 400.9450908 | 0.011247385 | 401.0416 | 0.035327397 |
| 450.8 | -0.3046 | 450.7510395 | -0.010860803 | 450.8356 | 0.007893753 |
| 500.6 | -0.3383 | 500.5274386 | -0.014494891 | 500.6 | -1.13551E-14 |

**Tab. 2-27**

| Linearity and errors for sensor #3 | | | | | |
|---|---|---|---|---|---|
| I [A] | $Vs_3$ [V] | Ieq. Regr. [A] | E%punt. Regr. | Ieq. EndP [A] | E%punt. EndP. |
| 50.8 | -0.0380 | 5.060.143.387 | -0.390878201 | 50.8 | -1,40E-09 |
| 100.4 | -0.0760 | 1.005.971.659 | 0.196380362 | 1.007.879.985 | 0.38645267 |
| 150.6 | -0.1140 | 1.504.746.115 | -0.083259322 | 1.506.577.288 | 0.038332554 |
| 200.5 | -0.1521 | 2.005.360.582 | 0.017984117 | 2.007.114.318 | 0.105452283 |
| 250.6 | -0.1902 | 2.506.369.337 | 0.014738093 | 2.508.045.575 | 0.081627111 |
| 300.8 | -0.2284 | 3.008.823.815 | 0.027387457 | 3.010.422.332 | 0.080529652 |
| 350.9 | -0.2666 | 3.510.095.428 | 0.031217683 | 3.511.616.407 | 0.074562757 |
| 400.9 | -0.3046 | 4.009.395.602 | 0.009867841 | 4.010.839.347 | 0.045880438 |
| 450.8 | -0.3425 | 4.507.512.911 | -0.010804998 | 4.508.879.605 | 0.01951209 |
| 500.6 | -0.3803 | 5.004.710.214 | -0.025764802 | 500.6 | -1,14E-09 |

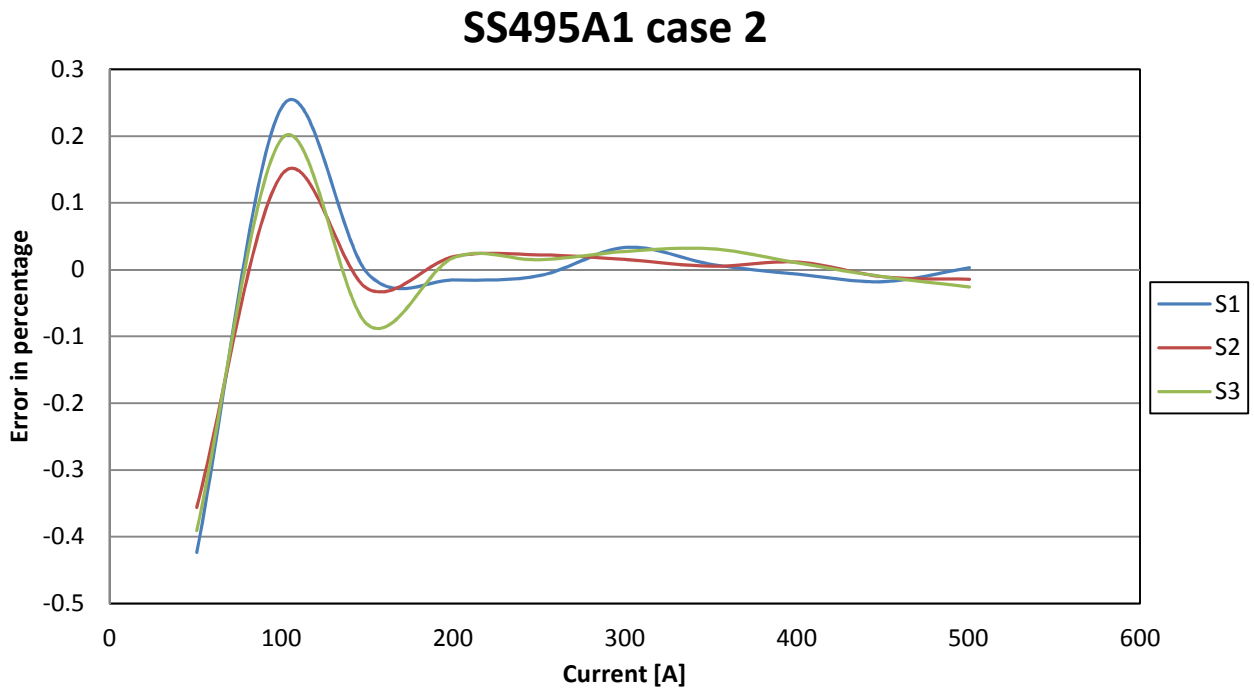


**Figure 2-19** Error in percentage referred to regression line (SS495A1 sensors)

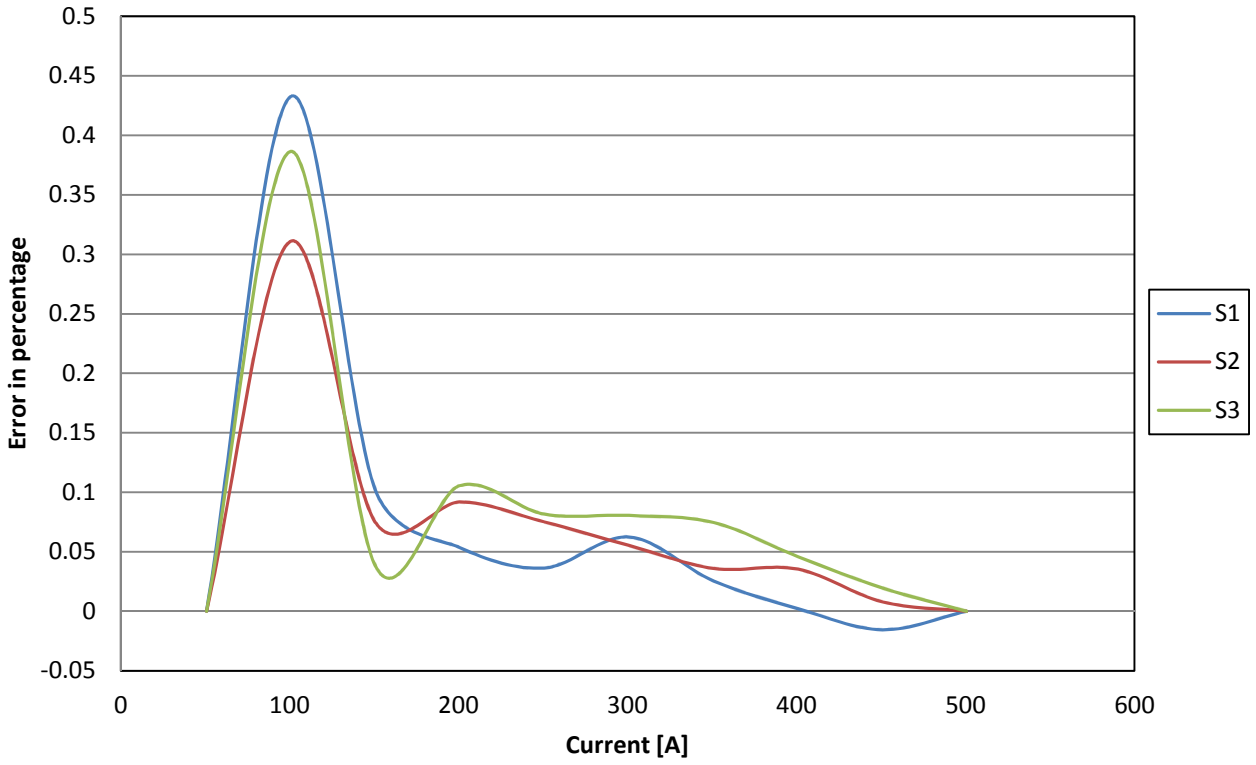


**Figure 2-20** Error in percentage referred to end points line (SS495A1 sensors)

## 2.7. Metrological Characterization of Type 5 Sensors

THE LAST sensors that we tested were again from Asahi-Kasei but this time we used hybrid ones. The EQ-732L [28] sensor is composed of an InAs Quantum Well Hall element and a signal processing IC chip right on the package. According to their datasheet these sensors are extremely linear, actually perfectly constant. As advised by the manufacturer's datasheet we drove the sensors with a 5 VDC which adds up to a power consumption of roughly 40mA (10mA/sensor, 4 sensors on the board) with a max allowed induction of 60mT per sensor. We did two tests with these sensors: first the linearity test from 50A to 2500A and we used a LEM APR transducer to sense the current passing through the cables that connected the generator to the bar, and secondly we did a temperature test to investigate the thermal drift using the temperature chamber and the more precise DC current generator.

*vii.* *Current from 100A to 1700A, measurement time greater than 1 second*

Below are shown the results of the tests with measurement time greater than 1 second. Every time that we wanted to read the hall voltage for the desired current value, a switch triggered the multimeters that processed a number of values during the measuring time that was set greater than 1 second.

**Tab. 2-28**

| Linearity and errors for sensor #1 | | | | | |
|---|---|---|---|---|---|
| I [A] | $Vs_1$ [V] | Ieq. Regr. [A] | E%punt. Regr. | Ieq. EndP [A] | E%punt. EndP. |
| 101.6 | -0.0968 | 103.0321604 | 1.407812332 | 101.6017978 | -1.39868E-14 |
| 151.4 | -0.1440 | 151.6729854 | 0.200026947 | 150.2618743 | -0.732198145 |
| 201.1 | -0.1929 | 201.9825552 | 0.462914472 | 200.5913563 | -0.22904578 |
| 250.9 | -0.2410 | 251.5916643 | 0.264100186 | 250.2201002 | -0.282494389 |
| 307.3 | -0.2958 | 307.9890629 | 0.222461319 | 306.6398205 | -0.216594541 |
| 357.3 | -0.3437 | 357.3921541 | 0.015533976 | 356.0624649 | -0.356577083 |
| 407.5 | -0.3925 | 407.6502195 | 0.036980322 | 406.340422 | -0.284442746 |
| 457.6 | -0.4407 | 457.2902312 | -0.05981292 | 456.0000808 | -0.341773615 |
| 507.2 | -0.4888 | 506.8375349 | -0.0802396 | 505.5669949 | -0.330718386 |
| 557.4 | -0.5370 | 556.4569448 | -0.17234595 | 555.2060437 | -0.396755975 |
| 607.6 | -0.5861 | 607.0137361 | -0.10318462 | 605.782845 | -0.305753522 |

| Linearity and errors for sensor #1 | | | | | |
|---|---|---|---|---|---|
| I [A] | $Vs_1$ [V] | Ieq. Regr. [A] | E%punt. Regr. | Ieq. EndP [A] | E%punt. EndP. |
| 657.2 | -0.6339 | 656.3035174 | -0.13802342 | 655.0921348 | -0.322345255 |
| 707.2 | -0.6825 | 706.345264 | -0.12749145 | 705.1536875 | -0.295972429 |
| 757.1 | -0.7310 | 756.356108 | -0.10358301 | 755.1843252 | -0.258347278 |
| 806.6 | -0.7789 | 805.6973937 | -0.11696338 | 804.5451399 | -0.259809335 |
| 856.8 | -0.8274 | 855.6567332 | -0.13339545 | 854.5242528 | -0.265571088 |
| 906.5 | -0.8758 | 905.5233646 | -0.10989579 | 904.410621 | -0.232644781 |
| 956.4 | -0.9242 | 955.286987 | -0.11507073 | 954.1939394 | -0.22935993 |
| 1006.4 | -0.9727 | 1005.328734 | -0.10526504 | 1004.255492 | -0.211907951 |
| 1105.8 | -1.0690 | 1104.495447 | -0.11404593 | 1103.461455 | -0.207555866 |
| 1206.0 | -1.1661 | 1204.506834 | -0.11980593 | 1203.512426 | -0.202264344 |
| 1304.6 | -1.2646 | 1305.929444 | 0.098733423 | 1304.975177 | 0.025589457 |
| 1404.6 | -1.3615 | 1405.81722 | 0.08726565 | 1404.902488 | 0.022141257 |
| 1503.4 | -1.4585 | 1505.728688 | 0.151659338 | 1504.853501 | 0.09344733 |
| 1604.1 | -1.5551 | 1605.205459 | 0.070894171 | 1604.369643 | 0.018788186 |
| 1704.2 | -1.6520 | 1704.998467 | 0.046726756 | 1704.202148 | -1.33419E-14 |

**Tab. 2-29**

| Linearity and errors for sensor #2 | | | | | |
|---|---|---|---|---|---|
| I [A] | $Vs_2$ [V] | Ieq. Regr. [A] | E%punt. Regr. | Ieq. EndP [A] | E%punt. EndP. |
| 101.6 | -0.0957 | 102.1193822 | 0.509424437 | 101.6017978 | -1.39868E-14 |
| 151.4 | -0.1432 | 151.6569855 | 0.189456952 | 151.143835 | -0.149546704 |
| 201.1 | -0.1909 | 201.5077217 | 0.226739794 | 200.999033 | -0.026273854 |
| 250.9 | -0.2385 | 251.1914537 | 0.104608581 | 250.687212 | -0.0963414 |
| 307.3 | -0.2923 | 307.3643403 | 0.019170849 | 306.8651263 | -0.143277941 |
| 357.3 | -0.3400 | 357.1242679 | -0.059433472 | 356.6295077 | -0.197891197 |
| 407.5 | -0.3880 | 407.1628837 | -0.082611422 | 406.6726022 | -0.202926037 |
| 457.6 | -0.4360 | 457.2954393 | -0.058674695 | 456.8096449 | -0.164844425 |
| 507.2 | -0.4836 | 506.947858 | -0.058490097 | 506.4665078 | -0.1533852 |
| 557.4 | -0.5315 | 556.9969115 | -0.07547661 | 556.5200409 | -0.161026576 |
| 607.6 | -0.5795 | 607.1085916 | -0.087574164 | 606.6362063 | -0.165315061 |
| 657.2 | -0.6272 | 656.9175767 | -0.04458925 | 656.4496495 | -0.115788222 |
| 707.2 | -0.6751 | 706.9248792 | -0.045537727 | 706.4614279 | -0.11106665 |
| 757.1 | -0.7230 | 756.8591174 | -0.037147586 | 756.4001355 | -0.097768041 |
| 806.6 | -0.7703 | 806.2819054 | -0.044500932 | 805.8273471 | -0.100852943 |
| 856.8 | -0.8183 | 856.3205212 | -0.055922496 | 855.8704416 | -0.108452822 |
| 906.5 | -0.8662 | 906.3904503 | -0.014245827 | 905.9448521 | -0.063400655 |
| 956.4 | -0.9138 | 956.0741823 | -0.0327615 | 955.633031 | -0.078888327 |
| 1006.4 | -0.9616 | 1005.904043 | -0.048099305 | 1005.467352 | -0.091491232 |
| 1105.8 | -1.0569 | 1105.375884 | -0.034422871 | 1104.948096 | -0.073110228 |
| 1206.0 | -1.1530 | 1205.693184 | -0.021431321 | 1205.274375 | -0.056159834 |
| 1304.6 | -1.2478 | 1304.653576 | 0.000938885 | 1304.243624 | -0.03048367 |

| Linearity and errors for sensor #2 | | | | | |
|---|---|---|---|---|---|
| I [A] | $Vs_2$ [V] | Ieq. Regr. [A] | E%punt. Regr. | Ieq. EndP [A] | E%punt. EndP. |
| 1404.6 | -1.3434 | 1404.480301 | -0.007916389 | 1404.079284 | -0.0364668 |
| 1503.4 | -1.4398 | 1505.096121 | 0.109584923 | 1504.70411 | 0.0835108 |
| 1604.1 | -1.5351 | 1604.495942 | 0.026661845 | 1604.112828 | 0.002777933 |
| 1704.2 | -1.6310 | 1704.576305 | 0.02195494 | 1704.202148 | 0 |

**Tab. 2-30**

| Linearity and errors for sensor #3 | | | | | |
|---|---|---|---|---|---|
| I [A] | $Vs_3$ [V] | Ieq. Regr. [A] | E%punt. Regr. | Ieq. EndP [A] | E%punt. EndP. |
| 101.6 | -0.0809 | 103.8611397 | 2.223722321 | 101.6017978 | 1.39868E-14 |
| 151.4 | -0.1206 | 152.4633035 | 0.722136379 | 150.2132984 | -0.764288953 |
| 201.1 | -0.1617 | 202.7912052 | 0.865124104 | 200.5508684 | -0.2491838 |
| 250.9 | -0.2020 | 252.0665292 | 0.453342946 | 249.8356585 | -0.435701753 |
| 307.3 | -0.2478 | 308.171369 | 0.28178538 | 305.9512765 | -0.440653052 |
| 357.3 | -0.2882 | 357.5078894 | 0.047922282 | 355.2972747 | -0.57071414 |
| 407.5 | -0.3288 | 407.2238273 | -0.067655924 | 405.0227634 | -0.607794929 |
| 457.6 | -0.3694 | 456.9152866 | -0.141756567 | 454.7237688 | -0.620709945 |
| 507.2 | -0.4100 | 506.6434638 | -0.118499452 | 504.4614991 | -0.548659762 |
| 557.4 | -0.4506 | 556.3104446 | -0.198627883 | 554.1380213 | -0.588357815 |
| 607.6 | -0.4915 | 606.3813215 | -0.207261681 | 604.2185171 | -0.563196414 |
| 657.2 | -0.5318 | 655.7056026 | -0.229001074 | 653.5522737 | -0.55664777 |
| 707.2 | -0.5728 | 705.8988723 | -0.190608264 | 703.7551859 | -0.493711224 |
| 757.1 | -0.6134 | 755.5658531 | -0.20795664 | 753.431708 | -0.489825781 |
| 806.6 | -0.6538 | 805.0492448 | -0.197314991 | 802.9246058 | -0.460708413 |
| 856.8 | -0.6946 | 854.9977289 | -0.210310078 | 852.8826854 | -0.457163997 |
| 906.5 | -0.7355 | 905.0563666 | -0.161411285 | 902.9509396 | -0.393665168 |
| 956.4 | -0.7760 | 954.6254332 | -0.18424289 | 952.5295288 | -0.403390922 |
| 1006.4 | -0.8168 | 1004.476003 | -0.189996823 | 1002.389675 | -0.397305292 |
| 1105.8 | -0.8978 | 1103.663093 | -0.189320532 | 1101.59582 | -0.376276092 |
| 1206.0 | -0.9799 | 1204.184265 | -0.146554053 | 1202.136302 | -0.316375334 |
| 1304.6 | -1.0634 | 1306.33326 | 0.129685689 | 1304.304921 | -0.025785318 |
| 1404.6 | -1.1451 | 1406.340382 | 0.124512183 | 1404.331255 | -0.018527768 |
| 1503.4 | -1.2270 | 1506.58005 | 0.208286574 | 1504.590179 | 0.075932843 |
| 1604.1 | -1.3083 | 1606.036404 | 0.122696531 | 1604.06564 | -0.000163829 |
| 1704.2 | -1.3901 | 1706.153679 | 0.114512874 | 1704.202148 | 0 |

**Tab. 2-31**

| Linearity and errors for sensor #4 | | | | | |
|---|---|---|---|---|---|
| I [A] | $Vs_4$ [V] | Ieq. Regr. [A] | E%punt. Regr. | Ieq. EndP [A] | E%punt. EndP. |
| 101.6 | -0.0826 | 102.5502498 | 0.933499271 | 101.6017978 | 0 |
| 151.4 | -0.1238 | 151.9398009 | 0.376293791 | 151.010623 | -0.237550838 |
| 201.1 | -0.1652 | 201.5569535 | 0.251226913 | 200.6471386 | -0.201300553 |
| 250.9 | -0.2070 | 251.5933722 | 0.264780841 | 250.703084 | -0.090016094 |
| 307.3 | -0.2536 | 307.4755589 | 0.055362391 | 306.6070785 | -0.227249068 |
| 357.3 | -0.2951 | 357.1645857 | -0.048150619 | 356.3154964 | -0.285766692 |
| 407.5 | -0.3371 | 407.5124593 | 0.003174101 | 406.6830181 | -0.200369977 |
| 457.6 | -0.3784 | 456.9259684 | -0.13942209 | 456.1158107 | -0.316480989 |
| 507.2 | -0.4200 | 506.7587436 | -0.095772792 | 505.9680331 | -0.251656279 |
| 557.4 | -0.4619 | 556.9628688 | -0.081583836 | 556.1917504 | -0.219921482 |
| 607.6 | -0.5037 | 606.9992875 | -0.105562439 | 606.2476957 | -0.229252604 |
| 657.2 | -0.5448 | 656.2930063 | -0.139622776 | 655.5606513 | -0.251056617 |
| 707.2 | -0.5868 | 706.5809847 | -0.094162114 | 705.8682545 | -0.194937418 |
| 757.1 | -0.6286 | 756.7012567 | -0.05799718 | 756.0080858 | -0.149548356 |
| 806.6 | -0.6698 | 806.0189335 | -0.077101795 | 805.3450087 | -0.160648864 |
| 856.8 | -0.7117 | 856.2470168 | -0.064501443 | 855.5926934 | -0.140869749 |
| 906.5 | -0.7532 | 905.9120856 | -0.067015198 | 905.2771439 | -0.137056894 |
| 956.4 | -0.7948 | 955.6849656 | -0.07345804 | 955.0694477 | -0.137816673 |
| 1006.4 | -0.8366 | 1005.841175 | -0.054346213 | 1005.24523 | -0.113562391 |
| 1105.8 | -0.9195 | 1105.111417 | -0.058340193 | 1104.554213 | -0.108731445 |
| 1206.0 | -1.0031 | 1205.208213 | -0.061646182 | 1204.690071 | -0.104611585 |
| 1304.6 | -1.0869 | 1305.604484 | 0.07382545 | 1305.125522 | 0.03711325 |
| 1404.6 | -1.1700 | 1405.19816 | 0.043191647 | 1404.758064 | 0.011858957 |
| 1503.4 | -1.2535 | 1505.163187 | 0.114045697 | 1504.762101 | 0.087368021 |
| 1604.1 | -1.3366 | 1604.7928 | 0.045168399 | 1604.430595 | 0.022588007 |
| 1704.2 | -1.4199 | 1704.525433 | 0.018969841 | 1704.202148 | 0 |

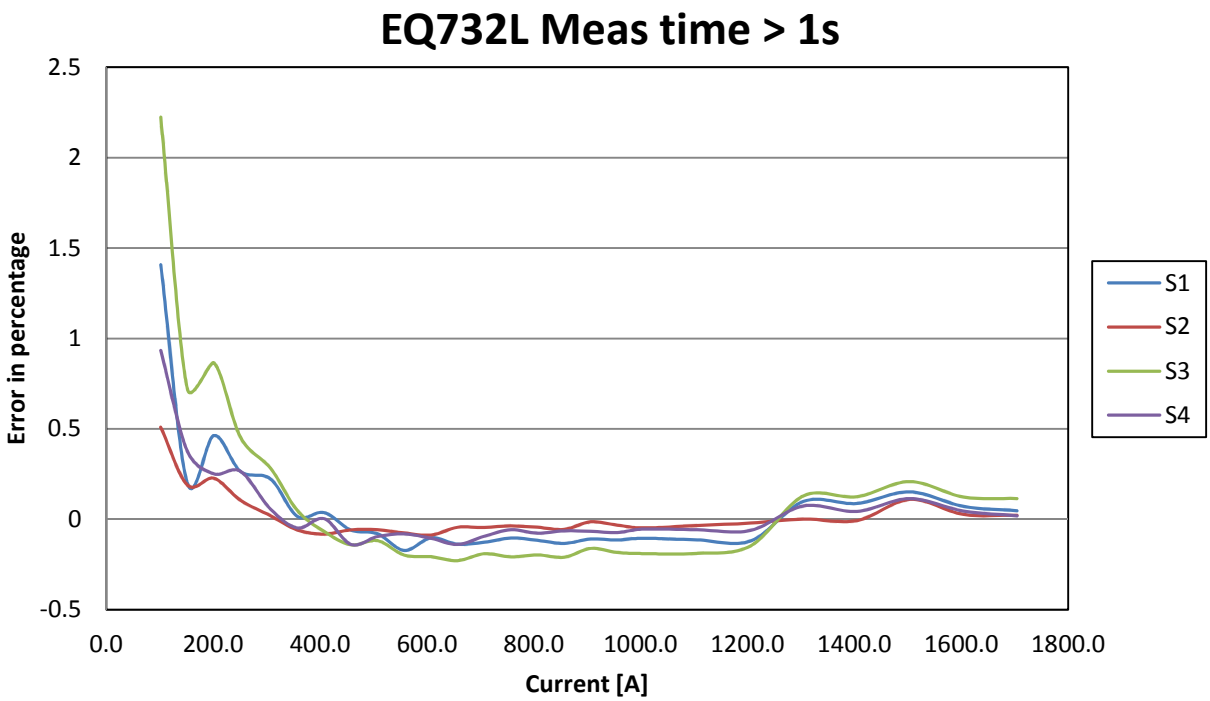


**Figure 2-21** Error in percentage referred to regression line (EQ732L sensors)

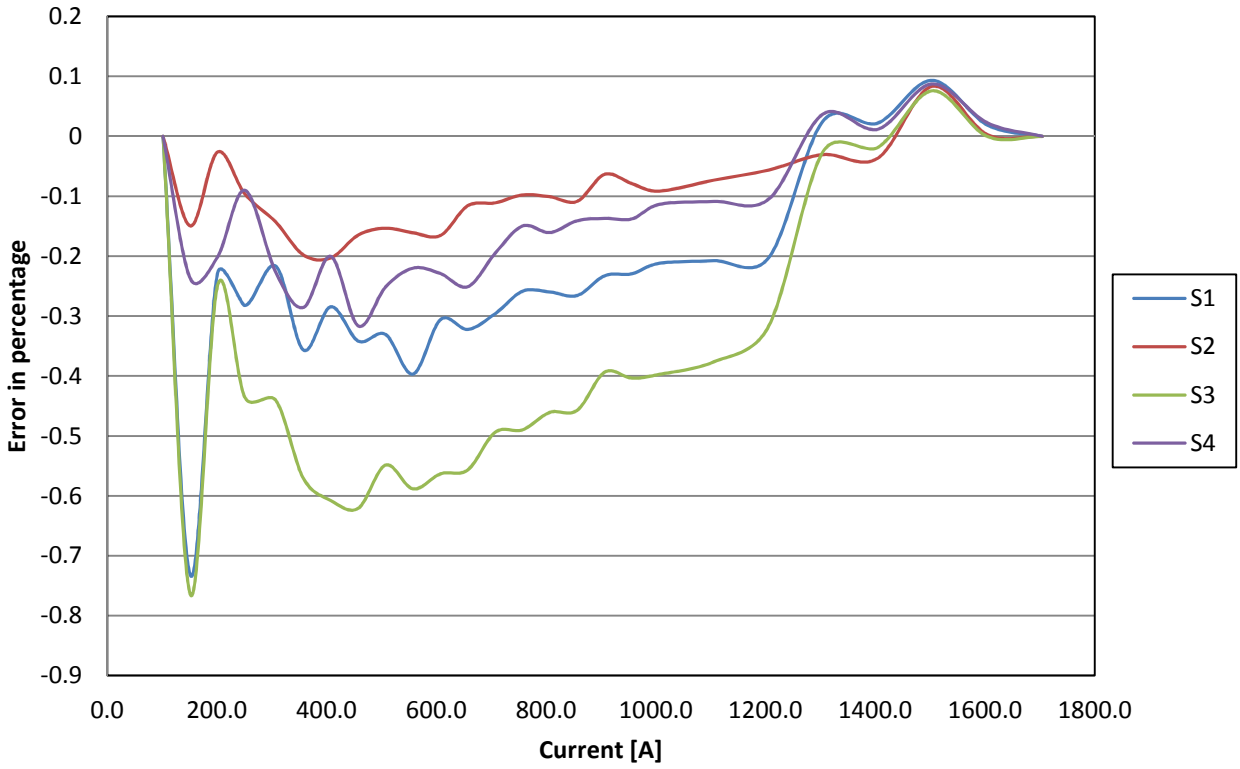


**Figure 2-22** Error in percentage referred to end points line (EQ732L sensors)

*viii.* *Current from 50A to 2500A, measurement time lower than 1 second*

We repeated the tests with the same sensors but now with a measurement time lower than 1 second.

**Tab. 2-32**

| Linearity and errors for sensor #1 | | | | | |
|---|---|---|---|---|---|
| I [A] | $Vs_1$ [mV] | Ieq. Regr. [A] | E%punt. Regr. | Ieq. EndP [A] | E%punt. EndP. |
| 52.1 | 0.0431 | 49.69913487 | -4.672202823 | 52.13498721 | -1.36289E-14 |
| 101.8 | 0.08452 | 99.52031625 | -2.267598352 | 102.0378702 | 0.204726946 |
| 151.6 | 0.12627 | 149.7384312 | -1.246462869 | 152.3383378 | 0.468193569 |
| 201.4 | 0.16816 | 200.1249423 | -0.621964095 | 202.8074775 | 0.710129142 |
| 251.3 | 0.20988 | 250.3069724 | -0.377944259 | 253.071801 | 0.722456209 |
| 306.9 | 0.25637 | 306.2264973 | -0.234294987 | 309.0830282 | 0.696335838 |
| 357.0 | 0.29844 | 356.8295176 | -0.05742351 | 359.7690323 | 0.765890294 |
| 407.8 | 0.34086 | 407.8535281 | 0.015729867 | 410.8767169 | 0.757090213 |
| 457.2 | 0.38218 | 457.5544266 | 0.069242724 | 460.6591197 | 0.748253296 |
| 507.5 | 0.4239 | 507.7364567 | 0.039709979 | 510.9234432 | 0.667644421 |
| 607.3 | 0.50774 | 608.5816486 | 0.202815531 | 611.9340109 | 0.754781141 |
| 707.0 | 0.5912 | 708.9697654 | 0.277602547 | 712.4867539 | 0.775049959 |
| 806.5 | 0.67421 | 808.8166091 | 0.2843207 | 812.4973362 | 0.74069018 |
| 906.8 | 0.75739 | 908.8679337 | 0.228582221 | 912.7127347 | 0.652581063 |
| 1006.4 | 0.84063 | 1008.991428 | 0.261221487 | 1013.000421 | 0.659586178 |
| 1504.9 | 1.25656 | 1509.284136 | 0.293099118 | 1514.113558 | 0.614017944 |
| 2004.1 | 1.66877 | 2005.10232 | 0.051358267 | 2010.744833 | 0.332910519 |
| 2504.1 | 2.07829 | 2497.684894 | -0.257585842 | 2504.135192 | 0 |

**Tab. 2-33**

| Linearity and errors for sensor #2 | | | | | |
|---|---|---|---|---|---|
| I [A] | $Vs_2$ [mV] | Ieq. Regr. [A] | E%punt. Regr. | Ieq. EndP [A] | E%punt. EndP. |
| 52.1 | 0.04148 | 51.36409454 | -1.478647481 | 52.13498721 | -1.36289E-14 |
| 101.8 | 0.08015 | 100.136574 | -1.662411919 | 101.0326103 | -0.78247313 |
| 151.6 | 0.12002 | 150.4225516 | -0.795280753 | 151.4476151 | -0.119244242 |
| 201.4 | 0.15954 | 200.2670922 | -0.551375301 | 201.4200502 | 0.02116052 |
| 251.3 | 0.19933 | 250.4521699 | -0.320155713 | 251.7338961 | 0.189970704 |
| 306.9 | 0.2438 | 306.5398906 | -0.132194405 | 307.9655305 | 0.332265608 |
| 357.0 | 0.28328 | 356.3339813 | -0.196215767 | 357.8873862 | 0.238869547 |
| 407.8 | 0.32399 | 407.6794077 | -0.026968752 | 409.3645581 | 0.386271625 |
| 457.2 | 0.36338 | 457.359986 | 0.026717683 | 459.1726102 | 0.42314686 |
| 507.5 | 0.40343 | 507.8729884 | 0.066610918 | 509.8152221 | 0.449290755 |
| 607.3 | 0.48273 | 607.8899942 | 0.08893482 | 610.0888584 | 0.450977245 |

| Linearity and errors for sensor #2 | | | | | |
|---|---|---|---|---|---|
| I [A] | $Vs_2$ [mV] | Ieq. Regr. [A] | E%punt. Regr. | Ieq. EndP [A] | E%punt. EndP. |
| 707.0 | 0.56201 | 707.8817752 | 0.1237158 | 710.3372049 | 0.471014965 |
| 806.5 | 0.64076 | 807.2050944 | 0.084510686 | 809.9153745 | 0.420555472 |
| 906.8 | 0.72089 | 908.2689365 | 0.162525711 | 911.238533 | 0.49000833 |
| 1006.4 | 0.79969 | 1007.655318 | 0.128455224 | 1010.879927 | 0.448877386 |
| 1504.9 | 1.19814 | 1510.199782 | 0.353944492 | 1514.713853 | 0.653908007 |
| 2004.1 | 1.59225 | 2007.270428 | 0.159543316 | 2013.059916 | 0.448429401 |
| 2504.1 | 1.98061 | 2497.088894 | -0.281386455 | 2504.135192 | 0 |

**Tab. 2-34**

| Linearity and errors for sensor #3 | | | | | |
|---|---|---|---|---|---|
| I [A] | $Vs_3$ [mV] | Ieq. Regr. [A] | E%punt. Regr. | Ieq. EndP [A] | E%punt. EndP. |
| 52.1 | 0.05125 | 48.2593959 | -7.433762843 | 52.13498721 | 1.36289E-14 |
| 101.8 | 0.10055 | 98.34766542 | -3.419182128 | 102.3948899 | 0.555332625 |
| 151.6 | 0.15025 | 148.8423306 | -1.837447447 | 153.0625808 | 0.945836884 |
| 201.4 | 0.19999 | 199.3776354 | -0.993061713 | 203.7710505 | 1.188620184 |
| 251.3 | 0.24962 | 249.8011814 | -0.579248843 | 254.3673785 | 1.238095428 |
| 306.9 | 0.30459 | 305.6501099 | -0.422076579 | 310.4076797 | 1.127894795 |
| 357.0 | 0.35463 | 356.4902115 | -0.152458063 | 361.4219906 | 1.228859044 |
| 407.8 | 0.40501 | 407.6757494 | -0.027865865 | 412.7829216 | 1.224538546 |
| 457.2 | 0.45397 | 457.4185825 | 0.039533007 | 462.6962042 | 1.193772973 |
| 507.5 | 0.50398 | 508.2282044 | 0.136599413 | 513.679931 | 1.21075736 |
| 607.3 | 0.6033 | 609.1362557 | 0.294131455 | 614.9337552 | 1.248688292 |
| 707.0 | 0.70214 | 709.5566322 | 0.360609744 | 715.6982335 | 1.229285796 |
| 806.5 | 0.80063 | 809.6214124 | 0.384107413 | 816.105897 | 1.188111844 |
| 906.8 | 0.90008 | 910.6615423 | 0.426378658 | 917.4922524 | 1.179659046 |
| 1006.4 | 0.99865 | 1010.807602 | 0.441690583 | 1017.981474 | 1.154542193 |
| 1504.9 | 1.49177 | 1511.812216 | 0.461091938 | 1520.702837 | 1.051880593 |
| 2004.1 | 1.98046 | 2008.315997 | 0.211715537 | 2018.907945 | 0.74023657 |
| 2504.1 | 2.45642 | 2491.886236 | -0.489149147 | 2504.135192 | 0 |

**Tab. 2-34**

| Linearity and errors for sensor #4 | | | | | |
|---|---|---|---|---|---|
| I [A] | $Vs_4$ [mV] | Ieq. Regr. [A] | E%punt. Regr. | Ieq. EndP [A] | E%punt. EndP. |
| 52.1 | 0.04746 | 49.86279442 | -4.358287816 | 52.13498721 | 2.72578E-14 |
| 101.8 | 0.09287 | 99.60229404 | -2.187093323 | 101.9764499 | 0.144410086 |
| 151.6 | 0.13887 | 149.9880457 | -1.081840401 | 152.4654894 | 0.552050991 |
| 201.4 | 0.18464 | 200.1218686 | -0.62349044 | 202.7020838 | 0.657792714 |
| 251.3 | 0.23067 | 250.5404805 | -0.285008146 | 253.2240509 | 0.7830516 |
| 306.9 | 0.2813 | 305.9976676 | -0.308845558 | 308.794922 | 0.602473558 |

| Linearity and errors for sensor #4 | | | | | |
|---|---|---|---|---|---|
| I [A] | $Vs_4$ [mV] | Ieq. Regr. [A] | E%punt. Regr. | Ieq. EndP [A] | E%punt. EndP. |
| 357.0 | 0.32746 | 356.558674 | -0.133282723 | 359.4595756 | 0.679216137 |
| 407.8 | 0.37413 | 407.6783051 | -0.027239129 | 410.683999 | 0.709831027 |
| 457.2 | 0.41969 | 457.5821061 | 0.07529636 | 460.6900998 | 0.755028785 |
| 507.5 | 0.46577 | 508.0554851 | 0.102568402 | 511.2669464 | 0.735325115 |
| 607.3 | 0.55767 | 608.7174542 | 0.225175895 | 612.1352666 | 0.787917855 |
| 707.0 | 0.64889 | 708.6345904 | 0.230194967 | 712.2572272 | 0.742585408 |
| 806.5 | 0.74004 | 808.4750527 | 0.241971478 | 812.3023566 | 0.716514868 |
| 906.8 | 0.83136 | 908.5017231 | 0.188197066 | 912.5340759 | 0.63287884 |
| 1006.4 | 0.92255 | 1008.385999 | 0.201061351 | 1012.623109 | 0.622093474 |
| 1504.9 | 1.38078 | 1510.304759 | 0.360920317 | 1515.570774 | 0.710851033 |
| 2004.1 | 1.83336 | 2006.034835 | 0.097889253 | 2012.317067 | 0.411362457 |
| 2504.1 | 2.28145 | 2496.846823 | -0.291053302 | 2504.135192 | 1.81599E-14 |

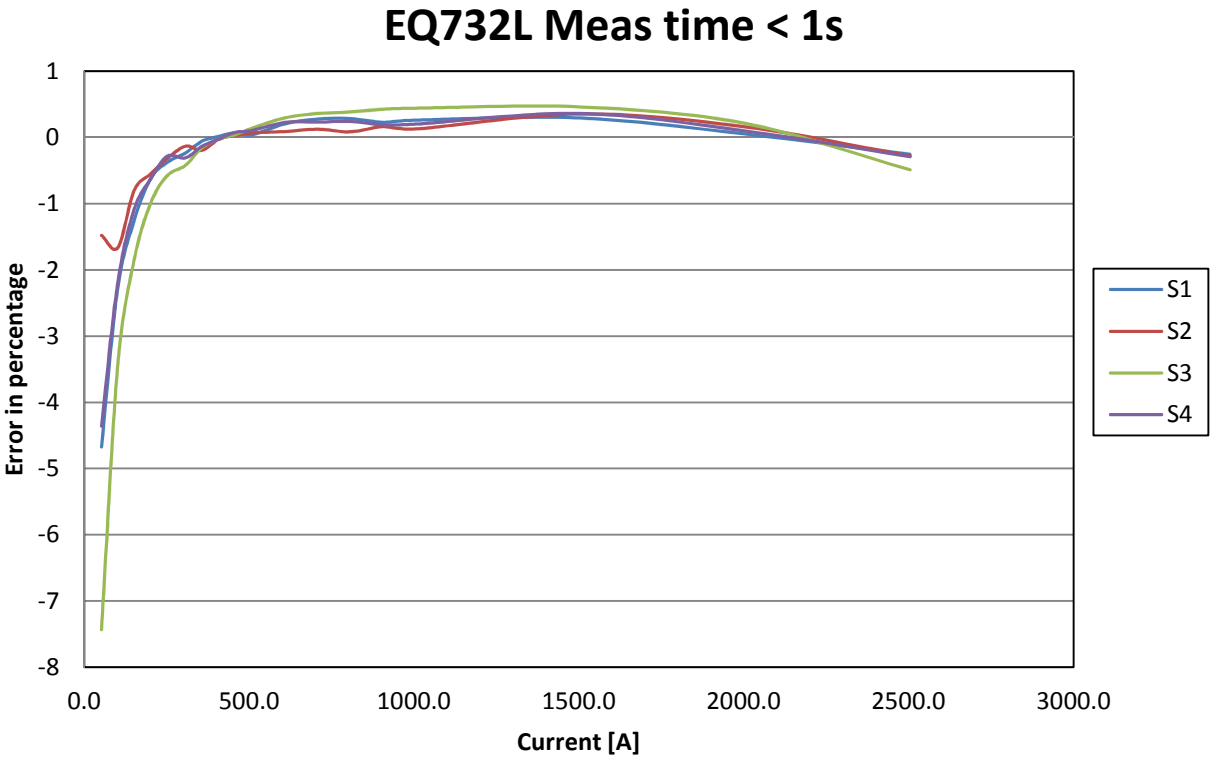


**Figure 2-23** Error in percentage referred to regression line (EQ732L sensors)

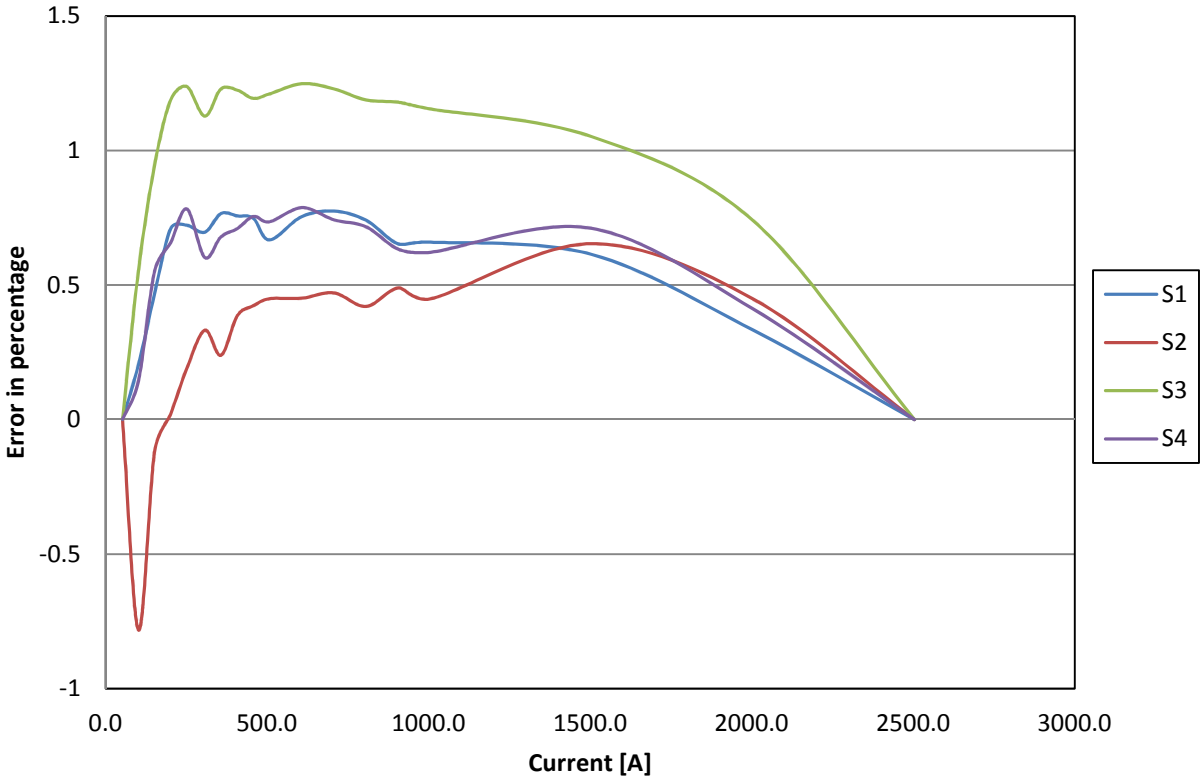


**Figure 2-24** Error in percentage referred to end points line (EQ732L sensors)

## 2.7.1. Temperature Test

THE TEMPERATURE TEST concludes the investigation performed on EQ732L sensors and it also completes the experimental activity on Hall-effect sensors. The sensors and the bar are put inside the climatic chamber, and we started with 20$^0$C, went down to -20$^0$C, up again until we reached 100$^0$C, and to conclude the test back to 20$^0$C to look for hysteresis. In this case we used the 500A DC current generator because as stated earlier it generated a more stable output. Again we measured the output of the generator with the LEM transducer to double check the on-screen value.

The tables below show the measures for both cases; first the generator was off (offset voltage) and second the generator output was 500A (gain voltage). We did the experiment for 8 sensors, mounted 4 at a time on two separated boards.

**Tab. 2-35 (1st batch of sensors)**

| Temp [°C] | I [A] | $Vs_1$ [V] | $Vs_2$ [V] | $Vs_3$ [V] | $Vs_4$ [V] | $V_{LEM}$ [mV] | $I_{LEM}$ [A] |
|---|---|---|---|---|---|---|---|
| 20 | 0 | 2.50821 | 2.49225 | 2.50691 | 2.48836 | | 0.7 |
| 20 | 500 | 2.97172 | 2.98758 | 2.90845 | 2.90907 | 98.0695 | 501.2 |
| 0 | 0 | 2.50841 | 2.49297 | 2.50645 | 2.48809 | | 0.7 |
| 0 | 500 | 2.97102 | 2.98755 | 2.90748 | 2.90752 | 98.0484 | 501.1 |
| -20 | 0 | 2.50847 | 2.49405 | 2.50583 | 2.48756 | | 0.7 |
| -20 | 500 | 2.97128 | 2.98975 | 2.90604 | 2.90545 | 98.0543 | 501.1 |
| 0 | 0 | 2.50845 | 2.49347 | 2.50644 | 2.48836 | | 0.7 |
| 0 | 500 | 2.97116 | 2.98889 | 2.90652 | 2.90693 | 98.0073 | 500.9 |
| 20 | 0 | 2.50866 | 2.49286 | 2.50669 | 2.48942 | | 0.7 |
| 20 | 500 | 2.97175 | 2.98921 | 2.90782 | 2.90927 | 98.0352 | 501.0 |
| 40 | 0 | 2.50866 | 2.49217 | 2.5069 | 2.49072 | | 0.7 |
| 40 | 500 | 2.97323 | 2.99051 | 2.90923 | 2.91239 | 98.0467 | 501.1 |
| 60 | 0 | 2.50955 | 2.49238 | 2.50668 | 2.49137 | | 0.7 |
| 60 | 500 | 2.97492 | 2.99177 | 2.91019 | 2.91459 | 98.0502 | 501.1 |
| 80 | 0 | 2.50995 | 2.49289 | 2.50655 | 2.49132 | | 0.7 |
| 80 | 500 | 2.97553 | 2.99202 | 2.91043 | 2.91528 | 98.0529 | 501.1 |
| 100 | 0 | 2.50937 | 2.49308 | 2.50717 | 2.49159 | | 0.7 |
| 100 | 500 | 2.97346 | 2.98964 | 2.90971 | 2.91484 | 98.0543 | 501.1 |
| 20 | 0 | 2.50967 | 2.49224 | 2.5063 | 2.48925 | | 0.7 |
| 20 | 500 | 2.97332 | 2.98953 | 2.90706 | 2.91117 | 98.0595 | 501.1 |

***Note:*** *the black values correspond to the offset voltage, and the red values to the gain voltage.*

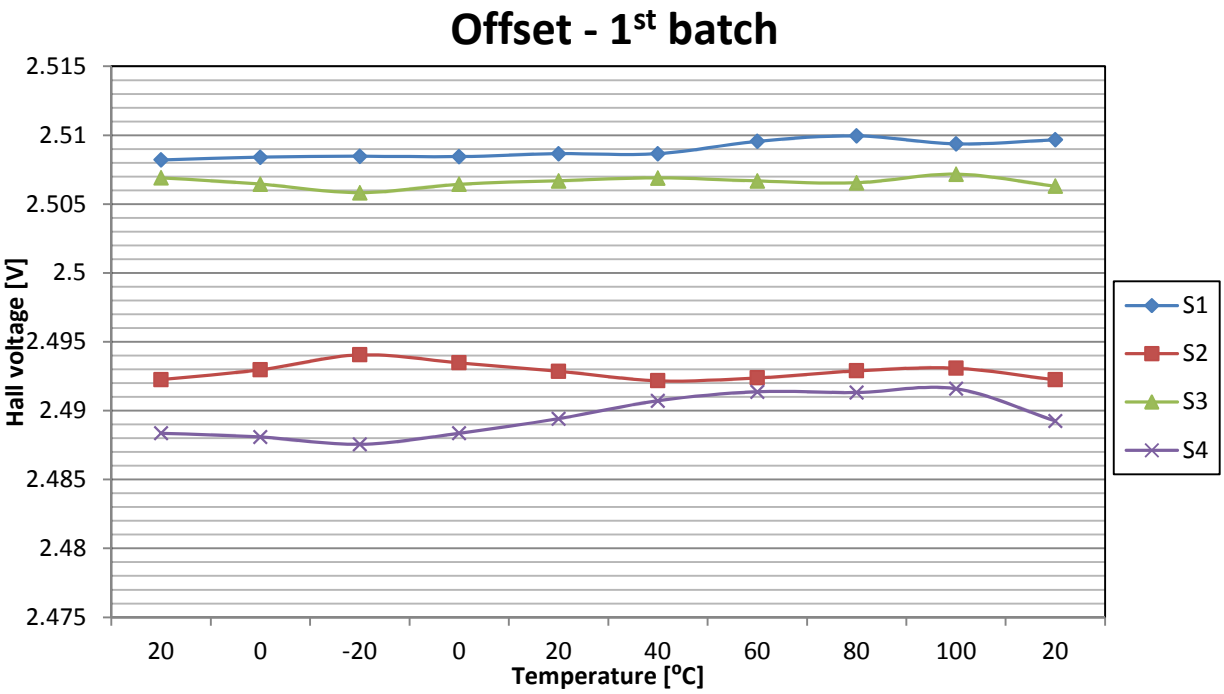
Offset - 1st batch
Hall voltage [V]
2.515
2.51
2.505
2.5
2.495
2.49
2.485
2.48
2.475
20
0
-20
0
20
40
60
80
100
20
Temperature [°C]
S1
S2
S3
S4

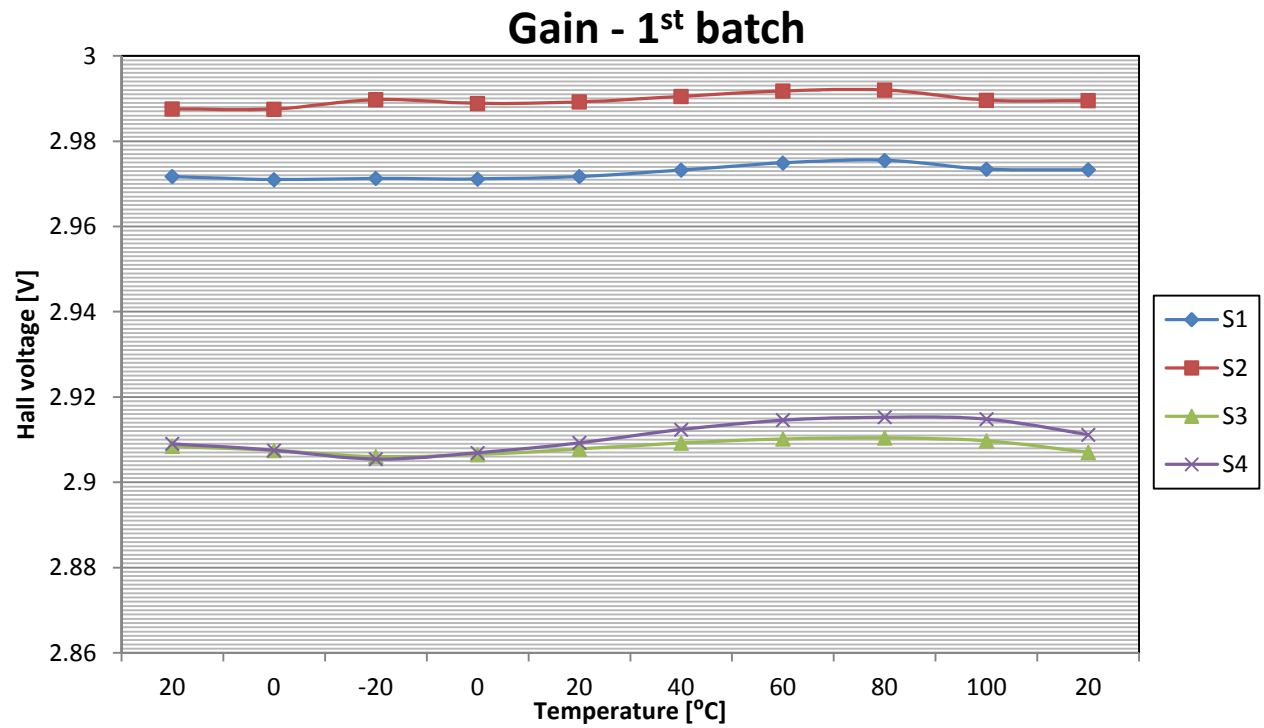
Gain - 1st batch
Hall voltage [V]
3
2.98
2.96
2.94
2.92
2.9
2.88
2.86
20
0
-20
0
20
40
60
80
100
20
Temperature [°C]
S1
S2
S3
S4

**Tab. 2-36 (2nd batch of sensors)**

| Temp [°C] | I [A] | $Vs_1$ [V] | $Vs_2$ [V] | $Vs_3$ [V] | $Vs_4$ [V] | $V_{LEM}$ [mV] | $I_{LEM}$ [A] |
|---|---|---|---|---|---|---|---|
| 20 | 0 | 2.4903 | 2.4881 | 2.49608 | 2.48277 | | 0.7 |
| 20 | 500 | 2.87936 | 2.9513 | 2.9931 | 2.90914 | 98.0496 | 501.1 |
| 0 | 0 | 2.49074 | 2.48915 | 2.49717 | 2.48105 | | 0.7 |
| 0 | 500 | 2.87769 | 2.95066 | 2.9924 | 2.90621 | 98.0525 | 501.1 |
| -20 | 0 | 2.49059 | 2.49066 | 2.49855 | 2.47935 | | 0.7 |
| -20 | 500 | 2.87636 | 2.95082 | 2.99489 | 2.90295 | 98.0441 | 501.0 |
| 0 | 0 | 2.4906 | 2.48943 | 2.4976 | 2.48016 | | 0.7 |
| 0 | 500 | 2.87639 | 2.95031 | 2.99441 | 2.90419 | 98.0532 | 501.1 |
| 20 | 0 | 2.49057 | 2.48865 | 2.49695 | 2.48157 | | 0.7 |
| 20 | 500 | 2.87725 | 2.95054 | 2.99445 | 2.90666 | 98.0477 | 501.1 |
| 40 | 0 | 2.49081 | 2.4881 | 2.49622 | 2.48348 | | 0.7 |
| 40 | 500 | 2.87888 | 2.95019 | 2.99504 | 2.91006 | 98.0448 | 501.1 |
| 60 | 0 | 2.49148 | 2.4872 | 2.49579 | 2.48699 | | 0.7 |
| 60 | 500 | 2.88148 | 2.95101 | 2.99563 | 2.91471 | 98.0509 | 501.1 |
| 80 | 0 | 2.49242 | 2.48689 | 2.49625 | 2.48941 | | 0.7 |
| 80 | 500 | 2.8838 | 2.95171 | 2.99609 | 2.91677 | 98.0539 | 501.1 |
| 100 | 0 | 2.49257 | 2.48551 | 2.49538 | 2.48989 | | 0.7 |
| 100 | 500 | 2.8848 | 2.95044 | 2.99302 | 2.91807 | 98.0583 | 501.1 |
| 20 | 0 | 2.49193 | 2.48797 | 2.49733 | 2.4872 | | 0.7 |
| 20 | 500 | 2.88405 | 2.9501 | 2.99292 | 2.91836 | 98.0539 | 501.1 |

***Note:*** *the black values correspond to the offset voltage, and the red values to the gain voltage.*

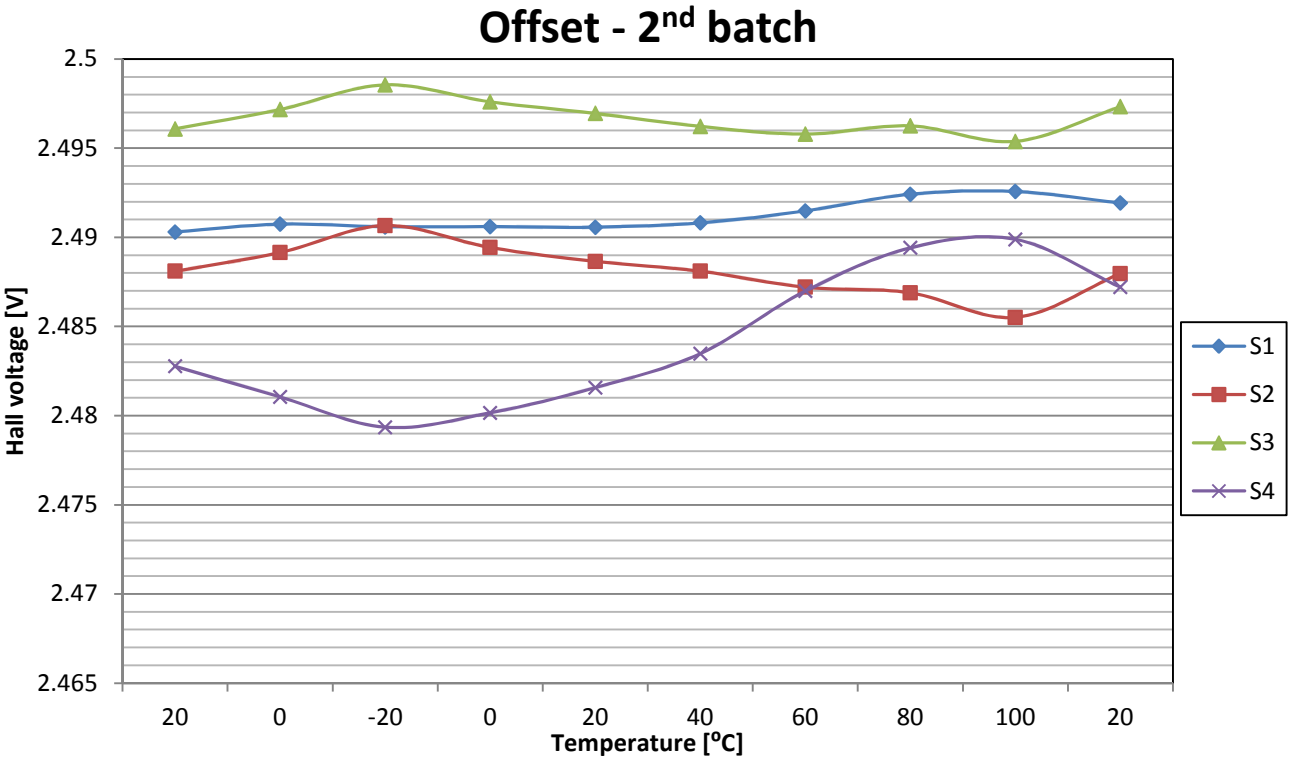
Offset - 2nd batch
Hall voltage [V]
2.5
2.495
2.49
2.485
2.48
2.475
2.47
2.465
20
0
-20
0
20
40
60
80
100
20
Temperature [°C]
S1
S2
S3
S4

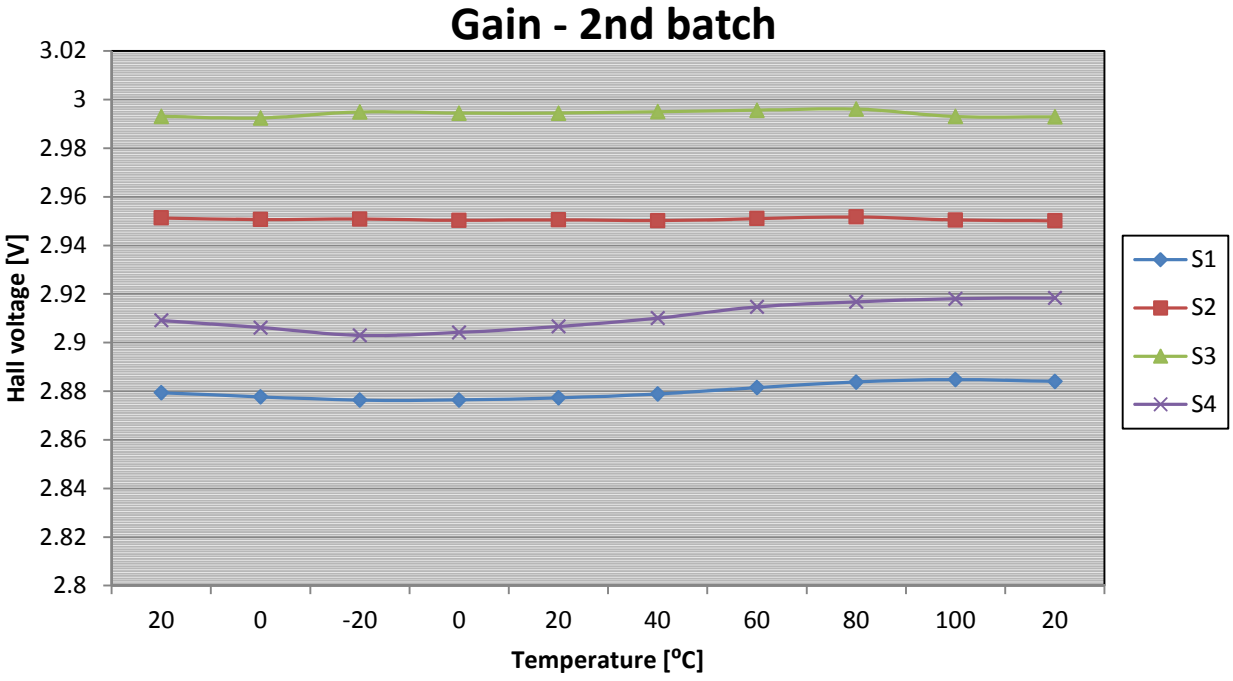
Gain - 2nd batch
Hall voltage [V]
3.02
3
2.98
2.96
2.94
2.92
2.9
2.88
2.86
2.84
2.82
2.8
20
0
-20
0
20
40
60
80
100
20
Temperature [°C]
S1
S2
S3
S4

## 2.8 Conclusions

NOW LET'S PUT together the two cases, that are the tests done with the generator able to go up to 2500A and the one that can generate up to 500A, and see if there is any repeatability of the measures. In order to compare the two cases, we discard the values greater the 500A from the measures collected for case#1, and recalculate the error in percentage referred to a new regression and endpoints line.

We show the graphics for case#1, first and immediately after for case#2. In this comparative analysis we show the error of only one sensor per batch, and that is sensor #1.

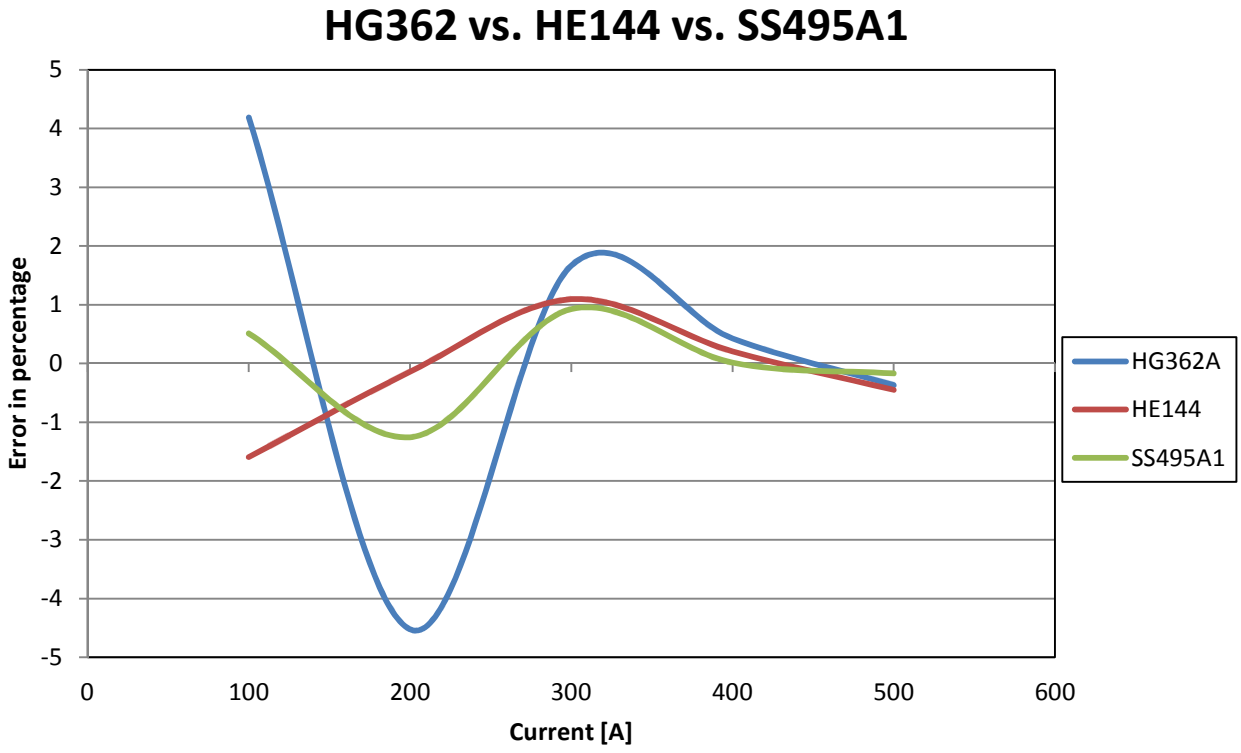


**Figure 2-25** Error in percentage referred to regression line (case#1)

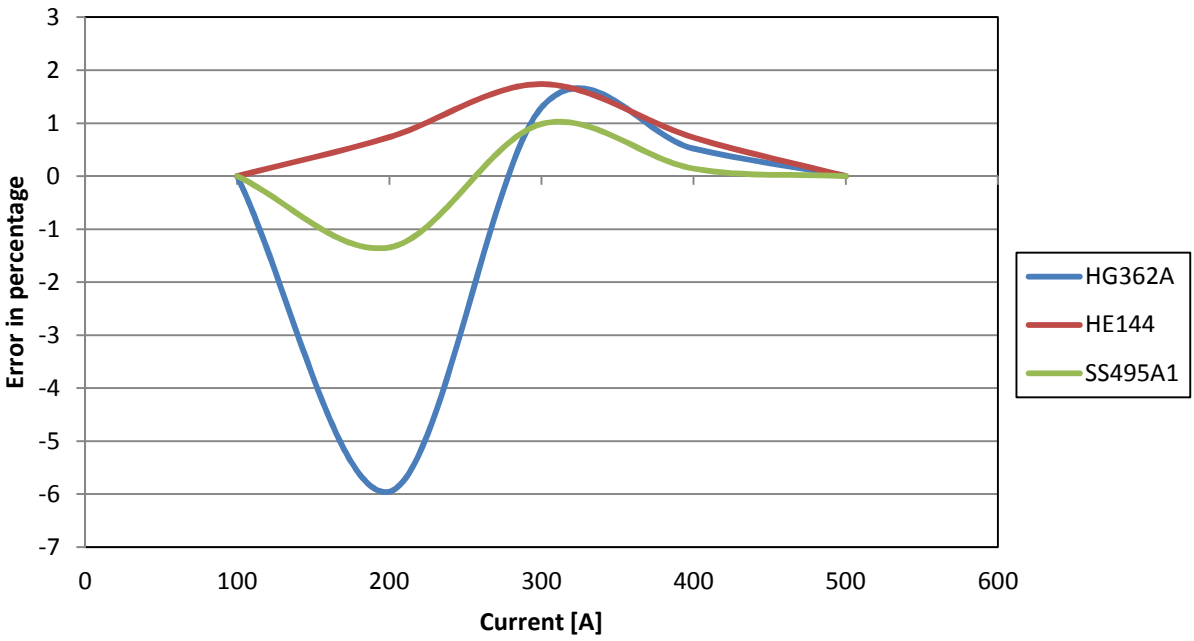


**Figure 2-26** Error in percentage referred to endpoints line (case#1)

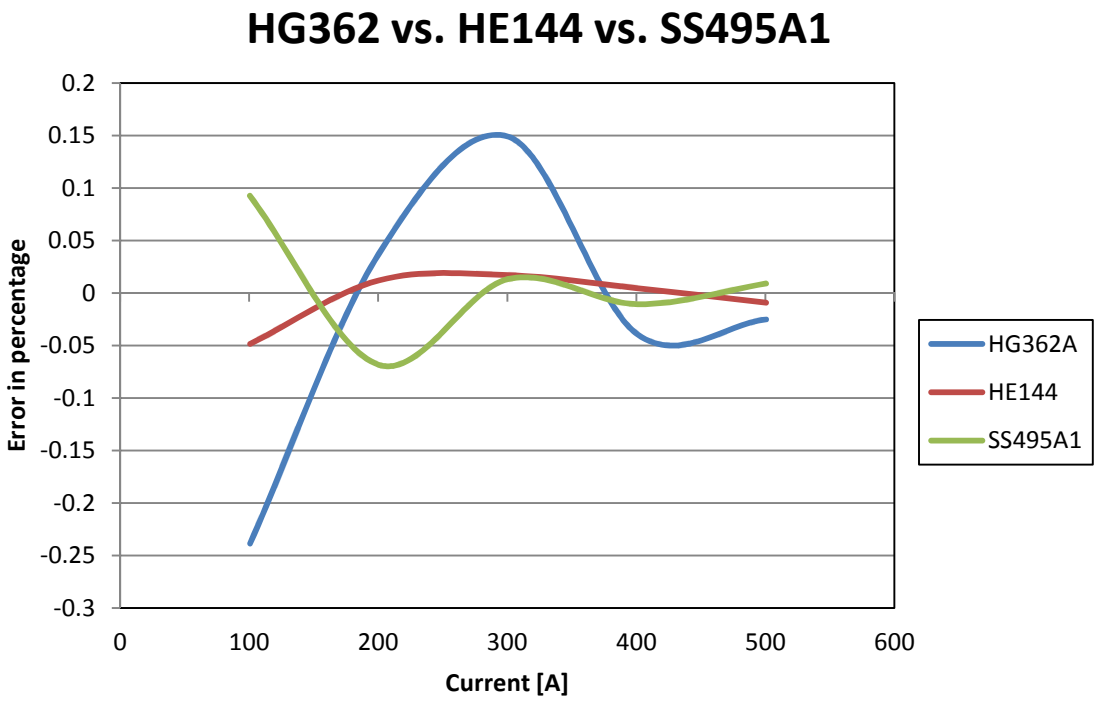


**Figure 2-27** Error in percentage referred to regression line (case#2)

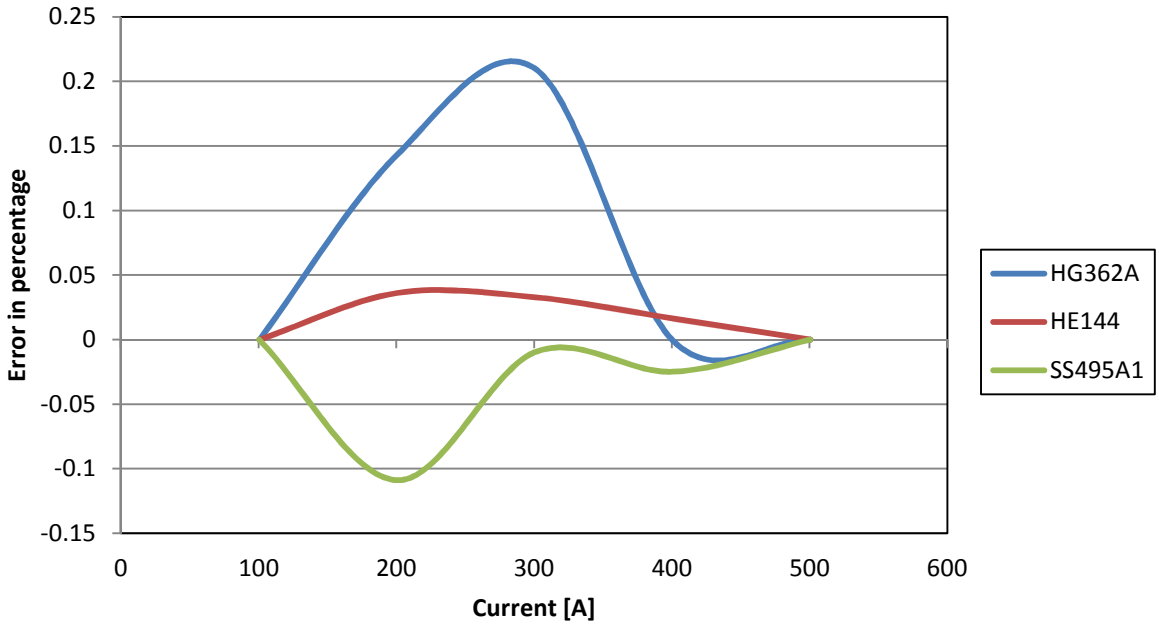


**Figure 2-28** Error in percentage referred to endpoints line (case#2)

From the graphs shown above we can immediately notice that in both cases the curves have the same trend. At smaller currents the error is greater with respect to higher currents, and for all the sensors the error oscillates before it becomes stable at increasing values of currents. Also is interesting to see that in case#1 the error in absolute value is greater than that in case#2, and since only the generator has changed in the experimental setup, that might be attributed to the fact that the first generator was not very stable. At last it is pretty obvious that the HG362A sensor compared to the other ones has the greater error even though it is well below 0.5% in case#2.

Conclusions EQ732L

From the first tests where we used different measuring times the graphs immediately show that sensor #3 had offset problems. Also it can be easily identified the same trend that at lower currents the error is greater and with higher currents it is lower.

The temperature test gives a good picture of the thermal drift of these sensors, especially for the first batch where the curves are almost perfectly constant during all the temperature range in which these sensors were tested. On the other hand the second batch wasn't as good as first one. We find the same offset for sensor #1, while the other three have much greater deviations with respect to the first batch.

Overall EQ372L sensors are quite linear and have a good immunity to temperature variations.

# 3

# Rogowski Coil

IN THIS CHAPTER we show the tests performed on two types of Rogowski coils, from two different manufacturers. The coils have a non-circular geometry. The purpose of these tests is to evaluate the crosstalk rejection of these new Rogowski coils designs. All the measurements were done at Dipartimento di Elettrotecnica of Politecnico di Milano, but this time the measurement setup was located at the Precision Measurements Laboratory which has a temperature of $23^0$C ±0.5 $^0$C and a relative humidity of 50% ±5%. The equipments used in this case were a current generator able to generate a current signal with a frequency that goes up to 5 kHz, and a FLUKE 8508A which is a very high accuracy digital multimeter. The experimental setup was the same for the two coils, and it consisted of a cylindrical bar with a diameter of six millimeters fixed on a mechanical platform that was able to move the bar with 0.5 millimeter steps on specified paths along the coils. With the aid of a caliber we took the exact measures of the casings of both coils, in order to refer all the measurements to the same center point. As the bar displaced along designated paths with 0.5 millimeter steps we measured the output voltage of the coil at each step, and then calculated the relative error with respect to the voltage measured at the center of each coil. The bar was fed in both cases with 30 Amperes @1kHz and the outputs of the coils were filtered with a low-pass second order filter with a gain of 20dB, and a cut-off frequency of 2kHz.

The tets consisted of two different scenarios:

i. The bar was displaced along a specified region at the top of the coil
ii. The bar was displaced along a specified region at the side of the coil

These two regions are enough to have a full view of the influence of an external bar right next to the coils.

The results of the tests for both coils are reported below.

***Note.*** *We will be referring to the air core coil as* ***Type A*** *and to the one that has a current transformer (CT) as* ***Type B****, although we removed the CT from the second coil for reasons that we explain later.*

## 3.1. Type A Rogowski Coil

BELOW ARE SHOWN the measurement results for the case of the first Rogowski coil that we tested. The calculation of the coordinates was done with the ***XY*** axis referred to the center point of the coil, and taking into account that the bar had a diameter of 6 mm. So each point given by its ***x,y*** coordinates identifies the position of the center of the bar against the center point of the coil which correspondents to the origin of the ***x,y*** plan.

*i.* *Case # 1 – the bar moves along the region at the top of the coil*

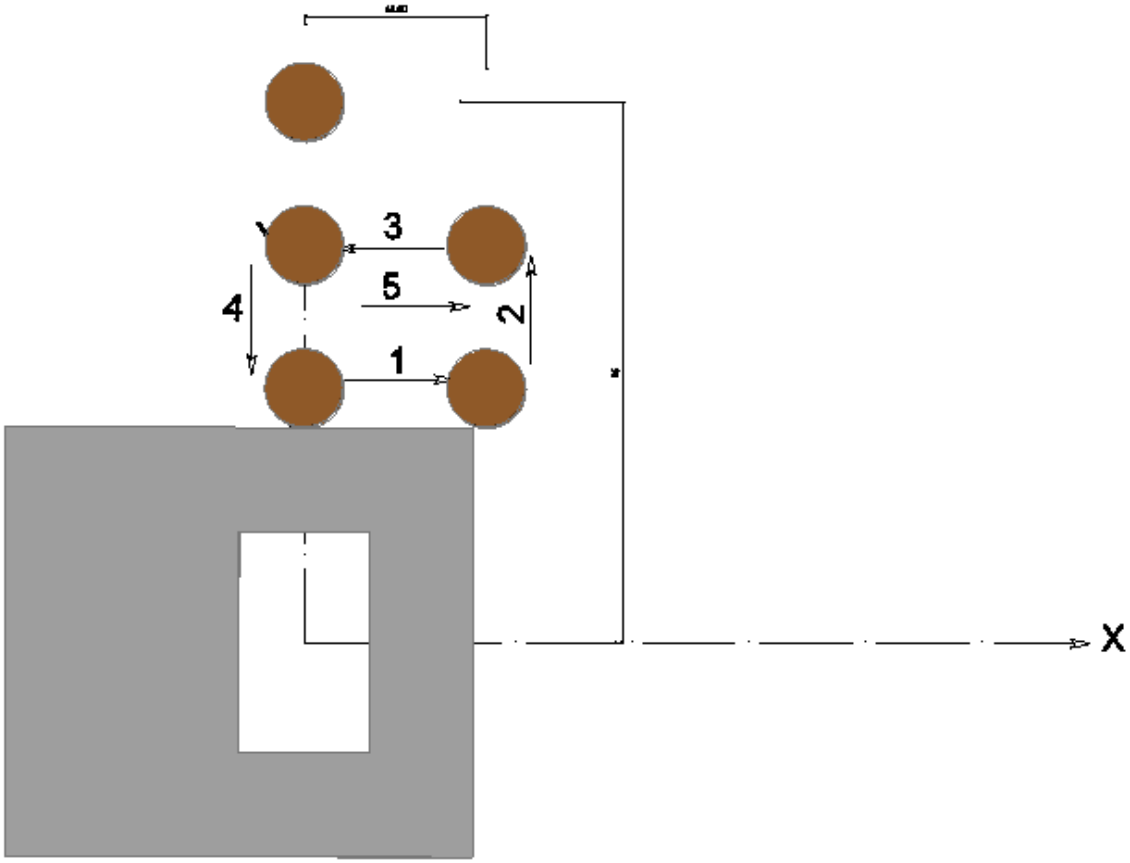


**Figure 3-1** Type A coil, case#1

We have divided the top region in 5 paths. The arrows show the displacement of the bar along these paths. From the starting point, @ ***x=0, y= 19.5*** mm, the bar was displaced along path #1 up to ***x=14mm*** while the ***y*** coordinate was fixed at 19.5 mm. During this first path the bar was touching the coil. Then we went up 5 mm along path #2 while the ***x*** coordinate was kept at 14 mm. Path #3 is the same as path #1 but @ ***y=24.5***

mm and then we turned at the starting point along path #4. At last we repositioned the bar @ ***x=0 mm, y=21.5 mm*** from the center of the coil, in order to go along path #5.

While at this region, we took a particular measure; after repositioning the bar at the starting point, we modified the setup slightly to place the bar @ ***x=0 mm, y=35 mm*** from the center of the coil. The reading was 5.314mV.

The following tables show the values obtained from the experimental test.

**Path #1**

| X [mm] | Y [mm] | Vrogowski [mV] | Relative error [%] |
|---|---|---|---|
| 0 | 19.50 | 66.628 | 2.786266884 |
| 0.5 | 19.50 | 66.915 | 2.798268724 |
| 1 | 19.50 | 67.198 | 2.810103291 |
| 1.5 | 19.50 | 67.174 | 2.809099653 |
| 2 | 19.50 | 66.723 | 2.790239619 |
| 2.5 | 19.50 | 65.855 | 2.753941371 |
| 3 | 19.50 | 64.458 | 2.695521265 |
| 3.5 | 19.50 | 62.519 | 2.614435663 |
| 4 | 19.50 | 59.736 | 2.498055451 |
| 4.5 | 19.50 | 56.088 | 2.345502446 |
| 5 | 19.50 | 52.132 | 2.180069418 |
| 5.5 | 19.50 | 47.118 | 1.970392673 |
| 6 | 19.50 | 41.996 | 1.756199557 |
| 6.5 | 19.50 | 35.804 | 1.497260904 |
| 7 | 19.50 | 28.941 | 1.2102622 |
| 7.5 | 19.50 | 21.982 | 0.919248944 |
| 8 | 19.50 | 13.776 | 0.57608832 |
| 8.5 | 19.50 | 6.255 | 0.261573203 |
| 9 | 19.50 | 0.946 | 0.039560072 |
| 9.5 | 19.50 | 9.176 | 0.383724334 |
| 10 | 19.50 | 16.982 | 0.710157655 |
| 10.5 | 19.50 | 24.503 | 1.024672772 |
| 11 | 19.50 | 31.049 | 1.298415088 |
| 11.5 | 19.50 | 34.402 | 1.438631707 |
| 12 | 19.50 | 36.649 | 1.532597332 |
| 12.5 | 19.50 | 37.935 | 1.586375612 |
| 13 | 19.50 | 38.443 | 1.607619287 |
| 13.5 | 19.50 | 38.281 | 1.600844729 |
| 14 | 19.50 | 37.585 | 1.571739221 |

**Path #3**

| X [mm] | Y [mm] | Vrogowski [mV] | Relative error [%] |
|---|---|---|---|
| 14 | 24.5 | 9.616 | 0.402124367 |
| 13.5 | 24.5 | 8.872 | 0.371011584 |
| 13 | 24.5 | 7.943 | 0.332162422 |
| 12.5 | 24.5 | 6.822 | 0.285284155 |
| 12 | 24.5 | 5.502 | 0.230084055 |
| 11.5 | 24.5 | 3.979 | 0.166394848 |
| 11 | 24.5 | 2.311 | 0.096641994 |
| 10.5 | 24.5 | 0.551 | 0.02304186 |
| 10 | 24.5 | 0.831 | 0.034750972 |
| 9.5 | 24.5 | 2.963 | 0.123907498 |
| 9 | 24.5 | 5.251 | 0.219587672 |
| 8.5 | 24.5 | 7.676 | 0.320996947 |
| 8 | 24.5 | 10.121 | 0.423242588 |
| 7.5 | 24.5 | 12.616 | 0.527579141 |
| 7 | 24.5 | 15.088 | 0.630953874 |
| 6.5 | 24.5 | 17.552 | 0.733994062 |
| 6 | 24.5 | 19.909 | 0.832559696 |
| 5.5 | 24.5 | 22.167 | 0.926985322 |
| 5 | 24.5 | 24.289 | 1.015723665 |
| 4.5 | 24.5 | 26.236 | 1.097143813 |
| 4 | 24.5 | 28.047 | 1.172876678 |
| 3.5 | 24.5 | 29.619 | 1.238614979 |
| 3 | 24.5 | 30.994 | 1.296115084 |
| 2.5 | 24.5 | 32.178 | 1.345627901 |
| 2 | 24.5 | 33.147 | 1.386149793 |
| 1.5 | 24.5 | 33.914 | 1.418224397 |
| 1 | 24.5 | 34.464 | 1.441224439 |
| 0.5 | 24.5 | 34.802 | 1.45535901 |
| 0 | 24.5 | 34.949 | 1.461506294 |

**Path #5**

| X [mm] | Y [mm] | Vrogowski [mV] | Relative error [%] |
|---|---|---|---|
| 0 | 21.5 | 50.386 | 2.10705474 |
| 0.5 | 21.5 | 50.331 | 2.104754736 |
| 1 | 21.5 | 50.024 | 2.091916531 |
| 1.5 | 21.5 | 49.401 | 2.065863756 |
| 2 | 21.5 | 48.458 | 2.026429139 |
| 2.5 | 21.5 | 47.171 | 1.972609041 |
| 3 | 21.5 | 45.506 | 1.902981642 |
| 3.5 | 21.5 | 43.491 | 1.818717852 |
| 4 | 21.5 | 41.043 | 1.716346757 |
| 4.5 | 21.5 | 38.151 | 1.595408355 |
| 5 | 21.5 | 34.958 | 1.461882658 |
| 5.5 | 21.5 | 31.367 | 1.311713294 |
| 6 | 21.5 | 27.461 | 1.148371179 |
| 6.5 | 21.5 | 23.339 | 0.97599632 |
| 7 | 21.5 | 18.932 | 0.791703258 |
| 7.5 | 21.5 | 14.505 | 0.60657383 |
| 8 | 21.5 | 10.029 | 0.419395308 |
| 8.5 | 21.5 | 5.631 | 0.23547861 |
| 9 | 21.5 | 1.442 | 0.060301928 |
| 9.5 | 21.5 | 1.677 | 0.070129218 |
| 10 | 21.5 | 5.319 | 0.222431314 |
| 10.5 | 21.5 | 8.547 | 0.35742065 |
| 11 | 21.5 | 11.464 | 0.479404508 |
| 11.5 | 21.5 | 13.899 | 0.581231966 |
| 12 | 21.5 | 15.935 | 0.666373939 |
| 12.5 | 21.5 | 17.745 | 0.742064986 |
| 13 | 21.5 | 18.849 | 0.788232342 |
| 13.5 | 21.5 | 19.576 | 0.818634216 |
| 14 | 21.5 | 19.974 | 0.835277882 |

**Path #2**

| X [mm] | Y [mm] | Vrogowski [mV] | Relative error [%] |
|---|---|---|---|
| 14 | 19.5 | 37.595 | 1.572157404 |
| 14 | 20 | 33.331 | 1.393844352 |
| 14 | 20.5 | 29.449 | 1.231505875 |
| 14 | 21 | 25.936 | 1.084598336 |
| 14 | 21.5 | 22.761 | 0.951825367 |
| 14 | 22 | 19.919 | 0.832977878 |
| 14 | 22.5 | 17.378 | 0.726717685 |
| 14 | 23 | 15.101 | 0.631497512 |
| 14 | 23.5 | 13.058 | 0.546062811 |
| 14 | 24 | 11.238 | 0.469953582 |
| 14 | 24.5 | 9.613 | 0.401998913 |

**Path #4**

| X [mm] | Y [mm] | Vrogowski [mV] | Relative error [%] |
|---|---|---|---|
| 0 | 24.5 | 34.951 | 1.46158993 |
| 0 | 24 | 37.575 | 1.571321039 |
| 0 | 23.5 | 40.401 | 1.689499435 |
| 0 | 23 | 43.459 | 1.817379668 |
| 0 | 22.5 | 46.751 | 1.955045373 |
| 0 | 22 | 50.288 | 2.102956551 |
| 0 | 21.5 | 54.098 | 2.262284113 |
| 0 | 21 | 58.151 | 2.431773512 |
| 0 | 20.5 | 62.458 | 2.611884749 |
| 0 | 20 | 66.635 | 2.786559612 |
| 0 | 19.5 | 66.864 | 2.796135993 |

The relative error is calculated against the voltage measured at the center point of the coil, which is

$$V_{cA} = 2391.3\ mV$$

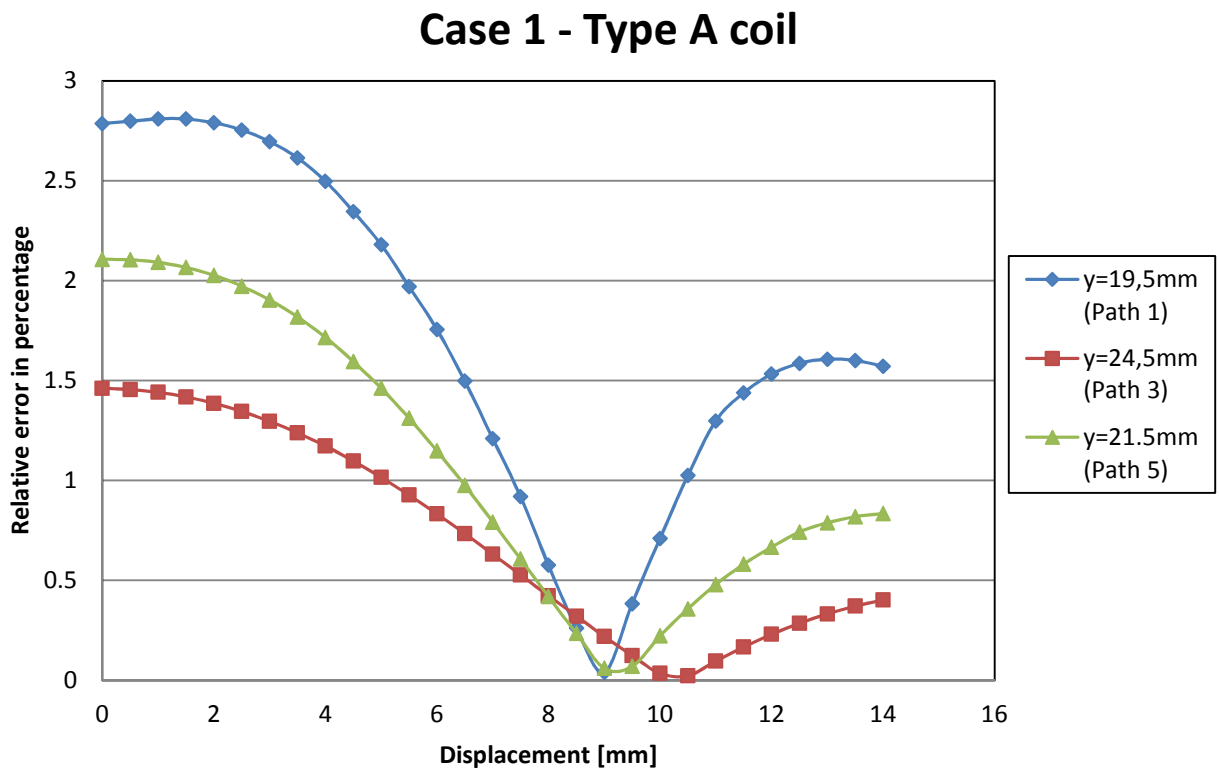


The figure shows the error plotted for path #1, #3, and #5. From the graph we can identify that at some point along the path the error dropped as low as 0.02%, because the output voltage of the coil was around 1mV. We can conclude that when the bar transited along these coordinates it disturbed the coil the less and the readings that we picked up were almost entirely background noise. The other two paths are not of any particular interest since in both paths it can be easily noted by looking at the values shown by the tables above (path #2 and path #4), the linear behavior of the error as the bar moves away or towards the coil.

*ii.* *Case #2 – the bar moves on the region at the side of the coil*

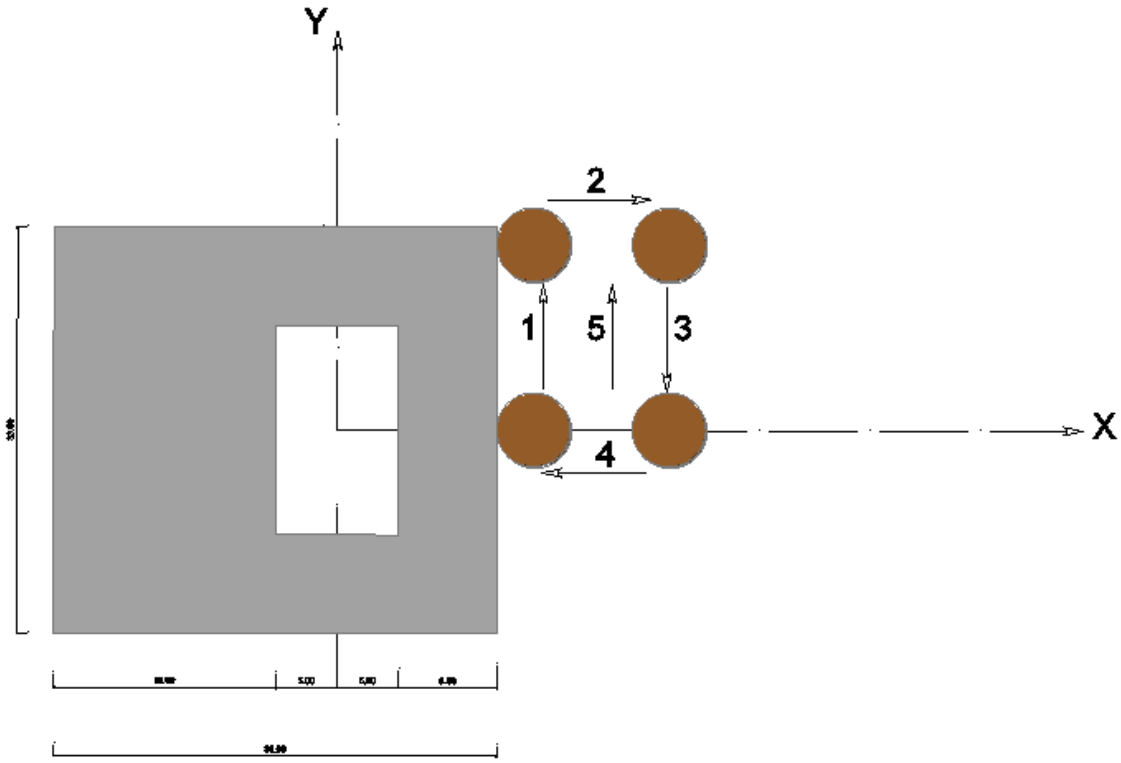


**Figure 3-2** Type A coil, case#2

The setup is the same as case one, but now we moved on the region at the side of the coil. The starting point had the coordinates ***x=16***, ***y=0 mm***. The bar was displaced then along path #1 from ***y=0*** to ***y=15 mm*** while ***x*** remained fixed at 16 mm. Along path #2 the bar moved away from the coil up to ***x=21 mm*** with ***y=15mm***. We came down to ***y=0*** and ***x=21 mm*** along path #3, and returned at the starting point going through path #4. Same as case one we repositioned the bar halfway through path #4, corresponding at ***x=18.5*** mm in order to go along path #5.

**Path #1**

| X [mm] | Y [mm] | Vrogowski [mV] | Relative error [%] |
|---|---|---|---|
| 16 | 0 | 140.615 | 5.880274328 |
| 16 | 0.5 | 140.445 | 5.873165224 |
| 16 | 1 | 139.552 | 5.83582152 |
| 16 | 1.5 | 137.774 | 5.761468657 |
| 16 | 2 | 134.904 | 5.641450257 |
| 16 | 2.5 | 131.612 | 5.503784552 |
| 16 | 3 | 127.451 | 5.329778781 |
| 16 | 3.5 | 122.747 | 5.133065696 |
| 16 | 4 | 116.971 | 4.891523439 |
| 16 | 4.5 | 110.372 | 4.615564756 |
| 16 | 5 | 103.005 | 4.30748965 |
| 16 | 5.5 | 94.794 | 3.964119935 |
| 16 | 6 | 85.889 | 3.591728349 |
| 16 | 6.5 | 76.212 | 3.187053067 |
| 16 | 7 | 65.735 | 2.74892318 |
| 16 | 7.5 | 54.719 | 2.288253251 |
| 16 | 8 | 43.085 | 1.80173964 |
| 16 | 8.5 | 31.076 | 1.299544181 |
| 16 | 9 | 19.031 | 0.795843265 |
| 16 | 9.5 | 6.788 | 0.283862334 |
| 16 | 10 | 4.147 | 0.173420315 |
| 16 | 10.5 | 15.181 | 0.634842972 |
| 16 | 11 | 25.422 | 1.063103751 |
| 16 | 11.5 | 34.597 | 1.446786267 |
| 16 | 12 | 42.352 | 1.771086857 |
| 16 | 12.5 | 48.888 | 2.04441099 |
| 16 | 13 | 53.616 | 2.242127713 |
| 16 | 13.5 | 56.952 | 2.381633421 |
| 16 | 14 | 58.928 | 2.464266299 |
| 16 | 14.5 | 59.625 | 2.493413624 |
| 16 | 15 | 59.316 | 2.480491783 |

**Path #3**

| X [mm] | Y [mm] | Vrogowski [mV] | Relative error [%] |
|---|---|---|---|
| 21 | 15 | 12.696 | 0.530924602 |
| 21 | 14.5 | 11.247 | 0.470329946 |
| 21 | 14 | 9.571 | 0.400242546 |
| 21 | 13.5 | 7.569 | 0.316522394 |
| 21 | 13 | 5.262 | 0.220047673 |
| 21 | 12.5 | 2.649 | 0.110776565 |
| 21 | 12 | 0.209 | 0.008740016 |
| 21 | 11.5 | 2.749 | 0.114958391 |
| 21 | 11 | 6.172 | 0.258102287 |
| 21 | 10.5 | 9.804 | 0.4099862 |
| 21 | 10 | 13.647 | 0.570693765 |
| 21 | 9.5 | 17.655 | 0.738301342 |
| 21 | 9 | 21.808 | 0.911972567 |
| 21 | 8.5 | 25.969 | 1.085978338 |
| 21 | 8 | 30.151 | 1.260862292 |
| 21 | 7.5 | 34.209 | 1.430560783 |
| 21 | 7 | 38.366 | 1.604399281 |
| 21 | 6.5 | 42.339 | 1.770543219 |
| 21 | 6 | 46.111 | 1.928281688 |
| 21 | 5.5 | 49.621 | 2.075063773 |
| 21 | 5 | 53.081 | 2.219754945 |
| 21 | 4.5 | 56.182 | 2.349433363 |
| 21 | 4 | 58.987 | 2.466733576 |
| 21 | 3.5 | 61.481 | 2.571028311 |
| 21 | 3 | 63.682 | 2.663070296 |
| 21 | 2.5 | 65.489 | 2.738635888 |
| 21 | 2 | 66.954 | 2.799899636 |
| 21 | 1.5 | 68.038 | 2.845230628 |
| 21 | 1 | 68.706 | 2.873165224 |
| 21 | 0.5 | 68.995 | 2.8852507 |
| 21 | 0 | 68.846 | 2.87901978 |

**Path #5**

| X [mm] | Y [mm] | Vrogowski [mV] | Relative error [%] |
|---|---|---|---|
| 18.5 | 0 | 98.983 | 4.139296617 |
| 18.5 | 0.5 | 98.895 | 4.13561661 |
| 18.5 | 1 | 98.264 | 4.10922929 |
| 18.5 | 1.5 | 97.095 | 4.060343746 |
| 18.5 | 2 | 95.347 | 3.987245431 |
| 18.5 | 2.5 | 92.992 | 3.888763434 |
| 18.5 | 3 | 90.077 | 3.766863212 |
| 18.5 | 3.5 | 86.611 | 3.621921131 |
| 18.5 | 4 | 82.547 | 3.451971731 |
| 18.5 | 4.5 | 77.984 | 3.26115502 |
| 18.5 | 5 | 72.977 | 3.051771003 |
| 18.5 | 5.5 | 67.631 | 2.828210597 |
| 18.5 | 6 | 61.881 | 2.587755614 |
| 18.5 | 6.5 | 55.552 | 2.32308786 |
| 18.5 | 7 | 49.018 | 2.049847363 |
| 18.5 | 7.5 | 42.293 | 1.768619579 |
| 18.5 | 8 | 35.476 | 1.483544516 |
| 18.5 | 8.5 | 28.474 | 1.190733074 |
| 18.5 | 9 | 21.502 | 0.89917618 |
| 18.5 | 9.5 | 14.645 | 0.612428386 |
| 18.5 | 10 | 7.961 | 0.332915151 |
| 18.5 | 10.5 | 1.705 | 0.07130013 |
| 18.5 | 11 | 3.563 | 0.148998453 |
| 18.5 | 11.5 | 9.007 | 0.376657048 |
| 18.5 | 12 | 13.817 | 0.577802869 |
| 18.5 | 12.5 | 18.187 | 0.760548656 |
| 18.5 | 13 | 21.752 | 0.909630745 |
| 18.5 | 13.5 | 24.797 | 1.03696734 |
| 18.5 | 14 | 27.151 | 1.135407519 |
| 18.5 | 14.5 | 28.886 | 1.207962196 |
| 18.5 | 15 | 30.092 | 1.258395015 |

**Path #2**

| X [mm] | Y [mm] | Vrogowski [mV] | Relative error [%] |
|---|---|---|---|
| 16 | 15 | 59.315 | 2.480449964 |
| 16.5 | 15 | 52.142 | 2.180487601 |
| 17 | 15 | 45.494 | 1.902479823 |
| 17.5 | 15 | 39.609 | 1.656379375 |
| 18 | 15 | 34.354 | 1.43662443 |
| 18.5 | 15 | 29.626 | 1.238907707 |
| 19 | 15 | 25.402 | 1.062267386 |
| 19.5 | 15 | 21.622 | 0.904194371 |
| 20 | 15 | 18.313 | 0.765817756 |
| 20.5 | 15 | 15.325 | 0.640864802 |
| 21 | 15 | 12.695 | 0.530882783 |

**Path #4**

| X [mm] | Y [mm] | Vrogowski [mV] | Relative error [%] |
|---|---|---|---|
| 21 | 0 | 68.855 | 2.879396144 |
| 20.5 | 0 | 73.806 | 3.086438339 |
| 20 | 0 | 79.161 | 3.31037511 |
| 19.5 | 0 | 85.008 | 3.554886463 |
| 19 | 0 | 91.418 | 3.822941496 |
| 18.5 | 0 | 98.367 | 4.11353657 |
| 18 | 0 | 106.122 | 4.43783716 |
| 17.5 | 0 | 114.271 | 4.778614143 |
| 17 | 0 | 123.425 | 5.161418475 |
| 16.5 | 0 | 133.486 | 5.582151968 |
| 16 | 0 | 140.793 | 5.887717978 |

Just like case one the relative error is calculated against the voltage measured at the center point of the coil, and the same value $\boldsymbol{V_{cA} = 2391.3\ mV}$ was used for this case.

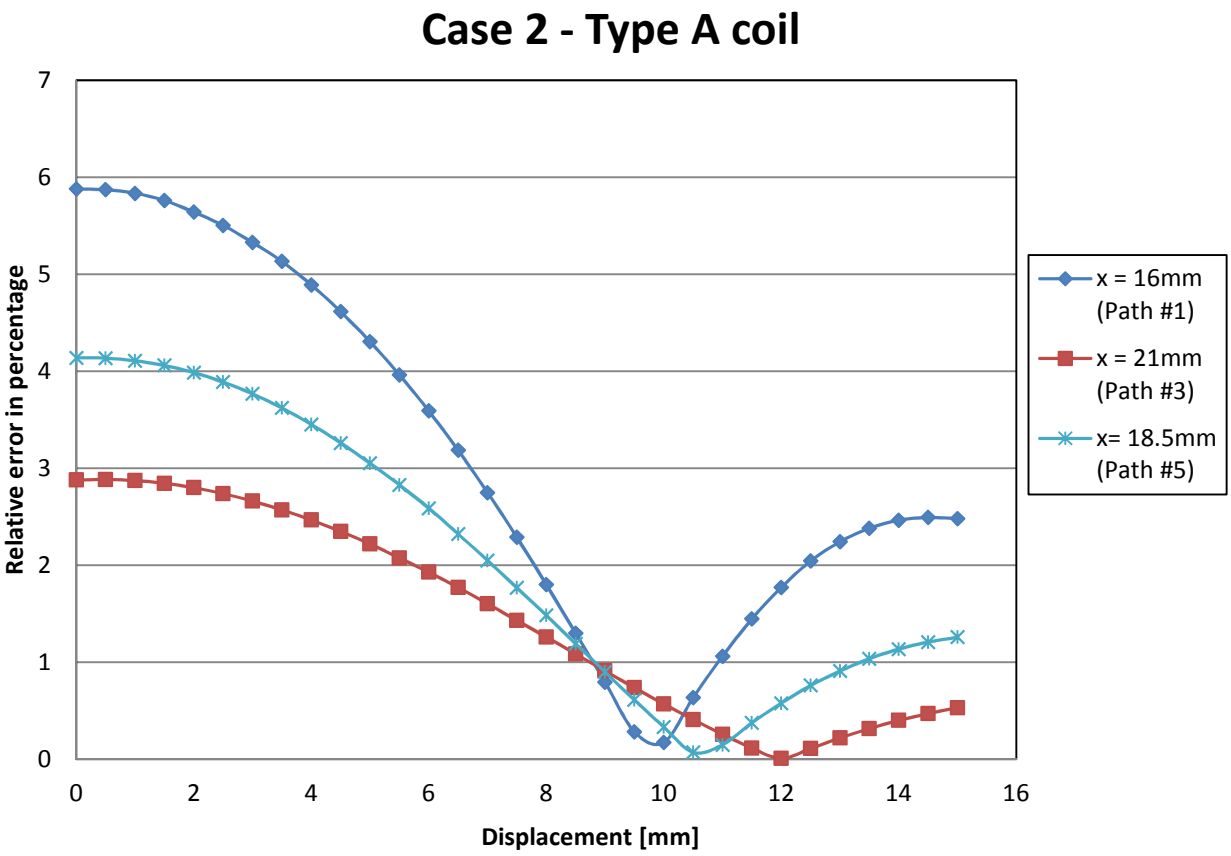


Same as case one path #1, #3, and #5 are the interesting ones, and we can make the same observations that we did in the first case for path #2 and #4. From the graph can be easily identified the same behavior as the one in the first case where the error is almost zero in specific points. Just like in the first case, we can conclude that at these points the influence of the bar is almost inexistent and the voltage readings that we get are background noise.

## 3.2. Type B Rogowski Coil

THE FOLLOWINGS show the tests performed on the second Rogowski coil that we had, a.k.a. Type B. The measurements for this coil were not done on the same day as the one of the first coil, but just after finishing the tests with the first coil, the Type B coil was repositioned exactly on the same footprint of the Type A coil to ensure that the experimental setup didn't change much. Due to the fact that the casing of the Type B coil was a bit different from that of Type A, some rearrangement of the base where the coil was positioned had to be done, in order to refer the measurements to the same center point. In other words, the two center points of the two coils, which correspond also with the origin of the ***X,Y*** plane, must overlap. But, the casing of the second coil is a bit different so the coordinates of the starting point of the region on the top of the Type B coil is slightly different from that of the Type A coil. Sidewise the casing of the coils has the same dimensions, so the paths overlap perfectly.

We anticipated on the note before that we removed the current transformer (CT) from this coil. This was done because in the preliminary tests we noted that the Type B coil overheated just after a couple of measures.

*iii.* *Case # 1 – the bar moves along the region at the top of the coil*

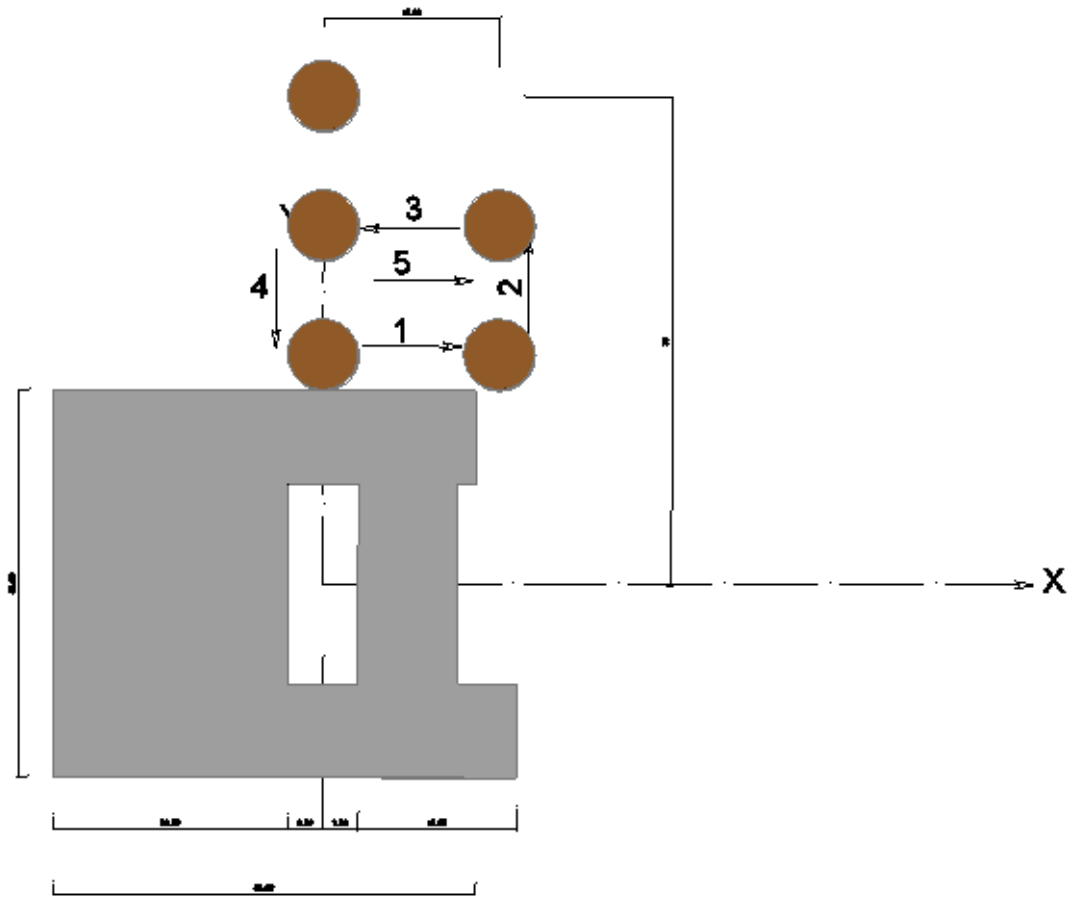


**Figure 3-3** Type B coil, case#1

The scenario is identical to the case of the Type A coil. We went through the same paths but as we anticipated, the different casing design of the coil changed a little bit the coordinates. The starting point had the coordinates ***x=0***, ***y=17.75 mm***; along path #1 the bar was displaced up to ***x=15 mm*** always in 0.5 mm steps. Again we went up along path #2 to ***y=22.75*** mm along while the ***x*** coordinate remained at 15 mm. Then path #3 was done and the bar was located at ***x=0***, ***y=22.75 mm*** at the end of it. We returned at the starting point going through path #4, and then we repositioned the bar at the middle of path #4, at coordinates ***x=0***, ***y=20.25*** mm in order to go along path #5. At last, just like in the case of the first coil, we did the measurement for the point ***x=0***, ***y=35*** mm from the center of the coil. The reading was 6.995 mV.

**Path #1**

| X [mm] | Y [mm] | Vrogowski [mV] | Relative error [%] |
|---|---|---|---|
| 0 | 17.75 | 73.956 | 3.9454773 |
| 0.5 | 17.75 | 74.194 | 3.9581744 |
| 1 | 17.75 | 73.852 | 3.939929 |
| 1.5 | 17.75 | 72.911 | 3.8897277 |
| 2 | 17.75 | 71.399 | 3.809064 |
| 2.5 | 17.75 | 69.252 | 3.6945237 |
| 3 | 17.75 | 66.416 | 3.543226 |
| 3.5 | 17.75 | 63.061 | 3.3642402 |
| 4 | 17.75 | 58.967 | 3.1458294 |
| 4.5 | 17.75 | 54.179 | 2.8903945 |
| 5 | 17.75 | 48.696 | 2.597882 |
| 5.5 | 17.75 | 43.035 | 2.2958735 |
| 6 | 17.75 | 37.021 | 1.9750327 |
| 6.5 | 17.75 | 30.659 | 1.6356265 |
| 7 | 17.75 | 24.088 | 1.2850703 |
| 7.5 | 17.75 | 17.429 | 0.9298194 |
| 8 | 17.75 | 10.623 | 0.5667262 |
| 8.5 | 17.75 | 4.591 | 0.2449252 |
| 9 | 17.75 | 0.416 | 0.0221932 |
| 9.5 | 17.75 | 5.538 | 0.2954467 |
| 10 | 17.75 | 9.808 | 0.5232468 |
| 10.5 | 17.75 | 13.548 | 0.722772 |
| 11 | 17.75 | 16.393 | 0.8745499 |
| 11.5 | 17.75 | 18.557 | 0.9899971 |
| 12 | 17.75 | 20.129 | 1.0738617 |
| 12.5 | 17.75 | 21.167 | 1.1292379 |
| 13 | 17.75 | 21.787 | 1.1623143 |
| 13.5 | 17.75 | 22.021 | 1.1747979 |
| 14 | 17.75 | 21.962 | 1.1716504 |
| 14.5 | 17.75 | 21.673 | 1.1562325 |
| 15 | 17.75 | 21.188 | 1.1303582 |

**Path #3**

| X [mm] | Y [mm] | Vrogowski [mV] | Relative error [%] |
|---|---|---|---|
| 15 | 22.75 | 5.342 | 0.28499 |
| 14.5 | 22.75 | 4.763 | 0.254101 |
| 14 | 22.75 | 4.091 | 0.218251 |
| 13.5 | 22.75 | 3.291 | 0.175572 |
| 13 | 22.75 | 2.406 | 0.128358 |
| 12.5 | 22.75 | 1.382 | 0.073728 |
| 12 | 22.75 | 0.354 | 0.018886 |
| 11.5 | 22.75 | 0.513 | 0.027368 |
| 11 | 22.75 | 1.838 | 0.098055 |
| 10.5 | 22.75 | 3.386 | 0.18064 |
| 10 | 22.75 | 5.063 | 0.270106 |
| 9.5 | 22.75 | 6.852 | 0.365547 |
| 9 | 22.75 | 8.738 | 0.466163 |
| 8.5 | 22.75 | 10.726 | 0.572221 |
| 8 | 22.75 | 12.753 | 0.68036 |
| 7.5 | 22.75 | 14.812 | 0.790205 |
| 7 | 22.75 | 16.874 | 0.900211 |
| 6.5 | 22.75 | 18.935 | 1.010163 |
| 6 | 22.75 | 20.921 | 1.116114 |
| 5.5 | 22.75 | 22.885 | 1.220891 |
| 5 | 22.75 | 24.687 | 1.317026 |
| 4.5 | 22.75 | 26.386 | 1.407666 |
| 4 | 22.75 | 27.986 | 1.493025 |
| 3.5 | 22.75 | 29.359 | 1.566273 |
| 3 | 22.75 | 30.599 | 1.632426 |
| 2.5 | 22.75 | 31.602 | 1.685935 |
| 2 | 22.75 | 32.429 | 1.730054 |
| 1.5 | 22.75 | 33.039 | 1.762597 |
| 1 | 22.75 | 33.444 | 1.784203 |
| 0.5 | 22.75 | 33.614 | 1.793273 |
| 0 | 22.75 | 33.571 | 1.790979 |

**Path #5**

| X [mm] | Y [mm] | Vrogowski [mV] | Relative error [%] |
|---|---|---|---|
| 0 | 20.25 | 48.858 | 2.606525 |
| 0.5 | 20.25 | 49.004 | 2.614314 |
| 1 | 20.25 | 48.783 | 2.602523 |
| 1.5 | 20.25 | 48.195 | 2.571154 |
| 2 | 20.25 | 47.223 | 2.519299 |
| 2.5 | 20.25 | 45.889 | 2.448131 |
| 3 | 20.25 | 44.206 | 2.358345 |
| 3.5 | 20.25 | 42.179 | 2.250207 |
| 4 | 20.25 | 39.754 | 2.120835 |
| 4.5 | 20.25 | 37.146 | 1.981701 |
| 5 | 20.25 | 34.161 | 1.822455 |
| 5.5 | 20.25 | 30.971 | 1.652271 |
| 6 | 20.25 | 27.588 | 1.471792 |
| 6.5 | 20.25 | 24.149 | 1.288325 |
| 7 | 20.25 | 20.577 | 1.097762 |
| 7.5 | 20.25 | 17.011 | 0.90752 |
| 8 | 20.25 | 13.508 | 0.720638 |
| 8.5 | 20.25 | 10.088 | 0.538185 |
| 9 | 20.25 | 6.861 | 0.366027 |
| 9.5 | 20.25 | 3.844 | 0.205073 |
| 10 | 20.25 | 1.153 | 0.061511 |
| 10.5 | 20.25 | 0.735 | 0.039212 |
| 11 | 20.25 | 2.853 | 0.152205 |
| 11.5 | 20.25 | 4.794 | 0.255755 |
| 12 | 20.25 | 6.471 | 0.345221 |
| 12.5 | 20.25 | 7.871 | 0.41991 |
| 13 | 20.25 | 9.051 | 0.482862 |
| 13.5 | 20.25 | 9.954 | 0.531036 |
| 14 | 20.25 | 10.669 | 0.56918 |
| 14.5 | 20.25 | 11.185 | 0.596708 |
| 15 | 20.25 | 11.545 | 0.615914 |

**Path #2**

| X [mm] | Y [mm] | Vrogowski [mV] | Relative error [%] |
|---|---|---|---|
| 15 | 17.75 | 21.192 | 1.1305716 |
| 15 | 18.25 | 18.986 | 1.0128838 |
| 15 | 18.75 | 16.918 | 0.9025581 |
| 15 | 19.25 | 14.988 | 0.7995945 |
| 15 | 19.75 | 13.219 | 0.7052202 |
| 15 | 20.25 | 11.595 | 0.6185815 |
| 15 | 20.75 | 10.095 | 0.538558 |
| 15 | 21.25 | 8.732 | 0.4658433 |
| 15 | 21.75 | 7.489 | 0.3995305 |
| 15 | 22.25 | 6.362 | 0.3394062 |
| 15 | 22.75 | 5.343 | 0.2850436 |

**Path #4**

| X [mm] | Y [mm] | Vrogowski [mV] | Relative error [%] |
|---|---|---|---|
| 0 | 22.75 | 33.573 | 1.7910854 |
| 0 | 22.25 | 36.114 | 1.9266451 |
| 0 | 21.75 | 38.831 | 2.0715943 |
| 0 | 21.25 | 41.861 | 2.2332418 |
| 0 | 20.75 | 45.196 | 2.4111606 |
| 0 | 20.25 | 48.869 | 2.6071114 |
| 0 | 19.75 | 52.935 | 2.8240284 |
| 0 | 19.25 | 57.394 | 3.0619115 |
| 0 | 18.75 | 62.293 | 3.3232682 |
| 0 | 18.25 | 67.679 | 3.6106058 |
| 0 | 17.75 | 73.699 | 3.9317667 |

The relative error is calculated against the voltage picked up at the center of the coil, which is

$$V_{cB} = 1874.45\ mV$$

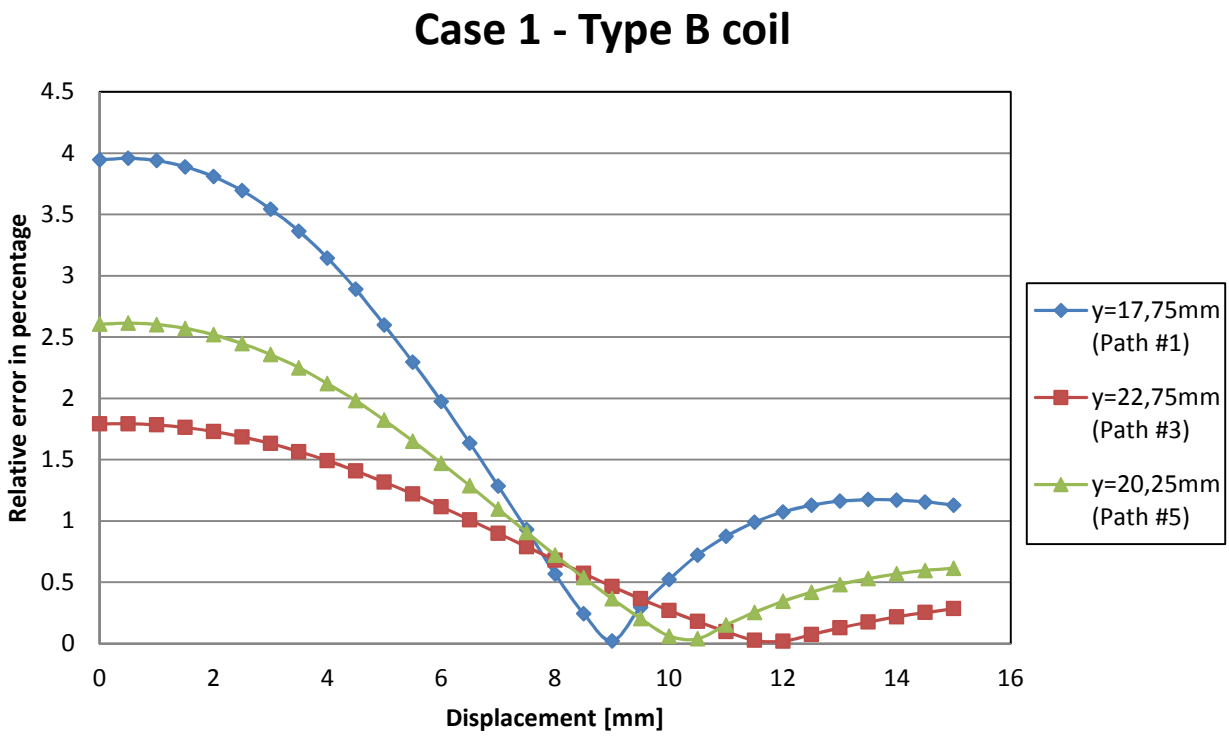


As we did for the first coil the above figure shows the error plotted for path #1, #3, and #5. From the graph we can identify the same trend as we did for the Type A coil and again the error dropped as low as 0.02%. We can conclude in this case too, that at some point along the bar's path its influence on the coil is almost zero and the readings that we picked up were almost entirely background noise. For path #2 and path #4 we can make the same observations that we did for the Type A Rogowski coil.

*iv.* *Case #2 – the bar moves on the region at the side of the coil*

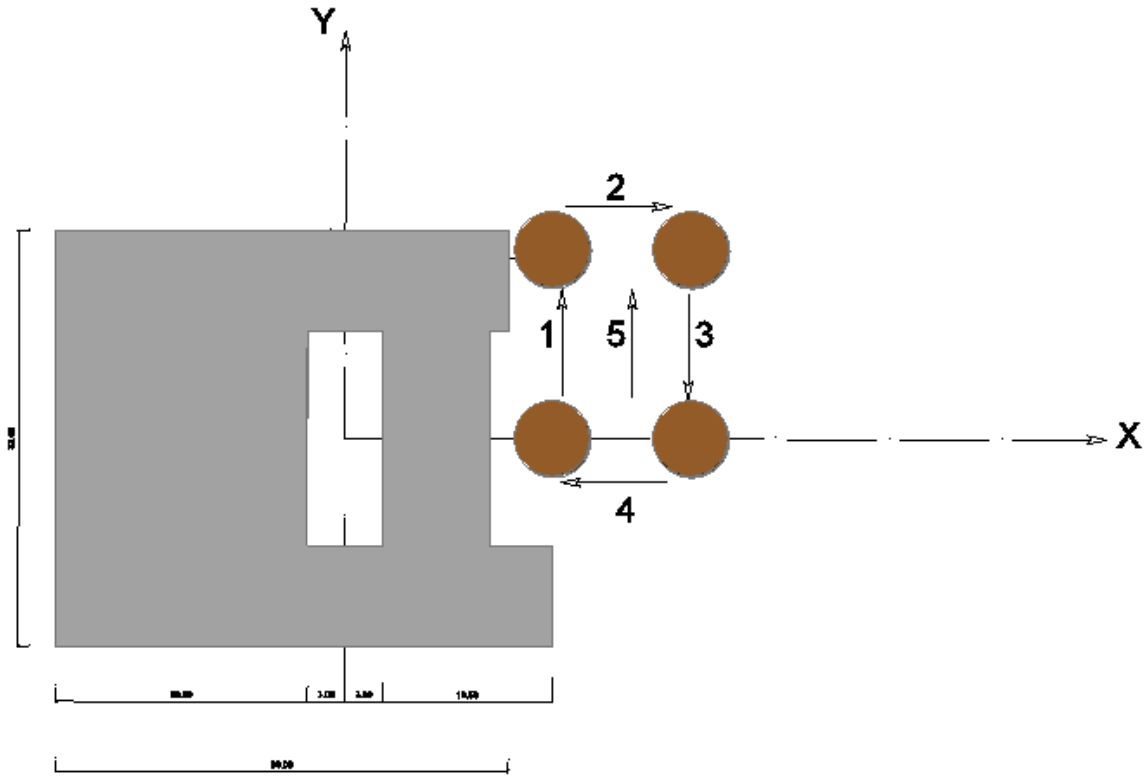


**Figure 3-4** Type B coil, case#1

We repeated the same test on the same setup as we did for the first coil in case two. The starting point had the coordinates ***x=16***, ***y=0*** same as the ones of the Type A coil. The bar then moved along path #1 from ***y=0*** to ***y=15mm*** while ***x*** remained fixed at 16 mm. We went through path #2 which displaced the bar away from the coil up to ***x=21mm*** while ***y=15mm*** remained constant. We came down to ***y=0*** and ***x=21mm*** along path #3, and returned at the starting point going through path #4. At last we repositioned the bar halfway through path #4, corresponding at ***x=18.5mm*** in order to go through path #5. As mentioned before, in this case the coordinates ***x,y*** of every single point that we measured were exactly like the ones for the first coil that we tested.

**Path #1**

| X [mm] | Y [mm] | Vrogowski [mV] | Relative error [%] |
|---|---|---|---|
| 16 | 0 | 27.828 | 1.484595481 |
| 16 | 0.5 | 27.369 | 1.460108298 |
| 16 | 1 | 26.709 | 1.42489797 |
| 16 | 1.5 | 25.665 | 1.369201632 |
| 16 | 2 | 24.188 | 1.290405186 |
| 16 | 2.5 | 22.117 | 1.179919443 |
| 16 | 3 | 19.392 | 1.034543466 |
| 16 | 3.5 | 15.612 | 0.832884313 |
| 16 | 4 | 11.305 | 0.603110246 |
| 16 | 4.5 | 6.366 | 0.339619622 |
| 16 | 5 | 1.152 | 0.061458028 |
| 16 | 5.5 | 3.502 | 0.186828136 |
| 16 | 6 | 9.073 | 0.484035317 |
| 16 | 6.5 | 14.523 | 0.774787271 |
| 16 | 7 | 19.517 | 1.041212089 |
| 16 | 7.5 | 24.099 | 1.285657126 |
| 16 | 8 | 27.919 | 1.489450239 |
| 16 | 8.5 | 31.113 | 1.659846888 |
| 16 | 9 | 33.601 | 1.792579157 |
| 16 | 9.5 | 35.225 | 1.879217904 |
| 16 | 10 | 36.143 | 1.92819227 |
| 16 | 10.5 | 36.436 | 1.943823522 |
| 16 | 11 | 36.089 | 1.925311425 |
| 16 | 11.5 | 35.292 | 1.882792286 |
| 16 | 12 | 34.057 | 1.816906293 |
| 16 | 12.5 | 32.785 | 1.749046387 |
| 16 | 13 | 31.067 | 1.657392835 |
| 16 | 13.5 | 29.145 | 1.554856091 |
| 16 | 14 | 27.154 | 1.448638267 |
| 16 | 14.5 | 25.071 | 1.337512337 |
| 16 | 15 | 23.043 | 1.229320601 |

**Path #3**

| X [mm] | Y [mm] | Vrogowski [mV] | Relative error [%] |
|---|---|---|---|
| 21 | 15 | 13.239 | 0.706287178 |
| 21 | 14.5 | 13.665 | 0.729013844 |
| 21 | 14 | 14.045 | 0.749286457 |
| 21 | 13.5 | 14.341 | 0.765077756 |
| 21 | 13 | 14.553 | 0.77638774 |
| 21 | 12.5 | 14.649 | 0.781509243 |
| 21 | 12 | 14.662 | 0.782202779 |
| 21 | 11.5 | 14.542 | 0.775800902 |
| 21 | 11 | 14.303 | 0.763050495 |
| 21 | 10.5 | 13.925 | 0.742884579 |
| 21 | 10 | 13.402 | 0.714983062 |
| 21 | 9.5 | 12.717 | 0.678439009 |
| 21 | 9 | 11.905 | 0.635119635 |
| 21 | 8.5 | 10.966 | 0.585024941 |
| 21 | 8 | 9.884 | 0.527301342 |
| 21 | 7.5 | 8.691 | 0.463656006 |
| 21 | 7 | 7.415 | 0.395582704 |
| 21 | 6.5 | 6.043 | 0.3223879 |
| 21 | 6 | 4.621 | 0.246525648 |
| 21 | 5.5 | 3.175 | 0.169383019 |
| 21 | 5 | 1.758 | 0.093787511 |
| 21 | 4.5 | 0.422 | 0.022513271 |
| 21 | 4 | 0.375 | 0.020005868 |
| 21 | 3.5 | 1.588 | 0.084718184 |
| 21 | 3 | 2.843 | 0.151671157 |
| 21 | 2.5 | 4.025 | 0.214729654 |
| 21 | 2 | 5.103 | 0.272239857 |
| 21 | 1.5 | 6.091 | 0.324948652 |
| 21 | 1 | 6.958 | 0.371202219 |
| 21 | 0.5 | 7.726 | 0.412174238 |
| 21 | 0 | 8.355 | 0.445730748 |

**Path #5**

| X [mm] | Y [mm] | Vrogowski [mV] | Relative error [%] |
|---|---|---|---|
| 18.5 | 0 | 16.434 | 0.876737176 |
| 18.5 | 0.5 | 15.512 | 0.827549414 |
| 18.5 | 1 | 14.494 | 0.77324015 |
| 18.5 | 1.5 | 13.248 | 0.706767318 |
| 18.5 | 2 | 11.763 | 0.62754408 |
| 18.5 | 2.5 | 10.032 | 0.535196991 |
| 18.5 | 3 | 8.098 | 0.432020059 |
| 18.5 | 3.5 | 5.899 | 0.314705647 |
| 18.5 | 4 | 3.511 | 0.187308277 |
| 18.5 | 4.5 | 0.989 | 0.052762144 |
| 18.5 | 5 | 0.901 | 0.048067433 |
| 18.5 | 5.5 | 3.605 | 0.192323081 |
| 18.5 | 6 | 5.883 | 0.313852063 |
| 18.5 | 6.5 | 8.549 | 0.45608045 |
| 18.5 | 7 | 11.089 | 0.591586865 |
| 18.5 | 7.5 | 13.471 | 0.718664141 |
| 18.5 | 8 | 15.616 | 0.833097709 |
| 18.5 | 8.5 | 17.522 | 0.934780869 |
| 18.5 | 9 | 19.126 | 1.020352637 |
| 18.5 | 9.5 | 20.409 | 1.088799381 |
| 18.5 | 10 | 21.394 | 1.141348129 |
| 18.5 | 10.5 | 22.043 | 1.175971618 |
| 18.5 | 11 | 22.444 | 1.19736456 |
| 18.5 | 11.5 | 22.508 | 1.200778895 |
| 18.5 | 12 | 22.387 | 1.194323668 |
| 18.5 | 12.5 | 21.994 | 1.173357518 |
| 18.5 | 13 | 21.461 | 1.144922511 |
| 18.5 | 13.5 | 20.767 | 1.107898317 |
| 18.5 | 14 | 19.931 | 1.063298568 |
| 18.5 | 14.5 | 19.021 | 1.014750994 |
| 18.5 | 15 | 18.025 | 0.961615407 |

**Path #2**

| X [mm] | Y [mm] | Vrogowski [mV] | Relative error [%] |
|---|---|---|---|
| 16 | 15 | 23.048 | 1.229587346 |
| 16.5 | 15 | 22.008 | 1.174104404 |
| 17 | 15 | 20.922 | 1.116167409 |
| 17.5 | 15 | 19.831 | 1.057963669 |
| 18 | 15 | 18.776 | 1.001680493 |
| 18.5 | 15 | 17.735 | 0.946144202 |
| 19 | 15 | 16.812 | 0.896903092 |
| 19.5 | 15 | 15.802 | 0.896903092 |
| 20 | 15 | 14.903 | 0.843020619 |
| 20.5 | 15 | 14.049 | 0.795059884 |
| 21 | 15 | 13.235 | 0.749499853 |

**Path # 4**

| X [mm] | Y [mm] | Vrogowski [mV] | Relative error [%] |
|---|---|---|---|
| 21 | 0 | 8.359 | 0.445944144 |
| 20.5 | 0 | 9.667 | 0.515724613 |
| 20 | 0 | 11.089 | 0.591586865 |
| 19.5 | 0 | 12.663 | 0.675558164 |
| 19 | 0 | 14.342 | 0.765131105 |
| 18.5 | 0 | 16.214 | 0.8650004 |
| 18 | 0 | 18.219 | 0.97196511 |
| 17.5 | 0 | 20.407 | 1.088692683 |
| 17 | 0 | 22.763 | 1.214382886 |
| 16.5 | 0 | 25.316 | 1.350582838 |
| 16 | 0 | 28.039 | 1.495852117 |

Just like case one the relative error is calculated against the voltage measured at the center point of the coil, and the same value ***1874.45 mV*** was used again.

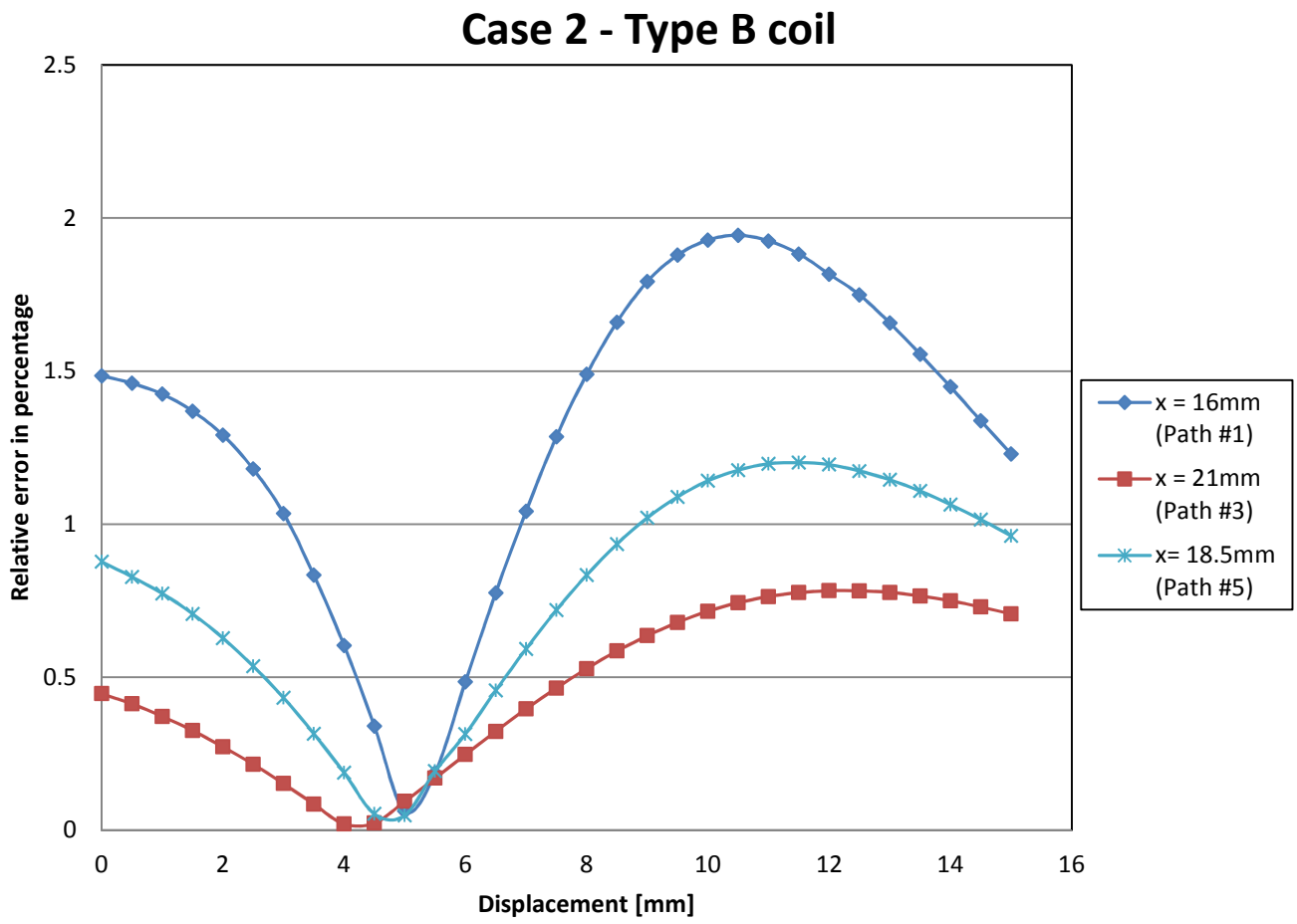


Again the figure shows path #1, #3, and #5, and we can make the same observations that we have done before for path #2 and #4. By now the form of the curve is quite familiar. We see the same trend that we saw in all the other cases that we analyzed, but in this case the points in which the error is almost zero are different from the ones that we saw in the previous cases. Just like before, we can conclude that at these points the influence of the bar is almost inexistent and the voltage readings that we get are background noise.

## 3.3. Comparative analysis of the two types of Rogowski coil.

IN THIS SECTION we make a side by side analysis of the two Rogowski coils that were tested for crosstalk rejection. As we saw in the previous paragraphs, the two coils have a slightly different casing so the region on the top of the coils is slightly displaced with respect to the same center point of the ***x,y*** plane. The regions on the side of the coils are completely overlapped.

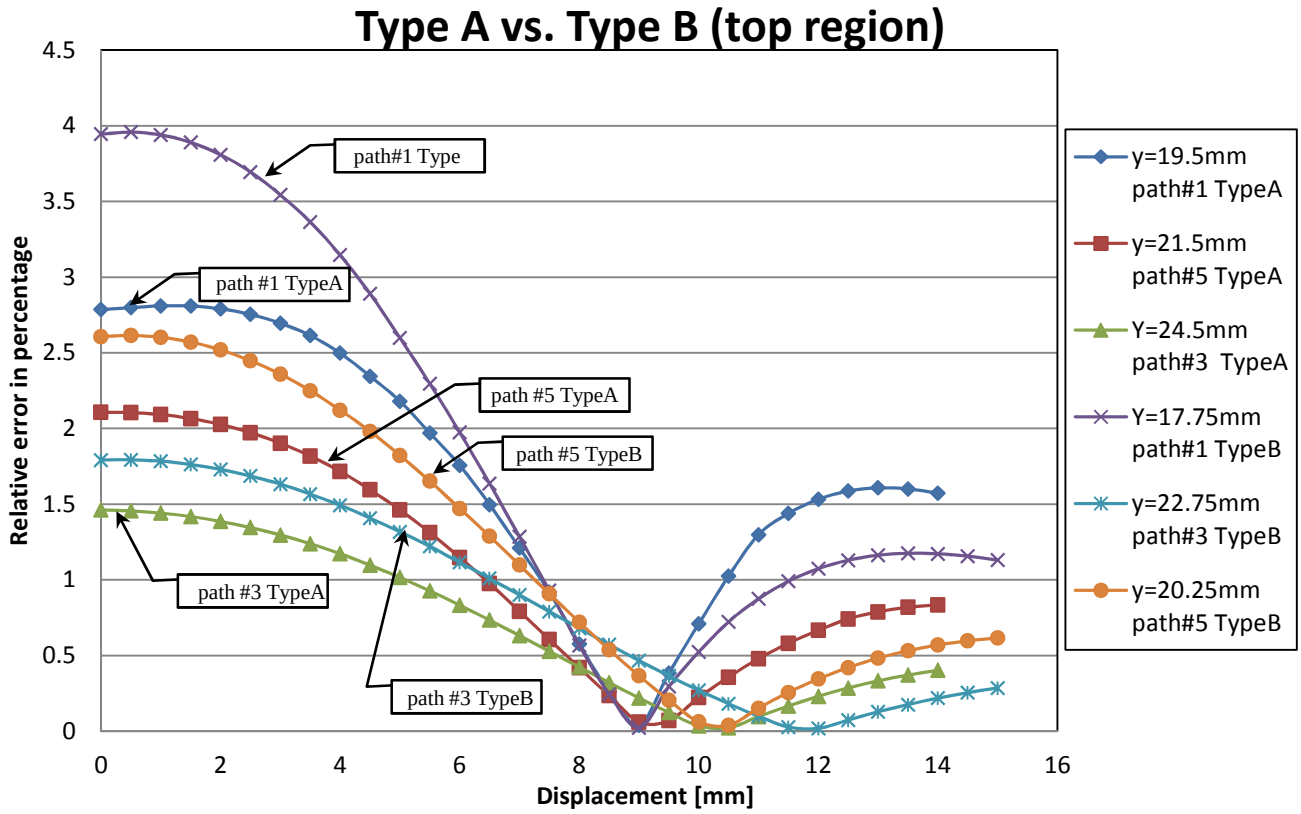


The graph shows the relative error for both coils for the first case. As we know the ***Y*** coordinate of the Type B coil is greater than that of the Type A coil, because of the different dimensions of the coils' casings. Looking at the graph and comparing the respective paths with each other, it can be easily seen that the Type A performs better. But, we have to keep in mind that the voltage measured at the center of the Type A coil was 2392.3 mV which is greater from 1874.45 mV for the Type B coil, so when we compute the ratios against the center voltage we divide for a number that's smaller so we end up with a greater error. If we were two compare two paths that have

almost the same coordinates we will see something like the graph shown below:

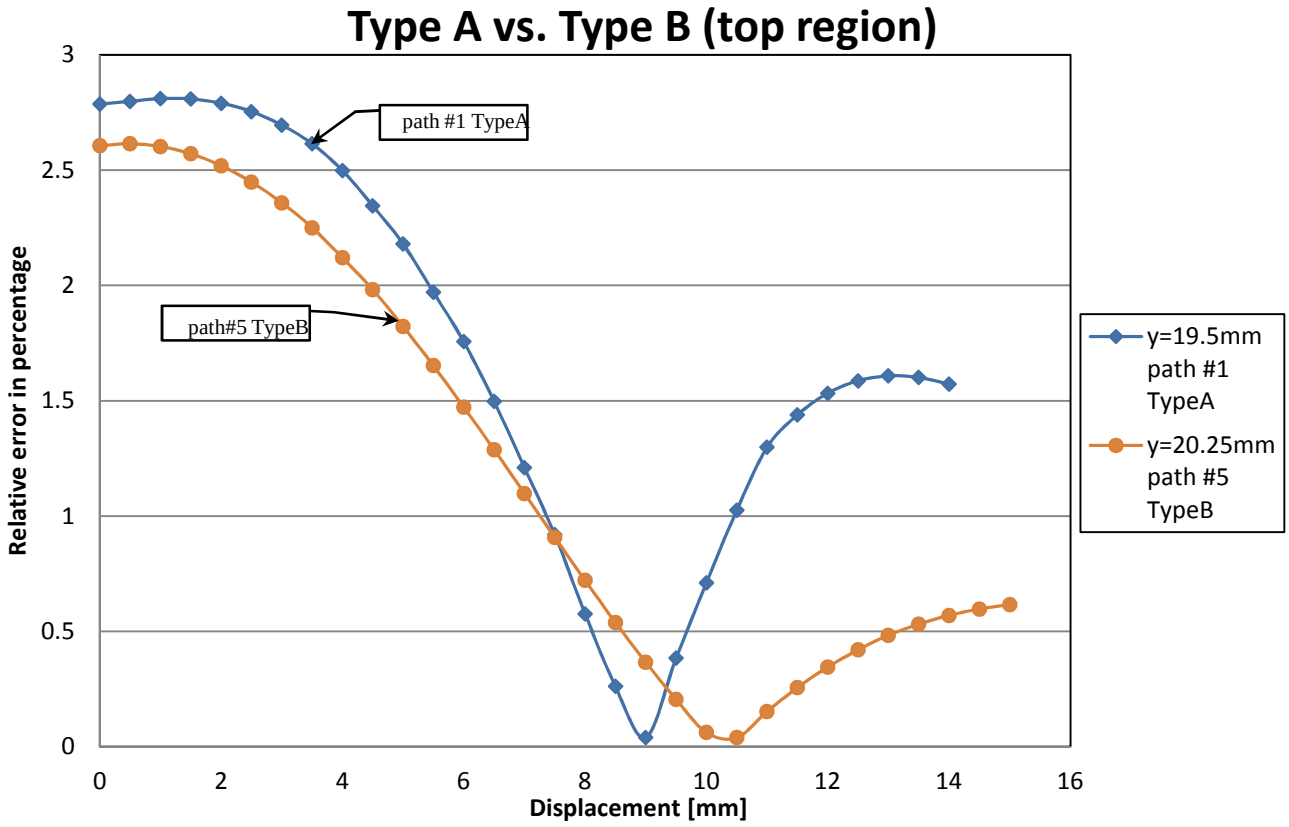


The center of the bar in the case of the Type B coil is 0.75 mm away from the center of the bar in the case of the Type A coil, so roughly one step (0.5 mm) above if we take into account errors during the repositioning of the Type B coil. With these observations in mind, from the graph we see clearly that the relative error is lower for the Type B coil and it is also interesting to notice that after the bar moves away from the points where its influence on the coil is almost inexistent the error stays much lower with respect to the Type A coil.

At last, let's compare the error for case #2 that is the bar was displaced on the region on the side of the coils.

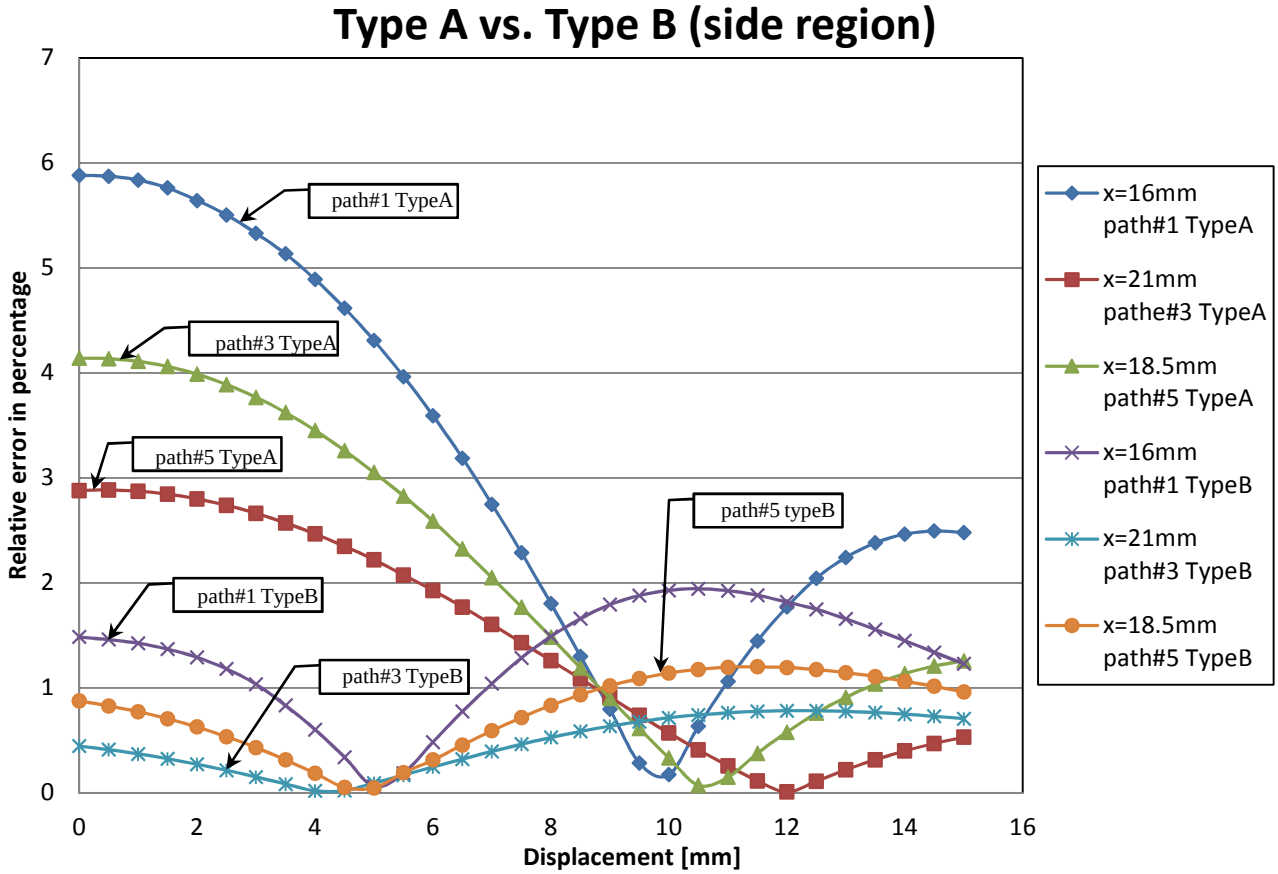


The above graph gives a clear answer: the Type B coil has better crosstalk rejection along the region on the side. It can be easily noticed that the relative error of the Type B coil never passes 2%. On the other hand for the Type A coil the error reaches a max value 5.88% at the most sensible point against 1.4% at the most sensible point of the Type B coil.

## 3.4. Conclusions

THIS CHAPTER was dedicated entirely in investigating two novel Rogowski coil designs from two well-known manufacturers. These coils can be used as current transducers in circuit breakers so it is very important to distinguish the short-circuit current from that of a bar that might be in the proximity of the coil. From this becomes clear the importance of the tests for crosstalk rejection that were performed with both these coils.

We can conclude that the Type A coil has a better sensitivity at the center because the measured voltage is up to 517 mV greater than the Type B coil. On the other hand the Type B coil has better crosstalk rejection especially sidewise where the error is considerably lower. On the other hand, if we look at the top region the overall performance of Type A coil is better. But when we compare the two paths that are almost overlapped, the Type B coil has a slightly lower relative error and after the “dead points” (where we get a reading of almost zero mV), the error rises very slowly for the Type B coil as opposed to the Type A coil. These “dead points” can be exploited in the case when cables or bars are placed in the immediate proximity outside the coils. By doing so, their influence on the coils will be very low.

# 4

# Final Conclusions

THE THESIS is presented as an experimental characterization of two kinds of magnetic sensors used in many applications today.

The Hall sensor is used widely in many fields for different purposes. The application of our interest in this case is the use of Hall sensors in magnetic sensor arrays for current measurements, so this work takes into account the problems related to this specific field of application and tries to give a complete view of the real performance of different sensors that are available on the market today. These tests were done on behalf of a well-known company, which will use later these types of sensors in arrays that can be used in circuit breakers instead of traditional current measurement techniques. From the pool of data that we collected, which for the record is wider but in this paper we expose only the most significant ones, if we were to rank the sensors from the most performing to the least performing one, the EQ732L will be the first followed by HE144. SS495A1 will be the third, HG362 fourth, and the least performing one CYSJ362A.

Last but not least, the two novel Rogowski coils tested for crosstalk rejection proved to have the same trend of the error referred to the voltage measured at their central points. For both coils we identified “dead points” so a possibility to reduce crosstalk problems due to external cables or bars that might be in the proximity of the coils, is to place these within those intervals where the error was below 0.5%. Overall, the Type B coil performed better than the Type A coil, in both quadrants in which the external conductor was placed.

# Reference

[1] S. Ziegler, R. C. Woodward, H. H. Iu, et al. Current sensing techniques: a riview[J], IEEE Sensors Journal., 2009, 9(4): p. 354-376.
[2] F. W. Grover, Inductance Calculations: Working Formulas and Tables. New York: D. Van Nostrand, 1946.
[3] C. M. Johnson and P. R. Palmer, "Current measurement using compensated coaxial shunts," Proc. IEE Sci., Measure. Technol., vol. 141, pp. 471–480, 1994.
[4] J. A. Ferreira, W. A. Cronje, and W. A. Relihan, "Integration of high frequency current shunts in power electronic circuits," IEEE Trans. Power Electron., vol. 10, pp. 32–37, 1995.
[5] R. Malewski, "New device for current measurement in exploding wire circuits," Rev. Scient. Instruments, vol. 39, pp. 90–94, 1968.
[6] F. Costa, P. Poulichet, F. Mazaleyrat, and E. Labouré, "The current sensors in power electronics, a review," EPE Journal, vol. 11, pp. 7–18, 2001.
[7] R. Malewski, C. T. Nguyen, K. Feser, and N. Hylten-Cavallius, "Elimination of the skin effect error in heavy-current shunts," IEEE Trans. Power Apparatus and Systems, vol. PAS-100, pp. 1333–1340, 1981.
[8] F. Castelli, "The flat strap sandwich shunt," IEEE Trans. Instrument. Measure., vol. 48, pp. 894–898, 1999.
[9] S. Ziegler, H. H. C. Iu, R. C. Woodward, and L. J. Borle, "Theoretical and practical analysis of a current sensing principle that exploits the resistance of the copper trace," in Proc. 39th IEEE Power Electronics Specialists Conf., PESC'08, Rhodes, Greece, 2008, pp. 4790–4796.
[10] W. F. Ray and C. R. Hewson, "High performance Rogowski current transducers," in Proc. IEEE Ind. Appl. Conf., Rome, Italy, 2000, pp. 3083–3090.
[11] D. A. Ward and J. L. T. Exon, "Using Rogowski coils for transient current measurements," Eng. Sci. Education J., vol. 2, pp. 105–113, 1993.
[12] A. Radun, "An alternative low-cost current-sensing scheme for highcurrent power electronics circuits," IEEE Trans. Ind. Electron., vol. 42, pp. 78–84, 1995.
[13] L. Dalessandro, N. Karrer, M. Ciappaz, A. Castellazzi, and W. Fichtner, "Online and offline isolated current monitoring of parallel switched high-voltage multi-chip IGBT modules," in Proc. 39th IEEE Power Electron. Specialists Conf., PESC'08, Rhodes, Greece, 2008, pp. 2600–2606.
[14] http://homepage.ntlworld.com/rocoil/
[15] http://www.electronics-tutorials.ws/electromagnetism/hall-effect.html
[16] HALL EFFECT SENSING AND APPLICATION.pdf available online at: http://sensing.honeywell.com
[17] K.-w. Ma and Y.-s. Lee, Isolated Current and Voltage Transducers Appl. Rep., LEM, 2004.
[18] P. Ripka, "Advances in fluxgate sensors," Sens. Actuators A: Physical, vol. 106, pp. 8–14, 2003.
[19] http://www.invasens.co.uk/FluxgateExplained.PDF
[20] R. Bazzocchi and L. Di Rienzo, "Interference rejection algorithm for current measurement using magnetic sensor arrays," Sensors & Actuators: A. Physical, Elsevier, vol. 85, No. 1-3, August 2000, pp. 38-41

[21] L. Di Rienzo, R. Bazzocchi, and A. Manara, "Circular arrays of magnetic sensors for current measurement," IEEE Transactions on Instrumentation and Measurement, vol. 50, No. 5, October 2001, pp. 1093-1096
[22] K. J. Binnis, P. J. Lawrenson, C.W.Trowbridge, The Analytical and Numerical Solution of Electric and Magnetic Fields, John Wiley & Sons, 1992.
[23] L. Di Rienzo, A. Manara, and R. Ottoboni, "Low-cost current transducer based on circular array of magnetic sensors," in Proc. of 11th IMEKO TC-4 Symposium, Lisbon, Portugal, 13-14 September 2001, pp. 135-139
[24] G. D'Antona, L. Di Rienzo, R. Ottoboni, and A. Manara, "Processing magnetic sensor array data for AC current measurement in multiconductor systems", IEEE Trans. Instrum. Meas., vol. 50, No. 5, pp. 1289-1295, Oct. 2001.
[25] A. Manara, E. De Bortoli, L. Di Rienzo, and A. Piazzesi, "An improved current sensing device for low-voltage power circuit breakers," European Patent 1 166 132 B1, 26 July 2006.
[26] G. D'Antona, L. Di Rienzo, R. Ottoboni. Metrological validation of a novel three phase current sensor[C]. Hungary: Proc. of IEEE Instrumentation and Measurement Technology Conference, 2011: 106-110.
[27] http://www.chenyang.de/
[28] http://www.asahi-kasei.co.jp/ake/en/product/hall_ic/index.html
[29] http://www.hoeben.com/products.html
[30 http://sensing.honeywell.com/